A COMPARATIVE STUDY OF CONTROL THEORIES FOR REALISING APFs IN DISTRIBUTION POWER SYSTEMS

A PROJECT REPORT

Submitted by

MAJ PRADEEP KUMAR

(EE14M039)

in partial fulfillment of the requirement
for the award of the Degree

of

MASTER OF TECHNOLOGY

in

ELECTRICAL ENGINEERING

DEPARTMENT OF ELECTRICAL ENGINEERING
INDIAN INSTITUTE OF TECHNOLOGY MADRAS
CHENNAI – 600036

JUNE 2016

To my Parents,

Sushama & Satendra

Whose discipline and love gave me the strength to face this Human Life and to understand the difference between a curator and an owner

THESIS CERTIFICATE

This is to certify that the thesis entitled "**A COMPARATIVE STUDY OF CONTROL THEORIES FOR REALISING APFs IN DISTRIBUTION POWER SYSTEM"** submitted by **Maj Pradeep Kumar** to the Indian Institute of Technology, Madras for the award of the degree of Master of Technology is a bonafide record of project work carried out by him under my supervision at Power Quality and Automation Laboratory, Department of Electrical Engineering from Jul 2015 to Jun 2016. The content of this thesis, in full or in parts, have not been submitted to any other Institute or University for the award of any degree or diploma.

Chennai – 600036

Date: Jun 2016

Prof. Mahesh K. Mishra

Project Guide
Department of Electrical Engineering
Indian Institute of Technology Madras
Chennai – 600 036, INDIA

ACKNOWLEDGEMENTS

Undoubtedly, many may agree with me that to a major extent, it is **always our guide or mentor** in our academician life, who not only teaches the importance of drawing pragmatic plans and setting firm goals in life, but also creates an **everlasting impression** of his virtues and pre-eminent personality as a whole. Reviving the same thoughtfulness in my heart and mind, I really feel **blessed & blissed** to have the singular honour and opportunity to serve under the esteemed guidance and supervision of Prof. Mahesh Kumar as my project guide.

One of the greatest lessons I have learnt from him as a *Guru* is to pay as much attention to the process of work as to its end. And, therefore now it appears to me that all the secret of success is there; to pay as much attention to the process as to the culmination of a work.

I take the opportunity to express my sincere thankfulness towards him for providing his **persistent support** in taking up one of the challenging task in hand, which was not much ventured around by the power quality engineers. As a guide, without his support and relentless guidance, this entire degree would have never been possible.

I would also like to place in record the assistance and friendship I nurtured from the Power Quality lab mates. Their ideas have helped me in approaching the given problem in more confident way.

Last but not the least; I would like to thank my organization, Indian Army, who not only gave me chance to pursue my PG in one of the prestigious institution of the country but also gave me the opportunity to learn from one of the best intellectual academicians of the world under the faculty of Power Systems group of Electrical Sciences. For this I shall always remain grateful and would put in my best in not only improving my personal learning curve but also utilizing this technical knowledge and evolving out of box solutions for the betterment of the society.

ABSTRACT

KEYWORDS: Control theories; Active power filters; Implementation strategies; DSP algorithms.

The increased use of power electronic components within the distribution systems and the reliance on renewable energy sources along with converters as an interface between the source and the power system lead to power quality problems for the smooth operation of various components of power systems, including various types of loads. Therefore, mitigation of power quality problems in power systems more so on dynamic and real time basis is a need of an hour in today's industrial world. Knowing the growing challenges of designing a grid interactive filter to provide real time mitigation/ reduction of the power quality problem, the implementation of APFs requires meticulous designing at each stage. Therefore, in order to design an efficient active power filter the vetting of a given control theory is an important aspect.

This thesis is primarily devoted to analyze the basic formulation of the given control theories in terms of computational time and memory. The same will not only assist in optimizing a given DSP algorithm designed to control APFs but also in reducing the overall operational time and cost of the various topologies or modifications of APFs designed so far. Finally, a comparative analysis is presented to derive their *Big-O* polynomial to comment upon their efficiency in time and space. A case study is also performed by analyzing the performance of the control theories on TMS320F28377S processor using CCS software. The thesis also incorporates simulation studies in the end to compare transient performance of the given theories.

TABLE OF CONTENTS

Page

LIST OF TABLES

Table **Title** **Page**

LIST OF FIGURES

Figure **Title** **Page**

ABBREVIATIONS

AC	Alternating Current
A/D	Analog to Digital Converter
APF	Active Power Filter
CT	Current Transformer
CCS	Code Composer Studio
DC	Direct Current
DSP	Digital Signal Processor
DSTATCOM	Distribution Static Compensator
DVR	Dynamic Voltage Restorer
FFT	Fast Fourier Transform
FPGA	Field Programmable Gate Array
IEEE	Institute of Electrical and Electronics Engineers
IGBT	Insulated Gate Bipolar Transistor
MAF	Moving Average Filter
PCC	Point of Common Coupling
PT	Potential Transformer
PLL	Phase-lock Loop
THD	Total Harmonic Distortion
VSI	Voltage Source Inverter

NOTATIONS

English Symbols

C_{dc}	DC storage capacitor
e_{dc}	Difference between reference and actual capacitor voltage
e_f	Difference between reference and actual filter current
h	Hysteresis band
$i_{df\,ref}$, $i_{qf\,ref}$	Reference filter currents in *d*-*q* plane
i_{la} , i_{lb} , i_{lc}	Instantaneous load currents in phase-*a*, *b* and *c* respectively
i_{fa} , i_{fb} , i_{fc}	Instantaneous filter currents in phase-*a*, *b* and *c* respectively
$i^*_{fa\,ref}$, $i^*_{fb\,ref}$, $i^*_{fc\,ref}$	Reference filter currents in phase-*a*, *b* and *c* respectively
i_0 , i_α , i_β	Load currents in $0-\alpha-\beta$ coordinates
i_{sa} , i_{sb} , i_{sc}	Instantaneous source currents in phase-*a*, *b* and *c* respectively
K_p , K_i	Gains of conventional proportional integral controller
L_f	Interface inductor
p	Instantaneous real power
p_0 , p_α , p_β	Instantaneous real power in $0-\alpha-\beta$ coordinates
$\overline{p}$, $\tilde{p}$	Dc and alternating component of instantaneous active power
P_{dc}	Power drawn by the load connected to dc link
P_{lav}	Average load power
P_{loss}	Losses in the inverter
q	Instantaneous reactive power
$\overline{q}$, $\tilde{q}$	Dc and alternating component of instantaneous reactive power
R_f	Internal resistance of the interface inductor
T	Half Time period of voltage or current waveform
v_{dc}	DC link voltage
$V_{dc\,ref}$	Reference value of dc link voltage
v_{sa} , v_{sb} , v_{sc}	Instantaneous supply voltages in phase-*a*, *b* and *c* respectively

Notations (continued)

v_0, v_α, v_β	Supply voltages in $0-\alpha-\beta$ coordinates

Greek Symbols

α	Harmonic compensation coefficient
β	Fundamental compensation coefficient
ω	Fundamental frequency of the supply voltages in rad/s
ϕ	Power factor angle between supply voltages and currents

CHAPTER 1

INTRODUCTION

The increased use of power electronic components within the distribution systems and the reliance on renewable energy sources along with converters as an interface between the source and the power system lead to power quality problems for the smooth operation of various components of power systems, including various types of loads. Thus, it would be prudent to say that the problem of power quality being faced is a reflection of the industrial growth achieved so far. Moreover, electrical networks with poor power quality result in financial loss, environmental impacts and/ or safety concerns. These losses are cascaded back to the utility power plants and results in increased CO_2 emissions. Even, one latest study shows that one unit of electricity saved is equivalent to three units generated. Therefore, mitigation of power quality problems in power systems more so on dynamic and real time basis is a need of an hour in today's industrial world. Knowing that the design of these APF is becoming challenging day by day, efforts are on to make them more grid interactive and simultaneously economically viable to accrue energy savings and management for both power grid and various industries.

1.1 NEED OF FILTERS IN POWER SYSTEMS

With the advancements in technology and improvements of power electronic devices, the implementation of harmonic filters has become an essential element of electric power networks. Therefore, the utilities are continually pressured to provide high-quality and reliable energy. But the non-linearity introduced by the power electronics based loads (e.g., computers, printers, fax, CFL tubes, electronic health assessment and diagnostic machines etc) is a matter of great concern for both the utility and consumer. They cause excessive neutral currents, over-heating of electrical apparatus, poor power factor, voltage distortion, high levels of neutral to ground voltage and

interference with communication systems. If this heating were continued to the point at which the insulation fails, a flash-over may occur. This would partially or permanently damage the device, which may result in loss of generation or transmission that could cause blackouts.

1.1.1 Harmonics in Power Systems: A Main Cause of Power Quality Problem

The harmonics disturbances in the power supply are caused by the nonlinear characteristic of the power electronic components used as an interface between Distribution Energy Systems and main power grid (e.g. VSIs, CSIs) and as a load as well. Therefore, with a network dominated by nonlinear components (power electronics coupling for generators and loads), deviation of power quality parameters from sinusoidal nature is be a common situation. Hence, given that the sensitive loads are connected to the system, injection of harmonic currents and reactive power into the supply grid is a serious problem, not only effecting the smooth operation of power electronic interface but polluting the electric distribution network as a whole.

The impact of harmonics on the power system can be categorized as; short term effects and long term effects. The short term effects are usually noticeable and are related to excessive voltage distortion such as nuisance tripping of sensitive loads or overheating of transformer. However, the long term effects will show the impact after certain period and it is undetected. This long term effects are usually related to increased resistive losses or voltage stress. Capacitors in power systems might fail or capacitor fuses may blow due to the over voltage stress on dielectric [1].

Over a period, various types of solutions were employed for mitigating/ limiting the injection of harmonics from nonlinear loads in power systems, like, one of the solution is implementing delta transformer connection to yield a net 12-pulse operation to eliminate the third harmonic component of the current. Also, standards such as IEEE-519, IEC-61000, and EN-50160 were introduced for the end-users and the electric utilities to attempt reasonable harmonics goals [2]. According to these standards, the end-users are required to limit the harmonic currents by controlling their loads and the utilities should limit the harmonic voltages by controlling the power system impedance.

The percentage total harmonic distortion (% THD) is a well known power quality term used to define the amount of distortion in voltage or current waveform. THD the compensated source currents indicates the quality of the load compensation. It is defined as

$$\%\text{THD} = \frac{\sqrt{\sum_{n=2}^{\infty} I_n^2}}{I_1} \text{x}100$$

where, I_n is the rms value of the n^{th} harmonic current.

The value of THD below 5% is generally accepted, while values above THD of 10% are definitely unacceptable. Also, higher THD leads to a poor power factor and lowers the efficiency of equipment.

1.2 FILTERS IN POWER SYSTEMS

The most traditional method for mitigating the power quantity issues is use of passive filters. The passive filters consist of inductors and capacitors which are tuned for a particular frequency. Thus the elimination of multiple harmonic components would require the installation of separate passive filters for each harmonic frequency. Inspite of the low cost and high efficiency of the passive filters, they suffer from disadvantages like bulk size, series/ parallel resonance, need of high rating and require the coordination with reactive power requirements of the loads.

Self-adaptable, dynamic solution known as APF has proved to be remarkable for mitigating power quality problems. Its basic principles were discussed by Sasaki and Machida (1971), Peterson *et al.* (1975), Gyugyi and Srycula (1976) and Mohan *et al.* (1977). However, the technology of those times was unable to support the real time implementation. But the significant progress in the speed and capacity of power semiconductor devices like IGBTs and GTOs in the recent years have enabled the practical realization of the APFs.

1.3 GENERAL CLASSIFICATION OF FILTERS IN POWER SYSTEMS

Filters are often the most common solution approaches that are used to mitigate the harmonics in power systems. Unlike other solutions, filters offer a simple and

inexpensive alternative with greater advantages. Classification of filters may be performed based on various criteria, including the following:

- Number and type of elements (e.g., one, two, or more passive and/or active filters)
- Topology (e.g., shunt-connected, series-connected or a combination of the two)
- Supply system (e.g., single-phase, three-phase three wire and three-phase four wire)
- Type of nonlinear load such as current-source and/or voltage-source loads
- Power rating (e.g., low, medium and high power)
- Compensated variable (e.g., harmonic current, harmonic voltage, reactive power and phase balancing as well as multiple compensation)
- Converter type (e.g., VSI and/or CSI to realise active elements of filter)
- Control technique (e.g., open loop, constant capacitor voltage, constant inductor current, linear voltage control or optimal control)
- Reference estimation technique (e.g., time and/or frequency current/voltage reference estimation)

Figure 1.1 depicts the classification of filters as used in power systems based on supply system with the topology as a sub-classification [3-7]. Further classification is made on the basis of the numbers and types of elements used in different topologies. As a matter of fact, according to Figure 1.1, there are 156 valid configurations of passive, active and hybrid filters – offering its own unique solution to improve the quality of electric power. Therefore, the choice of filter depends on the nature of the power quality problem, the required level and speed of compensation, as well as the economic cost linked with its implementation.

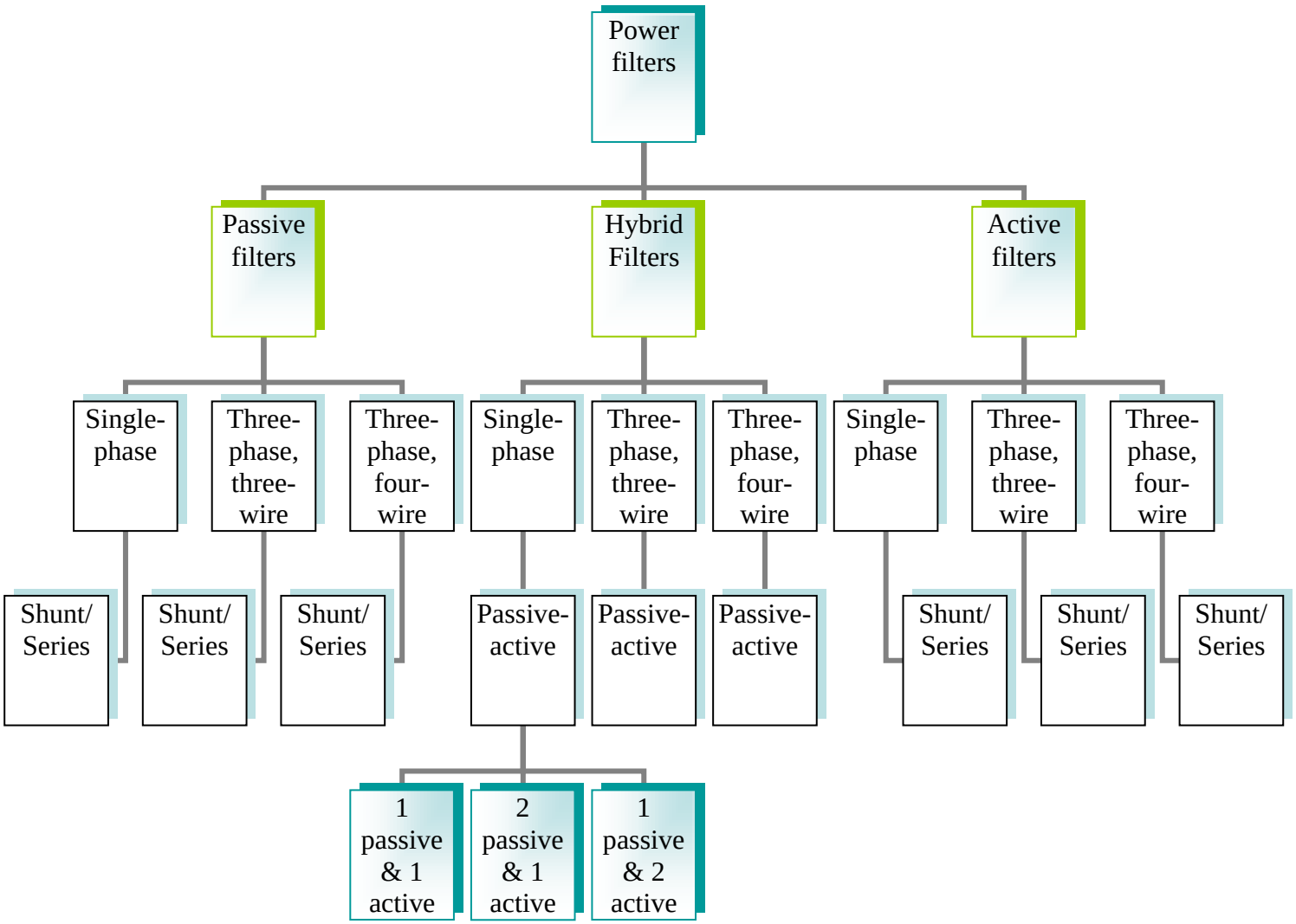

Fig. 1. 1 Classification of filters used for power quality improvement [3 – 7]

1.4 A BRIEF INTRODUCTION OF APFs

APFs are feasible alternatives to passive filters. For applications where the system configuration and/ or the harmonics of non-linear loads (e.g., orders, magnitudes and phase angles) change, active elements may be used instead to provide dynamic compensation.

An APF is implemented when the order numbers of harmonic currents are varying. This may be due to the nature of non-linear loads injecting time-dependent harmonics or may be caused by a change in the system configuration. APFs rely on active power conditioning to compensate undesirable harmonic currents replacing a portion of the distorted current wave stemming from the non-linear load. This is

achieved by generating harmonic components of equal magnitude but opposite phase angles, which cancel the injected harmonic components of the non-linear loads.

1.4.1 Working Principle of an APF

The working principle of an APF can be explained with the help of a typical shunt APF as shown in Figure 1.2. A Shunt APF draws a current in such a way that the source current, which is a sum of load and active filter current, becomes sinusoidal i.e.

$$i_s = i_l + i_f$$

where, i_s, i_l and i_f are instantaneous source, load and filter current, respectively. In other words, the shunt APF acts as a controlled (using VSI) non-sinusoidal current source that injects or draws, non-sinusoidal current at the PCC to make the supply current sinusoidal. These APFs compensate harmonics continuously, regardless of the changing of the applied loads.

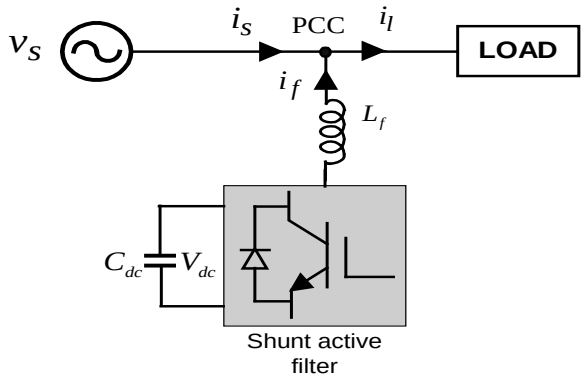

Fig. 1. 2 Schematic Diagram to explain working principle of a shunt APF

The main advantage of APFs over passive filters is their fine response to changing loads and harmonic variations. In addition, a single APF can compensate more than one harmonic and improve/ mitigate power quality problems such as flicker. Active filters are expensive compared with their passive counterparts and are not feasible for small facility. The main disadvantage of APFs is that their ratings are generally, close to the load (approximately, upto 80%). Also, a single APF might not be able to provide a complete solution to the given number of power quality problems,

sometimes involving both voltage and current quality problems. In that case, hybrid filters, which are having a more complicated design, are employed. Table 1.1, shows a brief summary of APFs used for different compensations in order of their preference in power systems [8].

Table 1. 1 Selection of an APF for a specific application [8]
APF configuration with higher number of # is more preferred

Compensation desired	APF			
	Series	Shunt	Hybrid (Active series & Passive shunt)	Hybrid (Active shunt & Active shunt)
A. Current harmonics		##	###	#
B. Reactive power		###	##	#
C. Load balancing		#		
D. Neutral current		##	#	
E. Voltage harmonics	###		##	#
F. Voltage regulation	###	#	##	#
G. Voltage balancing	###		##	#
H. Voltage flicker	##	###		#
I. Voltage sag & dip	###	#	##	#
A+B		###	##	#
A+B+C		##		#
A+B+C+D		#		
E+F	##			#
E+F+H+I	##			#
A+E			##	#
A+B+E+F			#	##
F+G	##		#	
B+C		#		
B+C+D		#		
A+B+G		##	#	
A+C		#		
A+D+G		#	##	

1.4.2 Block Diagram of APFs

The generalized block diagram of shunt connected APF is shown in Fig. 1.3. It consists of the following basic elements [9].

- **Sensors and transformers** are used to measure waveforms and inject compensation signals. Non-sinusoidal voltage and current waveforms are sensed via PTs, CTs, Hall effect sensor, and isolation amplifiers. Connection, transformers in shunt and series with the power system are used to inject the compensated current (I_{APF}) and voltage (V_{APF}), respectively.

- **Distortion Identifier** is a signal-processing function that takes a measured distorted waveform, d(t) (e.g., line current or phase voltages) and generates a reference waveform, r(t), to reduce the distortion.

- **Inverter** is a power converter (along with coupling inductance and transformer) that reproduces the reference waveform with appropriate amplitude for shunt (I_{APF}) and/or series (V_{APF}) active filtering.

- **Inverter Controller** is usually a pulse-width modulator with local current control loop to ensure I_{APF} and/or V_{APF} tracks r(t).

- **Synchronizer** is a signal-processing block (basically, PIL technique) to ensure compensation waveforms (I_{APF} and/or V_{APF}) are correctly Synchronized.

- **DC bus** is an energy storage device that supplies the fluctuating instantaneous power demand of the inverter.

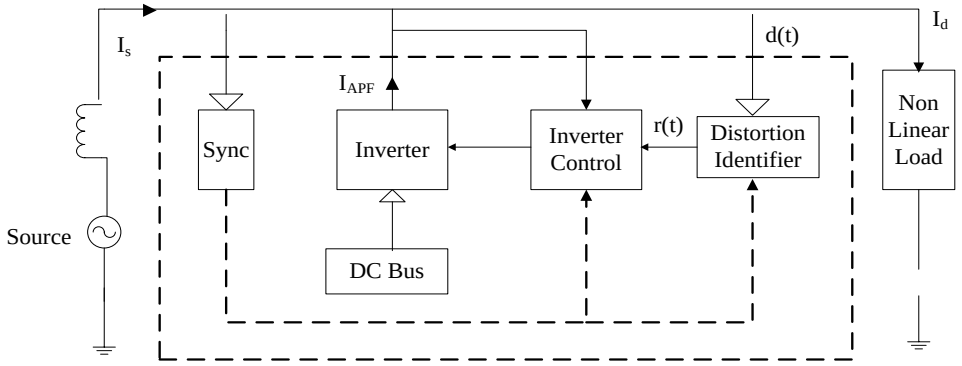

Fig. 1. 3 Control diagram of shunt-connected APF [9]

An essential component of the APF is the control unit, which consists of a microprocessor. The control theory is implemented online by the microprocessor after receiving input signals through A/D converter channels, PLL and synchronised interrupt signals. All control tasks are carried out concurrently in specially designed processors.

1.4.3 Implementation of Active (or Hybrid) Power Filters

The initial stage for any filtering process is the selection of the filter configuration. Depending upon the nature of the distortion and system structure, as well as the required precision, speed and accuracy of the compensation, an appropriate filter configuration (e.g., series, shunt, passive, active or hybrid) is selected. The important aspects in the realization of any APF are as under:

- Choice of Topology of the VSI, which is determined by the type of distribution system where it is to be installed and the loads it intends to compensate.

- The choice of a control algorithm for the generation of the reference quantities, which should be injected into the distribution network for proper compensation. Here, the algorithm uses the instantaneous values of source, load and capacitor voltages along with the load currents in order to calculate the reference quantities.

- The current control of the voltage source inverter, i.e. the switches of the inverter should be operated so that the actual injected quantity should track the reference values generated using control algorithm. Also, the parameters of the VSI should be properly designed for the effective working of the selected switching strategy.

This thesis primarily focuses on the second aspect mentioned above to compare various control theories for generation of reference currents.

1.5 AN OVERVIEW OF DIFFERENT CONTROL THEORIES USED FOR REFERENCE CURRENT GENERATION FOR IMPLEMENTING APFs

The applicability of a particular power theory to 'switching compensation control' depends on the goals of compensation as well as expected system conditions. As the

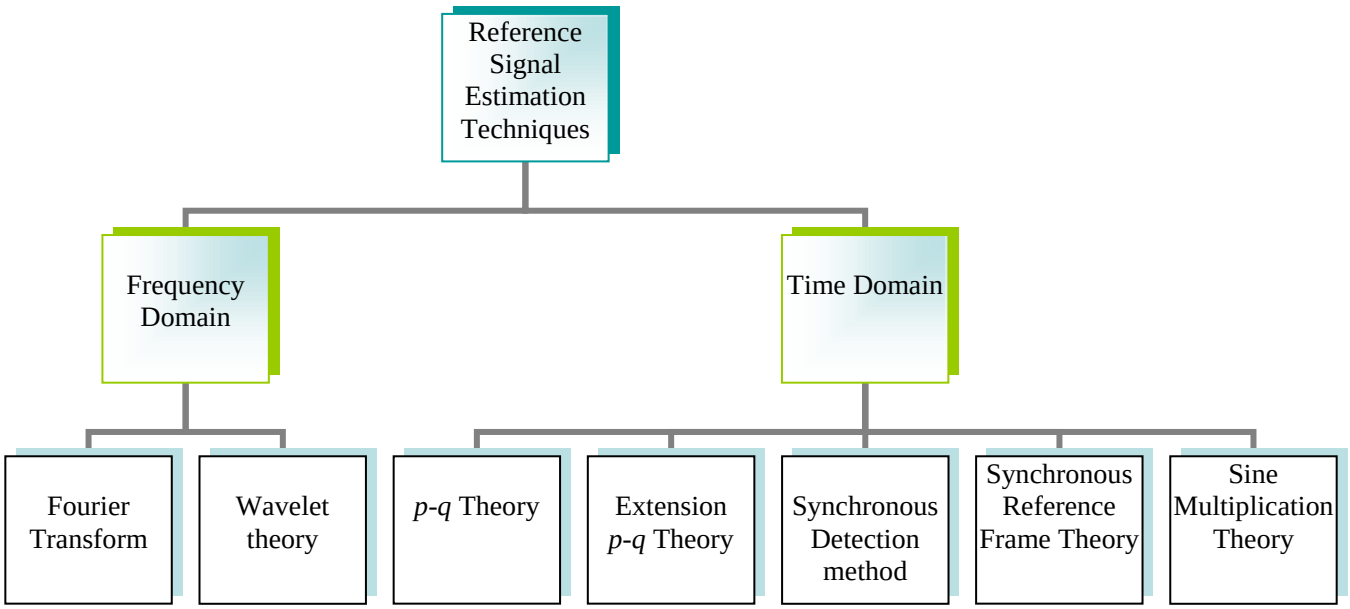

Fig. 1. 4 Reference current estimation techniques

performance of any APF mainly depends on the reference current generation strategy, control technique and topology of the filter inverter [10], accordingly a number of control methods (theories) exist in the literatures. For the ease of understanding the same may be classified as current estimation techniques, when compensation is implemented in time or frequency domain. Compensation in frequency domain is based on Fourier analysis of a distorted signal.

In time domain a number of control strategies such as IRP theory (*p-q* theory) initially developed by Akagi *et al*. [11], SRF theory (*d–q*) [12-13], synchronous detection method, notch filter and fuzzy logic controller method, sliding mode controller, etc. are used in the development of three-phase APFs. Out of these theories, more than 60% research works consider using *p-q* theory and *d-q* theory due to their accuracy, robustness and easy in calculation [14]. Figure 1.4 depicts the considered reference signal estimation techniques proposed by Motano *et al*, 2002 and Gobrio *et al*, 2008.

The following sub-sections briefly explain some of the commonly used time domain control theories used for generating the reference signal for implementing APFs. The overview of these theories in terms of their characteristic differences established so far is presented in Table 1.2 as a ready reference.

1.5.1 Instantaneous Reactive Power Theory (IRP)

In 1983, *Akagi et al.* has proposed the generalized theory of the instantaneous reactive power in three-phase circuits, also known as *p-q* theory [11]. It is based in instantaneous values in three-phase power systems with or without neutral wire, and is valid for steady-state or transitory operations, as well as for generic voltage and current waveforms. The *p-q* theory consists of an algebraic transformation (Clarke transformation) of the three-phase voltages and currents in the *a-b-c* coordinates to the α-β coordinates, followed by the calculation of the instantaneous active and reactive powers components. This scheme is most widely used because of its fast dynamic response but gives inaccurate results under distorted and asymmetrical source conditions. From [14] it is evident that under balanced and unbalanced sinusoidal voltage conditions the THD for *p-q* theory is 2.41% and 7.04 % respectively. The main characteristics of *p-q* theory are as under.

- It is inherently a three-phase system theory
- It is based in instantaneous values, allowing excellent dynamic response
- Its calculations are relatively simple (it only includes algebraic expressions that can be implemented using standard processors)
- It allows two control strategies: constant instantaneous supply power and sinusoidal supply current.

If the supply voltage is close to ideal and all the components of reactive power must be compensated, then time domain *p-q* provides as instantaneous response from the reference generator. However, under a non ideal supply condition or if the selection of a particular components of the fundamental or harmonics is required then the theory is no longer instantaneous. Therefore, when the source voltages are unbalanced and non-sinusoidal *p-q* theory fails, requiring more modifications from its original formulation.

1.5.2 Synchronous Reference Frame Theory (SRF or *d-q* theory)

In the SRF theory proposed by Divan [12-13], the compensation signals are calculated based on a synchronously rotating reference frame. It has an edge against rest of the theories as it performs the operation in steady-state and transient state as well as for generic voltage and current waveforms. The SRF method becomes quite complicated under asymmetrical source and load conditions. From [14] it is evident that under balanced and unbalanced sinusoidal voltage conditions the THD using SRF theory is 2.27% and 5.18 % respectively. Also from [14] it is observed that *d-q* method always give better result under un-balanced and non-sinusoidal voltage conditions over the instantaneous active and reactive power *p-q* method. Since *p-q* method is frequency variant, on providing additional PLL circuit it becomes frequency independent. Thus, problem of synchronization with unbalanced and non-sinusoidal voltages is also overcome. The theory has following established features [15].

- Like IRP theory, this is also an inherent three phase system theory.
- It can be applied to any three-phase system (balanced or unbalanced, with or without harmonics in both voltages and currents)
- It is based on instantaneous values, which gives it a good time dynamic response.
- Net decoupling between the fundamental and harmonic components.

Table 1. 2 Overview of different control theories

Differentiating Characteristics	Control Theories			Comments
	ISC	*p-q*	*d-q*	
Results with balanced and sinusoidal source condition	Accurate	Accurate (obtains sinusoidal and balanced currents, constant instantaneous power and unity power factor in the source side)	Accurate	

Results with unbalanced and/ or distorted source condition	Inaccurate	Inaccurate (instantaneous power is constant after compensation in the source side, but the current is not balanced and sinusoidal and the power factor is not unity)	Accurate	• Additional computational burden on p-q and ISC theory for. • However, positive sequence extraction is inherently a part of *d-q* theory (using PLL)
Harmonic Mitigation	Harmonic mitigation as per IEEE- 519 standard is achieved only under ideal source voltage condition but it fails under unbalanced and non-sinusoidal source voltage conditions	Harmonic mitigation as per IEEE- 519 standard is achieved only under ideal source voltage condition but it fails under unbalanced and non-sinusoidal source voltage conditions	Harmonic mitigation excellent as per IEEE- 519 standard is achieved only under ideal source voltage and unbalanced sinusoidal source voltage condition	
Valid for steady and/ or transient state	Both	Both	Both	
Transient response	good	good	Better than rest	
Design of controller	Easy	Easy	Easiest	• As in *d-q* model we deal with DC quantities, implementation of regular PID is much easier
Computational complexity	Simpler (doesn't require complex transformation. Compensator currents can be calculated directly)	Average (requires complex transformation. It deals with the power components for calculation of compensator currents)	High (numbers of complex transformation required more than IRP. currents)	• Uses only load current component for computation of compensation
Overall ease of execution	Simplest	Simpler	Complex	• Requirement of PLL in *d-q*

1.5.3 Instantaneous Symmetrical Component Theory (ISC theory)

The theory of instantaneous symmetrical components is widely used for the purpose of load balancing, power factor correction and harmonics suppression [16-17]. The control algorithm based on the instantaneous symmetrical component theory can practically compensate any kind of unbalance and harmonics in the load, even when the source voltages are unbalanced. The symmetrical component theory originally defined for steady state analysis of a 3-phase unbalanced system uses a transformation matrix based of phasor representing an unbalanced 3-phase system. It is the simplest scheme, which predominantly requires implementation of algebraic equations with least computational efforts.

The Table 1.2 highlights that so far the control theories have been characterised and compared based on their applicability in meeting the compensation goals and to achieve desired THD % (quantified parameter) as specified in IEEE-519. Though, the symmetrical component theory is superior to other theories, in terms of its computational efficiency and simplicity, however, a very little information is available with the power quality engineers to comment upon the very basic nature of these theories, specifically their performance in terms of computational time and memory.

1.6 MOTIVATIONS

Knowing the growing challenges of designing a grid interactive filter to provide real time mitigation/ reduction of the power quality problem, the implementation of APFs requires meticulous designing at each stage. The advent of micro grids and their unpredicTable operation also impinges sudden variations in the source conditions for implementing an APF. As over a period, the use of digital control systems has taken over the analog control everywhere, the implementation of more complex digital signal processing algorithms has also been made possible. In order to implement such APFs in digital domain, henceforth as Digital Filters, aspects starting from currents and voltage measurements, signal galvanic isolation, choice of sampling rate, choice of number of bits, choice of sequential versus simultaneous sampling, synchronization with line voltage, signal filtration and separation etc. needs to be deliberated.

Therefore, in order to design an efficient digital filter the vetting of a given control theory assumes importance.

This thesis is primarily devoted to analyze the basic formulation of the given control theories in terms of computational time and memory. The same will not only assist in optimizing a given DSP algorithm designed to control APFs but also in reducing the overall operational time and cost of the various topologies or modifications of APFs designed so far.

1.7 OBJECTIVES

As brought out in preceding sections that the performance of a given DSP based control algorithm will improve drastically, when we have *a priori* knowledge of computational efficiency and memory requirement of the theories working behind the control algorithms. Therefore, this necessitates a need to establish a generic comparison amongst commonly existing control theories for generation of reference current. Based on the above requirement, following objectives are formulated:

1. To understand the mechanism of popular transformations involved in power systems and to obtain their various combinations followed by their generalization.

2. To formulate the control theories based on a given source condition. A comparative study to be carried out amongst various theories in terms of their computational speed and memory requirement. Finally, a generic analytic polynomial to be developed of the theories to perform various case studies on different microprocessors.

3. To perform simulation studies on the control theories to understand the transient performance amongst each other.

1.8 ORGANIZATION OF THE THESIS

Chapter 1 begins with an introduction to power quality issues. It describes the need of filters in power system. Emphasis is also given on understanding the causes of harmonics in power system and their mitigation. The chapter also reviews the general

classification of existing filters. Working principle and implementation of APF is also discussed in brief. Finally an overview of commonly used reference current generation techniques are brought out along with the motivations and objectives of the thesis.

A literature survey of various control strategies employed in APFs is provided in **Chapter 2**. A detailed study of various Transformations is covered in **Chapter 3**. It discusses about the inter-conversions of commonly used transformations and their interpretation in different reference frames. The applications of these transformations in developing control theories are also discussed. **Chapter 4** elucidates the generalization of *α-β-0* and *d-q-0* transformations.

Chapter 5 gives the formulation of ISC theory, SRF theory and IRP theory under balanced and unbalanced source voltage conditions. It gives the implementation algorithm of these theories and their sequential depiction in the form of flowcharts. Chapter focuses on the main work of the project by analyzing the theories based on their performances in terms of computational efforts and memory allocations in a generic form. Finally a comparative analysis is presented to derive their *Big-O* polynomial to comment upon their efficiency in time and space. A case study is also performed by analyzing the performance of the control theories on TMS32OF28377S processor using CCS software.

In **Chapter 6** simulation studies on DSTATCOM are performed using different control theories. In addition performance analysis of control theories is discussed when used for reference current generation (ideal current) for shunt active filter.

The important conclusions are summarized in **Chapter 7**. The suggestions for future work are also brought out. The mathematical derivation used in positive sequence extraction is given at **Appendix "A"**.

CHAPTER 2

LITERATURE SURVEY

Ray P. Stratford *et al* (1980) discussed static power converters which have increased in number and applications in the past decade, and there has been an increased use of static power capacitors for improving power factor. These two trends have set the stage for possibly uncontrolled harmonic resonances in power systems.

Mansoor *et al* (1994) explained net harmonic currents produced by large numbers of single-phase desktop computers in a facility, such as a commercial office building. Providing estimates of the net harmonic current injection due to distributed single-phase computer loads in Amps/ KW, as well as in percent of the fundamental current, for a wide range of system loading and voltage distortion conditions.

Al-Yousif *et al* (2004) discussed different types of passive harmonics filters to mitigate harmonics in commercial application. The passive filters considered are the single tuned and double tuned harmonic filters. The effects of power factor correction capacitor and load parameter variation on harmonic distortion were also investigated. The study also proves that both filters give better performance in reducing harmonics when they are placed close to the harmonic producing loads.

Akagi *et al* (1996) and Oku *et al* (1995) proposed active filters for power conditioning which provides the following functions:

- Reactive power compensation
- Harmonic compensation
- Flicker/ unbalance compensation and
- Voltage regulation.

Fujita *et al* (1991), (1996) and Peng *et al* (1990), (1993) presented the study of a parallel operation of a current controlled active filter and passive filters. The effects of the impedance characteristics have been discussed in terms of the effectiveness of filters. The idea of sharing the compensation tasks of reactive power and harmonics between the two types of filters were discussed.

In order to implement an APF, selection of control strategy plays a crucial role. Control of an APF includes overall system control, extraction of reference signals, controlling dc-link capacitor voltage or inductor current and gating signal generation. Therefore, it is realised in three stages:

- Sensing of required voltage and current signals with the help of current CTs, PTs, hall-effect sensors or isolation amplifier [18].
- Deriving compensating signals in terms of voltage and current level and regulating dc-link.
- Generation of gating signal for solid-state devices of the APF.

Very accurate and fast sensing of signals, fast processing of reference signals and high dynamic response of controller are the key requirement of a good compensating device [19]. Keeping this in mind, researchers have proposed and implemented large number of control techniques for reference signal generation, dc-link voltage balance and switching pattern. These methods are discussed under succeeding sections.

2.1 REFERENCE SIGNAL EXTRACTION SCHEMES

Grady *et al*(1990) proved that Active Power Line Conditioning (APLC) is a relatively new concept that can potentially correct network distortion caused by power electronic loads by injecting equal but opposite distortion at carefully selected points in a network. Existing and proposed line conditioning methodologies are compared and a list of the advantages and limitations of each methodology is presented. Two fundamental approaches were employed for improving power quality with:

- Correction in the time domain and
- Correction in the frequency domain.

Time domain and frequency domain correction techniques have both been successfully implemented, but a specific trend towards either technique has not been identified in the references. Both techniques have been used with voltage-type and current-type converters. The greatest advantage of time-domain correction is its fast response to changes in the power system. Also, it is easy to implement and has little computational burden. Since, time-correction techniques take measurements at only one point in the power system, they are generally limited to single-node applications and are not well suited for overall network correction.

Reference signal generation affects the rating, steady-state performance and transient response of APF [20]. Control strategy for generating compensating command can be extracted either by frequency based techniques or time domain techniques discussed in following sub sections.

2.1.1 Frequency-domain Compensation Schemes

Frequency domain compensation is based on the principle of Fourier analysis, wavelet analysis and infinite impulse response and the periodicity of distorted signal to be compensated. Among frequency domain schemes, conventional Fourier based method and modified Fourier method have gained popularity. Apart from this two methods, another approach which takes the advantage of decomposing three-phase signals into synchronously rotating direct and quadrature components has also been reported [21].

1. Conventional Fourier based techniques*:* In conventional Fourier based techniques conventional FT or FFT is applied to capture voltage or current signals. Compensating signal in time domain is obtained by subtracting the fundamental component from the FT and then applying IFT to the resultant, which is the compensating harmonic signal. Sampling time delay is a major demerit associated with this method [7]-[23].
2. Modified Fourier Transform technique: Modified Fourier transform was introduced to overcome the issue of sampling time delay in conventional method. It is based on calculating only fundamental component of current which is used to separate total harmonic signal from sampled load current waveform [24]. For

practical implementation it requires modifying the main Fourier series equation to generate recurring formula with a sliding window. The components of sine and cosine coefficient computed at each sub-cycle are stored in two different circular arrays. Coefficient values are continuously updated. It is applicable to both single and three-phase. Computation is fast.

2.1.2 Time-domain Compensation Schemes

Time-domain approaches are mainly based on instantaneous derivation of reference signals in terms of voltage or current signals from distorted/ harmonic polluted signals. There are a large number of time domain approaches. Some of them are briefly discussed here.

1. Instantaneous reactive power (*p-q*) theory: This theory relies on Clarke's Transformation (transformation of *abc* to *αβ0* in stationary reference frame). Real and reactive power of load consisting of dc-component and oscillating component are calculated from the transformed quantities. These components are separated by passing through filter and the compensating components are selected for reference current generation. This method is only applicable to three-phase system. It gives good performance for balanced sinusoidal supply condition. For contaminated supply, performance is poor [25]. The original '*p-q*' theory was proposed by Akagi *et al* [11] and then revised by Marshal *et a1* [26]. Thereafter it was further modified/extended by Nabae *et al* [27] to make it applicable to eliminate neutral current of 3-phase, 4-wire systems where source voltages are unbalanced and loads are non-linear and unbalanced. These modified forms are known as 'modified *p-q* theory' [28] 'extended pq theory [29] and '*p-q-r* theory' [30].

2. Synchronous reference frame (d-q) theory: SRFT [31] or *d-q* theory relies on Park's Transformation where three-phase signals are transformed to synchronously rotating reference frame. The active and reactive components of the signal are represented by the direct and quadrature component respectively. The fundamental quantities become dc quantities. The system is very sTable since the controller deals mainly with dc-quantities. To generate the transformation

angle 'θ' required for determining the synchronous reference frame a PLL is used. This method is ideally designed for three-phase system but recently it has been implemented in single-phase systems [70-71]. A modified version of SRFT which calculate the transformation angle directly from voltage waveform without using PLL is proposed in [32]. This method is named Modified-SRFT or *id-iq* method. It has the advantage of eliminating the PLL and phase error [48-50] and therefore has gained more popularity than the conventional SRFT.

3. Instantaneous power balance theory: Instantaneous power balance method [33] is based on principle that power supplied from mains equals power demanded by load at steady state. So, mains current magnitude is determined from power balance of mains, APF and the load. The compensating signal is calculated by processing the error signal generated at time of unbalance. The component of peak of supply currents is computed using the difference of average dc-bus voltage and the reference value. The main component of peak of supply currents to feed load currents is computed using sensed load currents and supply voltages. These two components add up to give the total peak value of supply current. Three-phase instantaneous reference supply currents are obtained by multiplying this peak magnitude with unit current templates derived in phase with supply voltages. This technique is simple and easy to implement. It gives fast dynamic response if proportional and integral constants are tuned properly [31].

4. Synchronous detection method (SDM): In the synchronous detection method [34-35], the active current in the power line tracks the same wave-shape and maintains in phase with the voltage waveform. The average power is obtained by monitoring the line currents and voltage. Average power is distributed proportionately among the three phases according to their instantaneous phase voltage. Instantaneous current for the three phases are calculated using these powers. Compensating current is obtained on subtracting this current from measured current. These signals are then synchronized relative to the mains voltage. Major drawback of this method is that it is highly dependent on voltage signal harmonics.

5. Direct detection method: Direct methods are those techniques that avoid transformation to α-β co-ordinates or *d-q* frame of reference for the generation of reference signal. Instead, in these methods the reference is calculated by using the

a-b-c phase voltage and line current directly. References [36-37] uses direct method of reference generation.

6. Notch filter method: In notch filter based method the fundamental component of distorted current or voltage signals are removed by passing through a notch filter. The resultant signal is used as compensating command for reference signal [19].

7. Flux based control: The flux-based controller enables direct implementation of a current regulator without explicit generation of reference voltage [38]. In this approach, harmonic components of load current are extracted using synchronous *d-q* transformation technique and the inductor reference flux (ϕ^*) is derived from the value of this current component. The AF terminal flux (ϕ^F) is estimated by integrating measured AF terminal voltage and integrating it through a special integrator. This flux is also used as feed forward quantity in generation of inductor reference flux. The inverter flux (ϕ^{inv}) is calculated by pure integration of measured inverter three-phase output voltage. The actual inductor flux (ϕ) is given by the difference of inverter flux (ϕ^{inv}) and AF terminal flux (ϕ^F).The inverter switching logics is obtained by using the value of the deviation between the actual inductor flux (ϕ) and the reference inductor flux (ϕ^*) in the synchronously rotating frame. This technique is associated with time delay due to presence of separate current and voltage loop.

8. Fictitious power detection method: This techniques is founded upon the basis that the apparent power (S) comprises only two real orthogonal subdivided components termed as active power (P) and fictitious power (F) of which fictitious power as can be sub-divided into orthogonal components reactive power (Q) and deactive power (D), where in active power hold the usual meaning. Reactive power (Q) represents the reciprocating component that contributes no net transfer between source and load. Deactive components accounts for non-similarity and un-correlation between voltage and current waveforms [39]. Here the compensation system forms an integral part of the load connected to network. The reactive power is compensated by means of cost effective low dynamic response compensation system like capacitor bank, TCR, synchronous condenser etc. The deactive power portion is compensated by high dynamic response APFs which are

either PWM based VSI or CSI. The instantaneous representation of the deactive current is derived directly from the cross correlation between the measured system voltage and load current. The system controller generates a reference current signal, which minimizes the undesired components of the power (fictitious power). This method finds application in single-phase systems. It has a drawback of large computation requirements that need microcontroller or DSP for implementation.

9. Adaptive detection method: This is a method based on adaptive interference canceling theory. In this technique the total harmonics components and reactive components present in current is extracted by taking undistorted voltage signal as the reference and distorted current signal as the primary input. It has the ability to continuously self-study and self-adjusts from start to end in order to maintain suiTable operating state [40-41]. This system is highly robust. This method shows advantage in situations where measurement error is plausibility. But it has a drawback of implementation complexity.

10. Other techniques: There are various other control techniques, apart from those mentioned in earlier sections, in the field of APF technology. Some of the techniques not covered earlier are unity power factor method [42] employed to achieve UPF condition. This method is suiTable for combined system of current harmonic and VAR compensation. Another method proposed in [43] multiplies load current and sine wave fundamental frequency. The resultant is integrated. The real fundamental component of load is calculated from this value so obtained. APF command current is obtained by subtracting the instantaneous load current from the fundamental. This technique is known as Sine-multiplication technique. Another approach is the Delta Modulation Method [44-45] which is a variation of traditional hysteresis current regulator. Use of soft computing based techniques like Neuro Controller and Fuzzy Logic Controller are also reported [46].

2.2 DC- LINK VOLTAGE REGULATION SCHEMES

The dc-link voltage regulation refers to regulating the voltage across the dc-link capacitor of the VSI, which is being used as compensator. The dc-link capacitor plays

two important roles in APF control, first it maintains a dc voltage with small ripple in steady state and second it serves as energy balancing medium that supplies or absorbs real power at times of transient period. So the load current variation is reflected upon dc-link voltage in terms of a rise or a fall. For balanced loading this voltage should remain constant. Therefore, a preset reference value is fixed and the rise or fall is regulated in such a way that it tracks the reference. The rise or fall in value of dc-link voltage occurring due to transients or load change can be translated in terms of requirement for change i.e. requirement for increasing or decreasing the amplitude of supply current. Hence, the peak value of reference current of the system under compensation is related to value of dc-link voltage. The regulator that regulates this voltage to a fixed value, in doing so, also gives the command for calculation of peak value of reference current. PI regulator and soft computing technique based controller like Fuzzy Logic Controller are used vastly for this purpose. In regulation scheme involving PI controller [47-50], the actual capacitor voltage is compared with reference value of link voltage. The error signal is then processed through a PI controller, which contributes to zero steady error in tracking the reference current signal. The output of the PI controller is considered as peak value of the supply current. This peak current has two components fundamental active power component of load current and the component that accounts for losses in the APF to maintain the average capacitor voltage to a constant value. Regulation scheme employing fuzzy controller [47-51] also uses the error signal between actual capacitor voltage and reference voltage to compute the peak of reference signal. In a fuzzy controller, linguistic control strategies are converted to automatic control strategy. The fuzzy rules are constructed by expert knowledge. Input error and change in input error are fed as numerical input to the controller. They are then converted to linguistic variable by using predefined number of fuzzy sets or levels (a set of seven levels is commonly used). Fuzzy logic is characterized by:

- Some fuzzy sets for each input and output variables
- A particular membership function
- Implication using Mamdani-type min-operator, and
- De-fuzzification.

2.3 SWITCHING CONTROL SCHEMES

Generation of the gating signals for the solid state devices of the APF based on the derived compensating command is the final step of APF control. Gating signal can be generated either in open loop or closed loop. Popular scheme of open loop type are PWM and SPWM [52]. For closed loop schemes hysteresis control is the most widely used scheme for lower order system. For second and higher order systems sliding mode [53], linear quadratic regulator (LQR) [54], pole shift control[73], dead bead control [26], Kalman Filter [55] are used. Further, advancement in microprocessors, microcontrollers and DSP has rendered possible the implementation of complex algorithms like fuzzy logic, neural network and genetic algorithm also for improving the dynamic and steady state performance [18]. Here three most extensively used methods are discussed:

1. Carrier based PWM technique: Use of carrier base PWM switching technique has been reported in many papers including [56-62]. In this method the reference signal (i_{ref}) is compared with the actual filter current (i_f). The difference is recorded as an error (e), i.e. ($e = i_{ref} - i_f$) this error is then amplified and compared with triangular carrier wave. When e> triangular carrier wave signal the upper switch of a particular phase leg (Sa or Sb or Sc) of the VSI is turned OFF and lower switch (Sa’ or Sb’ or Sc’) is turned ON. So current in that phase decays. When e < carrier signal lower switch is turned OFF and Upper Switch is turned ON so current increases. Carrier based PWM technique has been extensively used for gating signal generation owing to its fast response, simplicity and ease in implementation.

2. Hysteresis band current control technique: Hysteresis band current control (HBCC), is the most widely used [48-50], [63-64] switching technique in APF technology. In this method the actual current is forced to follow the reference current by trapping the actual current within a certain preset limit or tolerance band, around the reference current, referred to as the Hysteresis Band (HB). When the actual current crosses or hits the upper limit of the band, the upper switch of a particular phase leg (Sa or Sb or Sc) of the VSI is turned OFF and lower switch (Sa’ or Sb’ or Sc’) is turned ON. Soc current in that phase decays until it reaches the lower limit of the HB. As it strikes lower limit of HB, lower switch is turned OFF and Upper Switch is turned ON. Further detail and generation of switching

logics are described in [64]. The major drawback of this method is that the switching frequency is not constant and its working is rough and it produces large current ripple in steady state.

3. Adaptive hysteresis band current-control technique: Adaptive Hysteresis Band Current Control Technique (Adaptive-HBCC) is an enhanced version of HBCC. Switching logic generation principle remains the same as in HBCC. The improvement here is that the band-width of the hysteresis band is made variable by modulating it as a function of dc-link voltage and slope of reference current so that switching frequency can be held nearly constant. Formulation of the adaptive-HBCC is explained in [65-69].

Simone Buso *et al* (1998) discussed the difference in the dynamic performance of the three most popular current control techniques (hysteresis control, deadbeat control and linear rotating frame control) for active filter applications. The results of the comparison show a certain superiority of the hysteresis control. Indeed, the performance of this control strategy is almost unaffected by the variation in the firing angle and, on the basis of the performance indices considered in the paper, i.e., harmonic content, THD and r.m.s. of the current error, turns out to be better than the other techniques. The deadbeat controller, which has the advantage of being suiTable for a fully digital implementation is limited in its performance by the inherent calculation delay. The linear control's bandwidth limitation turns out to be not so satisfactory in providing quality of compensation, especially in correspondence of high di/dt in the current reference.

Bhim Singh *et al* (1999) proposed active filtering of electric power for harmonic and reactive power compensation in two wire (single phase), three-wire (three phase without neutral) and four wire (three phase with neutral) ac power networks with nonlinear loads. They presented a comprehensive review of Active Filter (AF) configurations, control strategies, selection of components, other related economic and technical considerations and their selection for specific applications. It is aimed at providing a broad perspective on the status of APF technology to researchers and application engineers dealing with power quality issues**.**

Bor-Ren Lin (2002) discussed a hybrid active filter topology and its control to suppress harmonic currents from entering the power source. The adopted hybrid active filter consists of one active filter and one passive filter connected in series. By controlling the equivalent output voltage of the active filter, the harmonic currents generated by the nonlinear load are blocked and flowed into the passive filter. The power rating of the converter is reduced compared with the pure active filters to filter the harmonic currents. The harmonic current detecting approach and dc link voltage regulation were proposed to obtain equivalent voltages of the active filter.

Peng (1998) discussed three phase active power filter, where calculation of reference values of filter current is based on instantaneous real and imaginary power. Both real and imaginary powers have dc and ac components, namely instantaneous value of the conventional fundamental active current, harmonic currents caused by the ac components of the instantaneous real power, the conventional fundamental reactive current and the harmonic currents caused by the ac components of the instantaneous imaginary power. Thus, by developing a simple algorithm instantaneous reference values of the filter current based on instantaneous real and imaginary power are calculated.

Mahesh K. Mishra *et al* (2001) derived a general instantaneous vector expression for filter currents in terms of active and reactive powers. This new compensation algorithm using the generalized IRP theory demonstrated the goals of compensation successfully both for balanced and unbalanced distribution system. This new algorithm was a revolutionary step in unifying both the instantaneous symmetrical component theory and generalized IRP theory to achieve shunt compensation for a balanced and unbalanced distribution system.

Dai (2004) showed that the APF has been an effective method to mitigate harmonic currents generated by nonlinear loads as well as to compensate reactive power. In this paper, *a-b-c* reference frame based strategy was proposed for simplifying the design of the control circuit of the APF. If the active power filter is solely used for reactive power compensation, there is no need for energy storage element in the filter. However, a sizable capacitor is required for harmonic current cancellation and switching losses in the filter.

Ziari *et al* (2007) and Peng et al (1992) presented a new control strategy based on two popular strategies: Synchronous d-q reference frame method, and Synchronous current detection method which have their own advantages and disadvantages. The proposed control strategy is based on both two aforementioned strategies in order to obtain a good accuracy as well as settling the current response to steady state value very quickly.

Mahesh K. Mishra *et al* (2007) researched a novel control algorithm to compensate the unbalanced and non-linear loads under unbalanced and distorted supply voltages. The approach used the positive sequence extraction of the supply voltage along with instantaneous symmetrical component theory to provide compensation to the load.

CHAPTER 3

A DETAILED STUDY ON VARIOUS TRANSFORMATIONS AND THEIR APPLICATION IN CONTROL THEORIES

3.1 INTRODUCTION

There are many transformations applied on voltages and currents in power engineering for various applications, some of them are studied in detail in this chapter. The transformations discussed in this chapter include natural reference frame (*abc* reference frame) to *αβ0*, *dq0*and symmetrical components. Transformations to *αβ0* and *dq0* were derived primarily for analyzing the dynamic models of electrical machines. *dq0* transformation was specifically derived to develop different dynamic machine models so that the parameters of the developed models are independent of the position of rotor. Hence the *dq0* reference frame was derived in such a way that it rotates at the same speed as that of the rotor and the *dq0* frame seems stationary to the rotor, hence *dq0* reference frame is also known as synchronous reference frame. Symmetrical component transformations are used to represent a set of unbalanced voltages as balanced quantities and it was applied to analyze the abnormal conditions (faults) in power system, the analysis of abnormal conditions using symmetrical components is much simpler than analysis using natural quantities. Now these transformations are extended on to many other applications in power engineering other than the specific applications for which they were developed [17], [74-75]. This study concentrates on observing how exactly the quantities appear after the transformation and what is the variation happening when different voltage profiles are transformed. The different voltage profiles used in this study includes balanced voltages, unbalanced voltages, balanced voltages with harmonics and unbalanced voltages with harmonics. A simulation study is done in MATLAB to observe the transformed quantities while transforming these *abc* voltage profiles.

3.2 TRANSFORMATION OF VOLTAGES IN *abc* REFERENCE FRAME TO *αβ0* REFERENCE FRAME

Transformation of *abc* voltages to *αβ0* frame is known as Clarke's transformation [76]. Let us consider an arbitrary set of $3-\phi$ voltages v_a, v_b, v_c along the *abc* axes and define α and β axes in quadrature with each other as shown in Fig. 3.1.

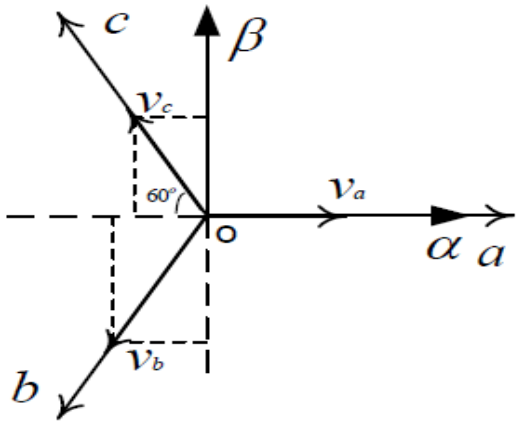

Fig. 3. 1 *abc* to *αβ0* reference frame

Resolving the *abc* voltages along α and β axes we get,

$$v_\alpha = v_a + v_b \cos 120^\circ + v_c \cos 120^\circ$$

$$v_\alpha = v_a - \frac{1}{2}v_b - \frac{1}{2}v_c$$

$$v_\beta = v_b \cos 150^\circ + v_c \cos 30^\circ$$

$$v_\beta = -\frac{\sqrt{3}}{2}v_b + \frac{\sqrt{3}}{2}v_c$$

Now we can represent the transformation in matrix form as follows,

$$\begin{bmatrix} v_\alpha \\ v_\beta \end{bmatrix} = \begin{bmatrix} 1 & -\frac{1}{2} & -\frac{1}{2} \\ 0 & -\frac{\sqrt{3}}{2} & \frac{\sqrt{3}}{2} \end{bmatrix} \begin{bmatrix} v_a \\ v_b \\ v_c \end{bmatrix} \tag{3.1}$$

Let,

$$C = \begin{bmatrix} 1 & -\frac{1}{2} & -\frac{1}{2} \\ 0 & -\frac{\sqrt{3}}{2} & \frac{\sqrt{3}}{2} \end{bmatrix}$$

While, using this transformation in power system to obtain power invariance property i.e.,

$$v_a i_a + v_b i_b + v_c i_c = v_\alpha i_\alpha + v_\beta i_\beta$$

where, *v* and *i* are voltage and current, respectively. We should multiply the transformation matrix *C* with a constant of $\sqrt{2/3}$. On observing (3.1) we understand that a transformation from *αβ0* to *abc* frame is cumbersome as matrix *C* is non invertible. Therefore we define zero sequence quantity in addition to *α* and *β* voltages which makes *C* a square matrix and let us assume all the elements of the third row is equal to K. So now we will define the new transformation matrix A,

$$\sqrt{\frac{2}{3}} \begin{bmatrix} 1 & -\frac{1}{2} & -\frac{1}{2} \\ 0 & -\frac{\sqrt{3}}{2} & \frac{\sqrt{3}}{2} \\ K & K & K \end{bmatrix} \qquad (3.2)$$

We have to choose the value of *K* in such a way that we get some advantage out of it. If we select the value of K as $1/\sqrt{2}$ we can get $A^{-1} = A^T$, which makes computations of inverse transform much easier. So, finally the transformation matrix A turns out as follows,

$$\sqrt{\frac{2}{3}} \begin{bmatrix} 1 & -\frac{1}{2} & -\frac{1}{2} \\ 0 & -\frac{\sqrt{3}}{2} & \frac{\sqrt{3}}{2} \\ \frac{1}{\sqrt{2}} & \frac{1}{\sqrt{2}} & \frac{1}{\sqrt{2}} \end{bmatrix} \qquad (3.3)$$

Therefore, *abc* to *αβ0* transformation and the inverse transformation can be concluded as shown in (3.4) and (3.5) respectively.

$$\begin{bmatrix} v_\alpha \\ v_\beta \\ v_0 \end{bmatrix} = \sqrt{\frac{2}{3}} \begin{bmatrix} 1 & -\frac{1}{2} & -\frac{1}{2} \\ 0 & -\frac{\sqrt{3}}{2} & \frac{\sqrt{3}}{2} \\ \frac{1}{\sqrt{2}} & \frac{1}{\sqrt{2}} & \frac{1}{\sqrt{2}} \end{bmatrix} \begin{bmatrix} v_a \\ v_b \\ v_c \end{bmatrix} \tag{3.4}$$

$$\begin{bmatrix} v_a \\ v_b \\ v_c \end{bmatrix} = \sqrt{\frac{2}{3}} \begin{bmatrix} 1 & 0 & \frac{1}{\sqrt{2}} \\ -\frac{1}{2} & -\frac{\sqrt{3}}{2} & \frac{1}{\sqrt{2}} \\ -\frac{1}{2} & \frac{\sqrt{3}}{2} & \frac{1}{\sqrt{2}} \end{bmatrix} \begin{bmatrix} v_\alpha \\ v_\beta \\ v_0 \end{bmatrix} \tag{3.5}$$

3.3 TRANSFORMATION OF VOLTAGES IN *αβ0* TO *dq0* REFERENCE FRAME

The *dq0* frame was first derived by R. H. Park for synchronous machine modeling known as Park's transformation [77]. To transform *αβ0* quantities to *dq0* Frame we need to define the *dq0* frame at an angle θ with respect to the *αβ0* frame as shown in the Fig. 3.2. The *dq0* frame is a rotating reference frame which rotates at the frequency of the balanced 3-ϕ quantities in natural reference frame.

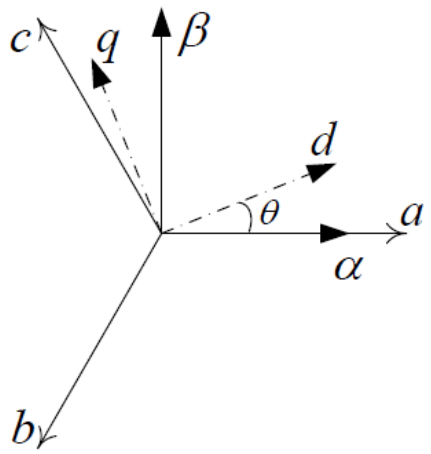

Fig. 3. 2 *αβ0* to *dq0* reference frame

Now resolving the $\alpha - \beta$ voltages along the *d*-*q* axes we get,

$$v_d = v_\alpha \cos\theta + v_\beta \cos(90^o - \theta) = v_\alpha \cos\theta + v_\beta \sin\theta$$

$$v_q = v_\alpha \cos(90^o + \theta) + v_\beta \cos\theta = -v_\alpha \sin\theta + v_\beta \cos\theta$$

Now we can represent the transformation in matrix form as follows,

$$\begin{bmatrix} v_d \\ v_q \\ v_0 \end{bmatrix} = \begin{bmatrix} \cos\theta & \sin\theta & 0 \\ -\sin\theta & \cos\theta & 0 \\ 0 & 0 & 1 \end{bmatrix} \begin{bmatrix} v_\alpha \\ v_\beta \\ v_0 \end{bmatrix} \tag{3.6}$$

So the whole transformation from natural reference frame to *dq0* reference frame can be obtained as shown in (3.7) by combining (3.4) and (3.6).

$$\begin{bmatrix} v_d \\ v_q \\ v_0 \end{bmatrix} = \sqrt{\frac{2}{3}} \begin{bmatrix} \cos\theta & \sin\theta & 0 \\ -\sin\theta & \cos\theta & 0 \\ 0 & 0 & 1 \end{bmatrix} \begin{bmatrix} 1 & -\frac{1}{2} & -\frac{1}{2} \\ 0 & -\frac{\sqrt{3}}{2} & \frac{\sqrt{3}}{2} \\ \frac{1}{\sqrt{2}} & \frac{1}{\sqrt{2}} & \frac{1}{\sqrt{2}} \end{bmatrix} \begin{bmatrix} v_a \\ v_b \\ v_c \end{bmatrix} \tag{3.7}$$

The transformation can be deducted as shown below using trigonometric simplification

$$\begin{bmatrix} v_d \\ v_q \\ v_0 \end{bmatrix} = \sqrt{\frac{2}{3}} \begin{bmatrix} \cos\theta & \cos(\theta+120^o) & \cos(\theta-120^o) \\ -\sin\theta & -\sin(\theta+120^o) & -\sin(\theta-120^o) \\ \frac{1}{\sqrt{2}} & \frac{1}{\sqrt{2}} & \frac{1}{\sqrt{2}} \end{bmatrix} \begin{bmatrix} v_a \\ v_b \\ v_c \end{bmatrix} \tag{3.8}$$

Thus, the transformation from natural reference frame to *dq0* reference in the chosen reference frame can be concluded as shown in (3.8).

3.4 INTERPRETATION OF VOLTAGES IN *αβθ* REFERENCE FRAME

We will perform an analysis on the *αβ0* frame when the *abc* reference frame quantities to be transformed are a set of balanced voltages. This analysis will help us to have an idea as of how the *abc* quantities will get transformed in the *αβ0* frame and its trace.

Consider a set of balanced 3-ϕ sinusoidal voltages as,

$$v_a = \sqrt{2}V\sin\omega t$$

$$v_b = \sqrt{2}V\sin(\omega t - 120^o)$$

$$v_c = \sqrt{2}V\sin(\omega t + 120^o)$$

Where, V is the rms value of phase voltage. The *αβ0* reference frame consists of two axes with one in quadrature with the other, so *αβ0* frame will have one component along *α*- axis (v_α) and one component along *β*-axis (v_β). We will define a quantity '$\vec{v}_{\alpha\beta}$' where,

$$\vec{v}_{\alpha\beta} = v_\alpha + jv_\beta$$

$\vec{v}_{\alpha\beta}$ can be looked upon as a position vector in the *αβ0*frame. With the help of (3.4), v_α and v_β can be obtained as follows,

$$\begin{aligned} v_\alpha &= \sqrt{\frac{2}{3}}\left[v_a - \frac{1}{2}v_b - \frac{1}{2}v_c \right] \\ &= \sqrt{\frac{2}{3}}\left[\frac{3}{2}v_a \right] \\ &= \sqrt{\frac{2}{3}}\left[\frac{3}{2}\sqrt{2}V\sin\omega t \right] \\ &= \sqrt{3}V\sin\omega t \end{aligned} \qquad (3.9)$$

$$\begin{aligned} v_\beta &= \sqrt{\frac{2}{3}}\left[-\frac{\sqrt{3}}{2}v_b + \frac{\sqrt{3}}{2}v_c \right] \\ &= -\frac{1}{\sqrt{2}}v_{bc} \\ &= -\frac{1}{\sqrt{2}}\left[\sqrt{3}v_a \angle -\pi/2 \right] \\ &= -\frac{1}{\sqrt{2}}\left[\sqrt{3}\sqrt{2}V\sin(\omega t - \pi/2) \right] \\ &= \sqrt{3}V\sin(\omega t - \pi/2) \end{aligned}$$

$$= \sqrt{3}V \cos \omega t \tag{3.10}$$

$$v_\alpha + jv_\beta = \sqrt{3}V \sin \omega t + j\sqrt{3}V \cos \omega t$$

$$= \sqrt{3}Ve^{j(\pi/2-\omega t)}$$

$$\vec{v}_{\alpha\beta} = v_\alpha + jv_\beta = \sqrt{3}Ve^{j(\pi/2-\omega t)} \tag{3.11}$$

$\vec{v}_{\alpha\beta}$ is a vector in *αβ0* frame, hence $\vec{v}_{\alpha\beta}$ gives us an acumen about the appearance of 3-ϕ voltages in *αβ0* frame. From the expression of $\vec{v}_{\alpha\beta}$ in (3.11), we understand that

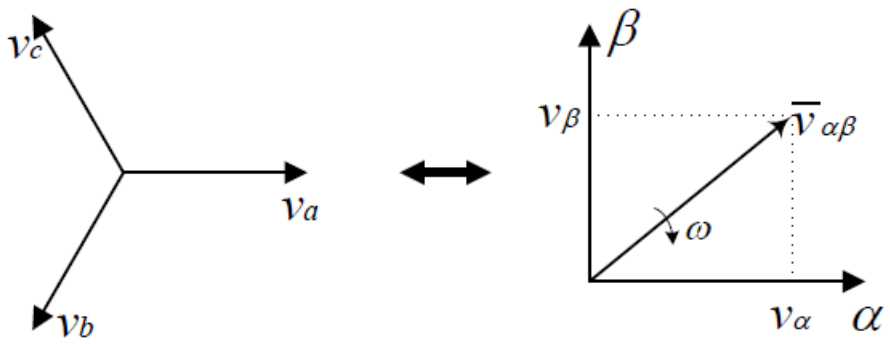

Fig. 3. 3 Appearance of *abc* quantities in *αβ0* reference frame

- 3-ϕ balanced quantities in *abc* reference frame gets transferred into a vector with a magnitude of '$\sqrt{3}V$' and rotates with a frequency 'ω' in *αβ0* reference frame.

- The sense of rotation of $\vec{v}_{\alpha\beta}$ is clockwise, as 'ωt' has a positive sense of rotation in clockwise direction. This can geometrically be interpreted as shown in Fig. 3.3.

3.5 INTERPRETATION OF VOLTAGES IN *dq0* REFERENCE FRAME

Now we will develop a relation between *dq0* frame and *αβ0* frame in such a way that we obtain a value for 'θ', which gives constant value for *d* and *q* voltages when

balanced voltages in natural reference frame are transformed. From Fig. 3.2, v_d and v_q can be written as follows,

$$v_d = v_\alpha \cos\theta + v_\beta \sin\theta$$

$$v_q = -v_\alpha \sin\theta + v_\beta \cos\theta$$

Therefore,

$$\begin{aligned} v_d + jv_q &= v_\alpha \cos\theta + v_\beta \sin\theta + j(-v_\alpha \sin\theta + v_\beta \cos\theta) \\ &= (v_\alpha + jv_\beta)\cos\theta - j(v_\alpha + jv_\beta)\sin\theta \\ &= (v_\alpha + jv_\beta)e^{-j\theta} \end{aligned} \quad (3.12)$$

Now substituting for '$v_\alpha + jv_\beta$' from (3.11) in (3.12), we get

$$\begin{aligned} v_d + jv_q &= \sqrt{3}Ve^{j(\pi/2-\omega t)}e^{-j\theta} \\ &= \sqrt{3}Ve^{j(\pi/2-\omega t-\theta)} \end{aligned} \quad (3.13)$$

We will get constant values for v_d and v_q if we get rid of the exponential term in (3.10) Therefore,

$\frac{\pi}{2} - \omega t - \theta = 0$, or

$$\theta = \frac{\pi}{2} - \omega t \quad (3.14)$$

Substituting the value 'θ' in (3.10) gives

$$v_d = \sqrt{3}V \quad (3.15)$$

$$v_q = 0 \quad (3.16)$$

The quantity along 0-axis is also zero when balanced *abc* quantities are transformed.

$$v_0 = \frac{1}{\sqrt{3}}(v_a + v_b + v_c) = 0 \quad (3.17)$$

Therefore 'θ' should be defined as ($\pi/2 - \omega t$) to obtain constant DC values along *d* and *q* axes when balanced *abc* quantities are transformed to dq0 frame, if the reference is selected as shown in Fig. 3.2. Substituting $\theta = \pi/2 - \omega t$ in (3.8) we obtain the final *abc* to *dq0* transformation as follows,

$$\begin{bmatrix} v_d \\ v_q \\ v_0 \end{bmatrix} = \sqrt{\frac{2}{3}} \begin{bmatrix} \sin\omega t & \sin(\omega t - 120^o) & \sin(\omega t + 120^o) \\ -\cos\omega t & -\cos(\omega t - 120^o) & -\cos(\omega t + 120^o) \\ \frac{1}{\sqrt{2}} & \frac{1}{\sqrt{2}} & \frac{1}{\sqrt{2}} \end{bmatrix} \begin{bmatrix} v_a \\ v_b \\ v_c \end{bmatrix} \quad (3.18)$$

3.6 ANALYSIS OF *dq0* TRANSFORMATION WITH A DIFFERENT REFERENCE FRAME

It has been seen that different reference frames have been used in various studies, so we will look at a different reference frame and perform the analysis. Consider the reference frame shown in the Fig. 3.4. On performing similar analysis shown in section 4, we get

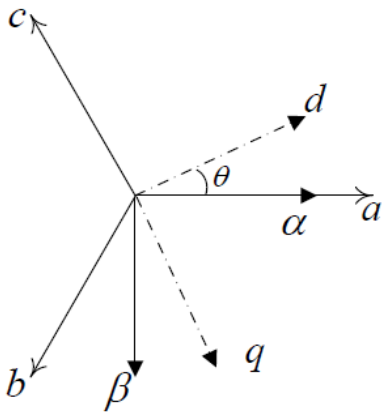

Fig. 3. 4 *abc* to $\alpha\beta 0$ reference frame

$$\vec{v}_{\alpha\beta} = v_\alpha + jv_\beta = \sqrt{3}Ve^{j(\omega t - \pi/2)}$$

On observing $\vec{v}_{\alpha\beta}$ we understand that this is a vector rotating in anticlockwise, direction, and now the positive sense of rotation of '*wt*' is clockwise. So there is shift in the rotation of $\vec{v}_{\alpha\beta}$ and positive sense of rotation of 'ωt'in the two reference frames considered in Fig. 3.2 and Fig. 3.4. Now on performing similar analysis shown in section 5 we get,

$$\begin{aligned} v_d + jv_q &= (v_\alpha + jv_\beta)e^{j\theta} \\ &= \sqrt{3}Ve^{j(\omega t - \pi/2)}e^{j\theta} \\ &= \sqrt{3}Ve^{-j(\pi/2 - \omega t - \theta)} \end{aligned}$$

Now in this reference frame also we find that on selecting $\theta = \pi/2 - \omega t$ we obtain constant DC values along *d* and *q* axes when balanced *abc* quantities are transformed to d-q frame i.e.,

$v_d = \sqrt{3}V$, $v_q = 0$

This makes it clear that we can define the reference frame by changing the alignment of *α-β* and *d-q* axis in many ways. But we should make sure that we define the value of '*θ*' in such a way that we obtain constant DC quantities along *d* and *q* axes. In the both the reference frames considered in this study it happened that $\theta = \pi/2 - \omega t$ gives us constant DC quantities along *d* and *q* axes but it not necessary that *θ* is always equal to $(\pi/2 - \omega t)$

3.7 TRANSFORMATION TO SYMMETRICAL COMPONENTS

The electrical power system operates as balanced 3-*ϕ* system but during abnormal condition (faults), this balance is broken and the result is an unbalanced system. Symmetrical components can transform the unbalanced quantities to symmetrical set of balanced phasors known as positive, negative and zero sequence components [78]. Symmetrical components reduce the complexity in solving for the electrical quantities during disturbances.

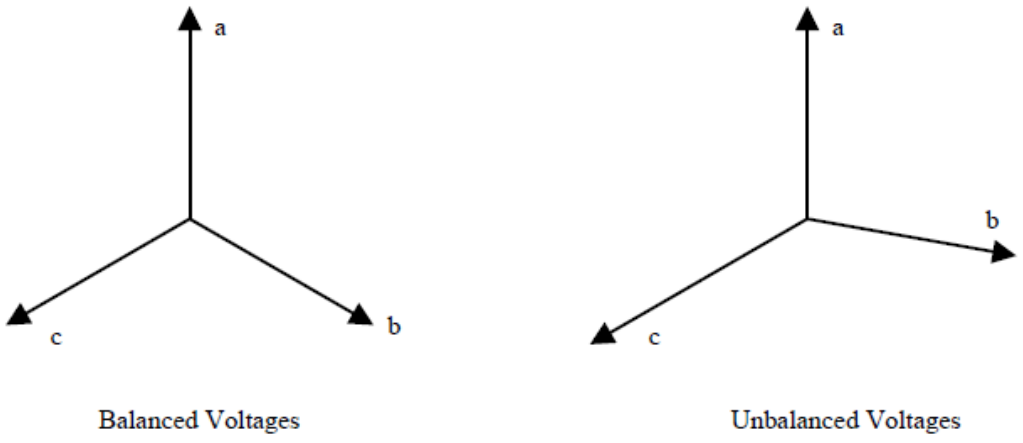

Fig. 3. 5 Balanced and unbalanced voltages

The positive sequence components can be notated as v_{a1}, v_{b1}, v_{c1}, the negative sequence components are v_{a2}, v_{b2}, v_{c2}. By the definition of symmetrical components

v_{b1} always lags v_{a1} by 120° and v_{b2} leads v_{a2} by 120°. Since the direction of rotation of v_{a1}, v_{b1}, v_{c1}, is same as that of the actual *abc* quantities they are known as positive sequence components and the direction of rotation of v_{a2}, v_{b2}, v_{c2} is opposite to that of *abc* hence they are known as negative sequence components. The rotation sequence is shown in the Fig. 3.6. For analysis we will use the voltages v_1, v_2 and v_0 as positive, negative and zero sequence respectively, these are components not specific to any phase but represents all the phases. The transformation is defined as shown in (3.19).

Positive sequence Negative sequence Zero sequence

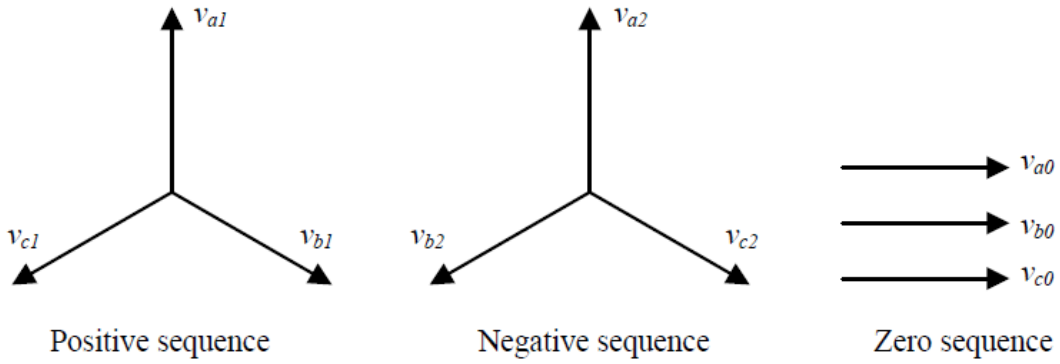

Fig. 3. 6 Symmetrical components

operator '*a*' = $1\angle 120^{o} = -\frac{1}{2} + j\frac{\sqrt{3}}{2}$

$$\begin{bmatrix} v_0 \\ v_1 \\ v_2 \end{bmatrix} = \frac{1}{\sqrt{3}} \begin{bmatrix} 1 & 1 & 1 \\ 1 & a & a^2 \\ 1 & a^2 & a \end{bmatrix} \begin{bmatrix} v_a \\ v_b \\ v_c \end{bmatrix} \tag{3.19}$$

From the transformation,

$$v_0 = \frac{1}{\sqrt{3}}(v_a + v_b + v_c) \tag{3.20}$$

and

$$v_1 = \frac{1}{\sqrt{3}}(v_a + av_b + a^2 v_c)$$

$$v_1 = \frac{1}{\sqrt{3}}\left(v_a + (-\frac{1}{2} + j\frac{\sqrt{3}}{2})v_b + (-\frac{1}{2} - j\frac{\sqrt{3}}{2})v_c\right)$$

$$v_1 = \frac{1}{\sqrt{3}}\left(v_a - \frac{1}{2}v_b - \frac{1}{2}v_c \right) + j\frac{1}{\sqrt{3}}\left(\frac{\sqrt{3}}{2}v_b - \frac{\sqrt{3}}{2}v_c \right)$$

From the definition of *α-β* transformation explained in (3.1)

$$v_1 = \frac{1}{\sqrt{2}}\left[v_\alpha - jv_\beta \right]$$

$$v_1 = \sqrt{\frac{3}{2}}V\sin\omega t - j\sqrt{\frac{3}{2}}V\cos\omega t \tag{3.21}$$

on performing similar analysis on v_2 we get,

$$v_2 = \sqrt{\frac{3}{2}}V\sin\omega t + j\sqrt{\frac{3}{2}}V\cos\omega t \tag{3.22}$$

Voltages in *abc* reference frame when subjected to symmetrical component transformation gets transformed into complex time varying quantities as shown in (2.21) and (2.22). We can plot the imaginary part Vs the real part of the symmetrical components, in this case $\sqrt{\frac{3}{2}}V\sin\omega t$ along x-axis and $\sqrt{\frac{3}{2}}V\cos\omega t$ along y-axis

$$x^2 + y^2 = \left(\sqrt{\frac{3}{2}}V\sin\omega t \right)^2 + \left(\sqrt{\frac{3}{2}}V\cos\omega t \right)^2 = (\sqrt{\frac{3}{2}}V)^2 \tag{3.22}$$

From (2.23) we can understand that the plot will be a circle with center at origin and radius $\sqrt{\frac{3}{2}}V$.

3.8 SIMULATION STUDIES

Simulations of these transformations are done in MATLAB. Simulations are done using various voltage profiles and the corresponding transformed voltages are observed. The various voltage profiles considered in this study includes balanced, unbalanced, balanced with harmonics, unbalanced with harmonics. The transformation used in (3.4) is used for *abc* to *αβ0* transformation and the transformation shown in (3.18) is made used for *abc* to *dq0* transformation.

3.8.1 Transformed Voltages, when Transformations are Applied to Balanced *abc* Voltages

In this section the transformed voltages are observed when a set of balanced voltages in *abc* reference frame are transformed. The balanced voltages selected are as shown below

$$v_a = 100\sin\omega t$$

$$v_b = 100\sin(\omega t - 120^o)$$

$$v_c = 100\sin(\omega t + 120^o)$$

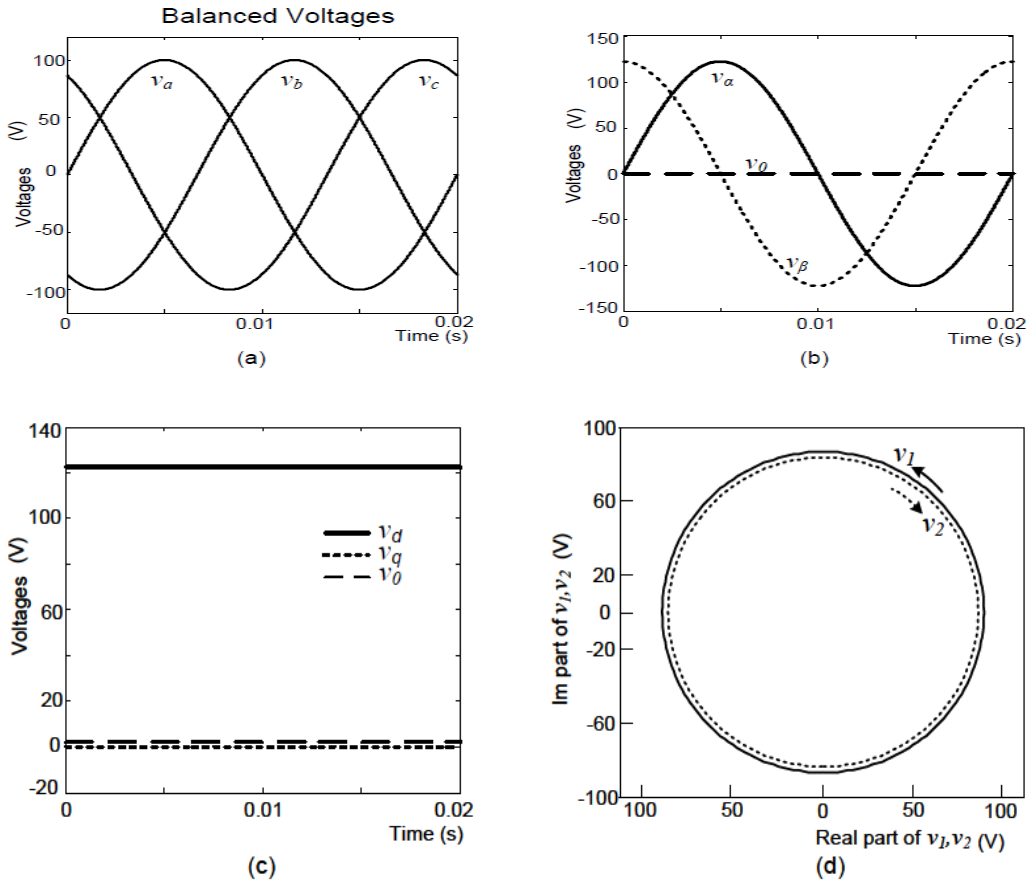

Fig. 3. 7 (a) Balanced voltages (b) *αβ0* voltages (c) *dq0* voltages (d) Loci of symmetrical components

and Fig. 3.7(a) shows its plot, frequency is chosen as 50Hz. Fig. 3.7(b), 3.7(c)and 3.7(d) shows the *αβ0* quantities, *dqo* quantities and loci of symmetrical components respectively, for selected voltages $v_\alpha = 122.47\sin\omega t$ and $v_\beta = 122.47\cos\omega t$ as per (3.11) and $v_d = 122.47V$, $v_q = v_0 = 0V$ as per (3.12).

It can be observed that the calculated values of the transformed quantities are matching with values obtained by performing the simulation. The loci of the symmetrical components turn out to be a circle when a set of balanced voltages are used for transformation. The loci of symmetrical components v_1 and v_2 has overlapped in this case but the direction is opposite to each other i.e, v_1 traces in the clockwise direction and v_2 traces in anti- clockwise direction.

3.8.2 Transformed Voltages, when Transformation is Applied to Unbalanced *abc* quantities

In this section the transformed quantities are observed when a set of unbalanced voltages in *abc* reference frame are transformed. The unbalanced voltages selected are as shown below and Fig. 3.8(a) shows its plot. (The phase shifts are shown in radians, frequency is selected as 50Hz).

$$v_a = 80\sin\omega t$$
$$v_b = 100\sin(\omega t - 0.5)$$
$$v_c = 50\sin(\omega t + 120^o)$$

Fig. 3.8(b), 3.8(c) and 3.8(d) shows the *αβ0* quantities, *dq0* quantities and loci of symmetrical components, respectively. It can be observed that the *α-β* voltages now has different magnitudes and *d, q* voltages oscillates at double the frequency of the *abc* quantities, with a non zero average. Average value of v_d = 41.05 V, Average value of v_q= -22.67 V. The *0*-quantity oscillates with the same frequency as that of *abc* quantities with a zero average. The loci of symmetrical components form two ellipses but do not overlap which reflects the unbalance.

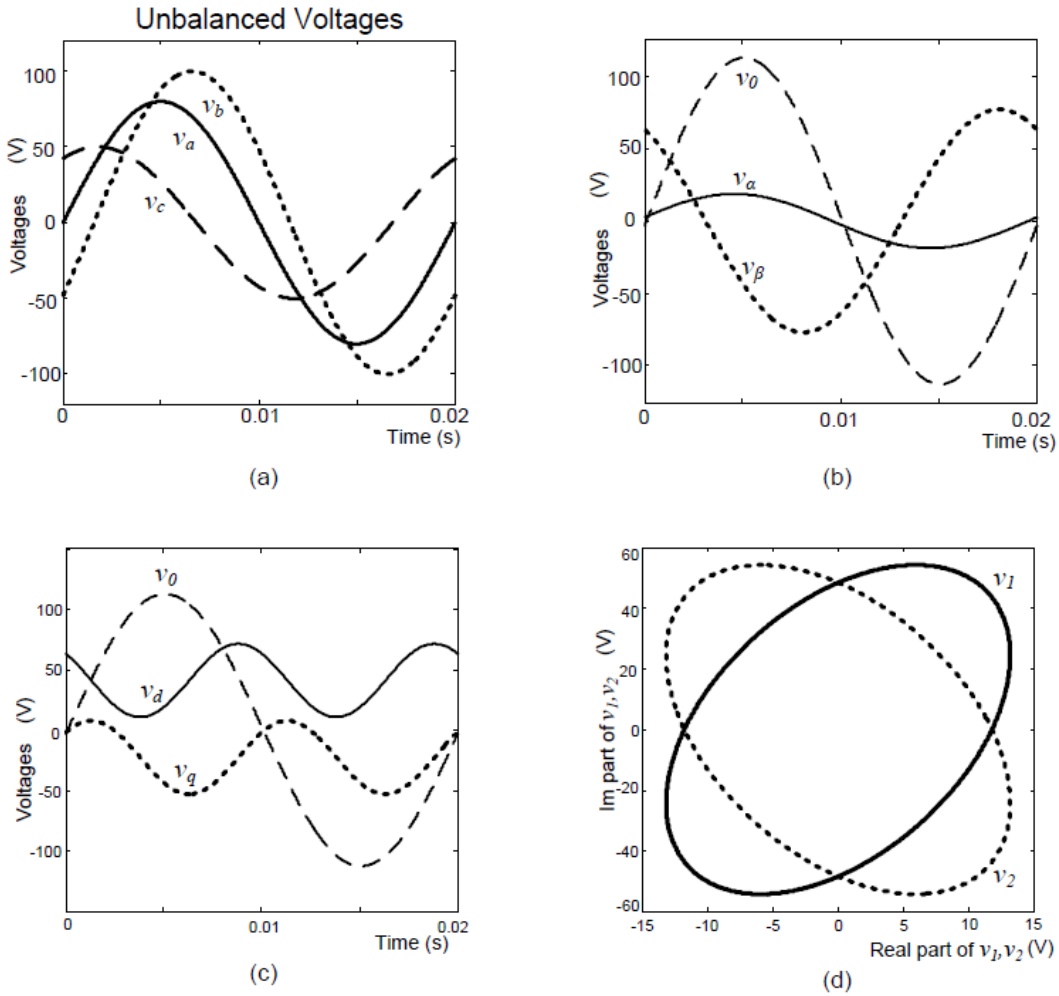

Fig. 3. 8 (a) Balanced voltages (b) *αβ0* voltages (c) *dq0* voltages (d) Loci of symmetrical components

3.8.3 Transformed Quantities, when Transformation is Applied to Balanced *abc* voltages with Harmonics

This section observes the different transformed quantities when transformations are applied to a set of balanced voltages with harmonics. The voltage profile in Fig. 3.9(a) is being transformed and the Fig. 3.9(b), 3.9(c) and 3.9(d) shows the $\alpha\beta 0$ quantities, *dq0* quantities and loci of symmetrical components respectively. It is observed that the *dq0* voltages have now become oscillatory but when the system is balanced the *q*-voltage has a zero average. Harmonics are introduced into $\alpha - \beta$ voltages. Loci of symmetrical components are no more a circle but the loci of positive and negative sequence overlaps each other even though they trace in opposite directions.

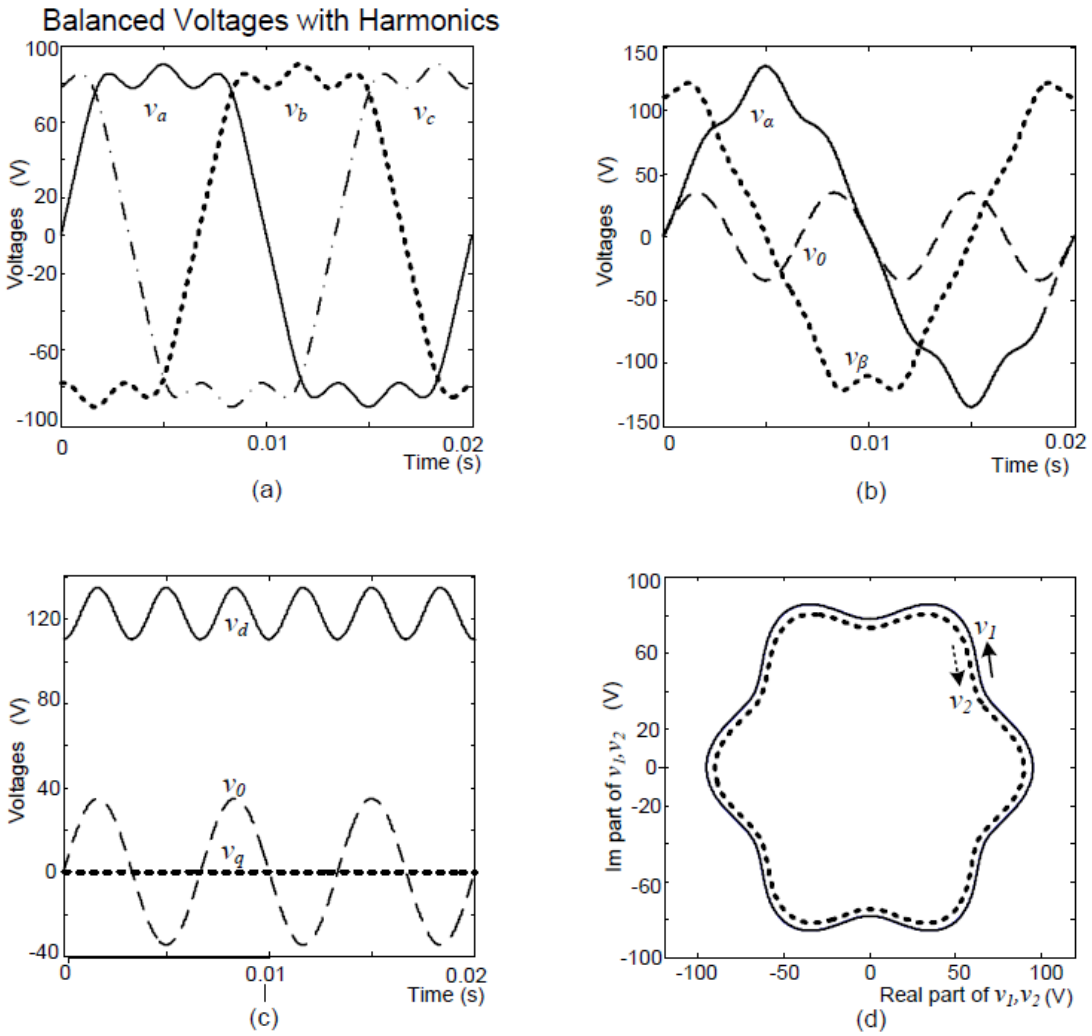

Fig. 3. 9 (a) Balanced voltage with harmonics (b) $\alpha\beta 0$ voltages (c) *dq0* voltages (d) loci of symmetrical components

3.8.4 Transformed Quantities, when Transformation is Applied to Unbalanced *abc* voltages with Harmonics

This section observes the different transformed quantities when transformations are applied to a set of unbalanced voltages with harmonics. The voltage profile in Fig. 3.10(a) has been transformed and the Fig. 3.10(b), 3.10(c) and 3.10(d) shows the *αβ0* quantities, *dqo* quantities and loci of symmetrical components respectively, it is observed that harmonics are introduced into all the transformed voltages.

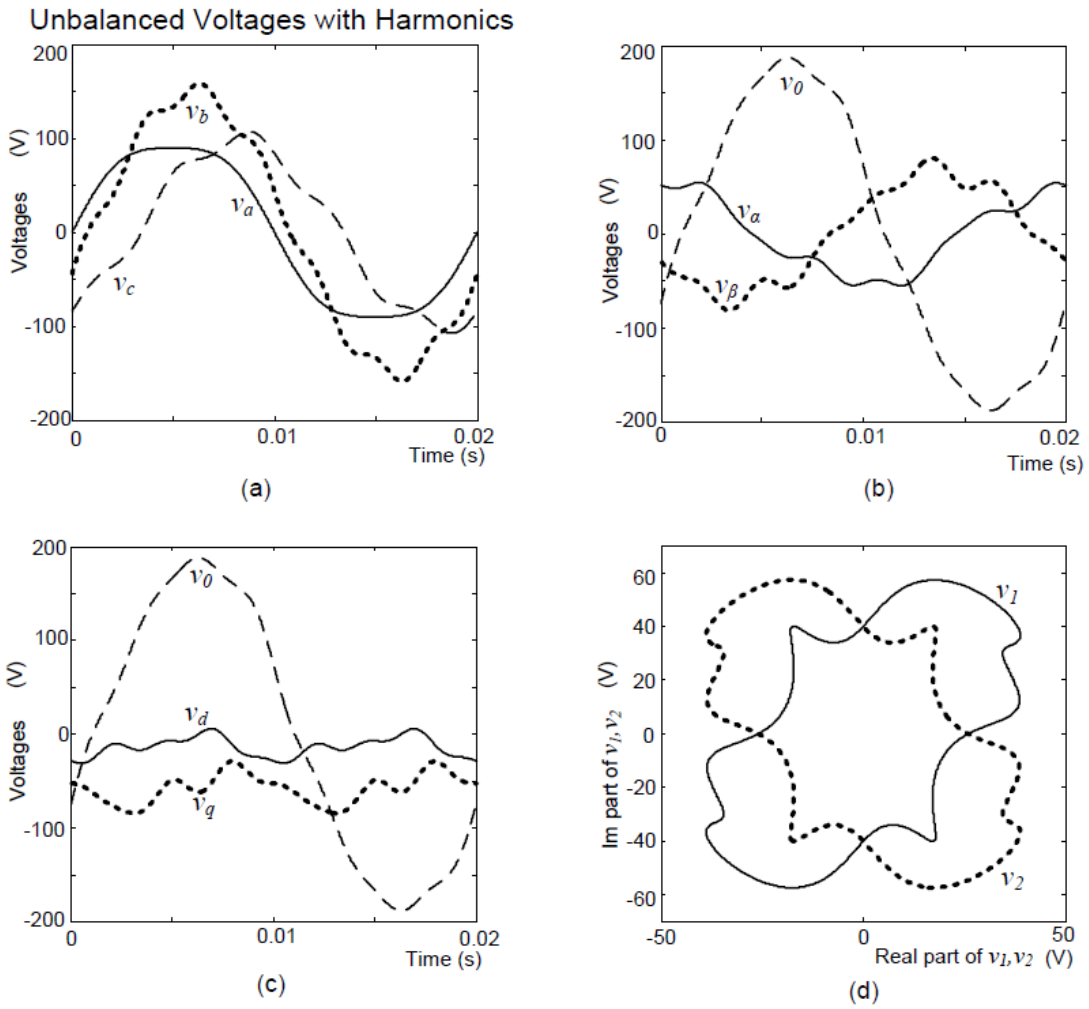

Fig. 3. 10 (a) Unbalanced voltage with harmonics (b) *αβ0* voltages (c) *dq0* voltages (d) loci of symmetrical components

3.9 APPLICATION OF TRANSFORMATIONS IN CONTROL THEORIES

This section describes one of the important application area of these transformation, when comes to implement APFs. The APF are widely in use to mitigate power quality problems uses the power control theories to derive reference currents (ideal current) needed for mitigating/compensating the load. Some of the commonly used power control theories are discussed in brief to explain the use of these transformations.

3.9.1 Application of *αβ0* Transformation in Instantaneous Reactive Power (IRP) Theory

The *pq* theory, not only aims to compensate the fundamental reactive power but also the harmonic currents in the load. Ideally, the compensation based on *pq* theory can eliminate all unbalances and harmonics caused by unbalanced non-linear loads

provided source voltages are balanced sinusoidal and the power converter has infinite bandwidth to track the reference filter currents. The *pq* theory makes use of *αβ0* transformation discussed above.

Using *αβ0* transformation, the instantaneous supply voltages and load currents in natural *abc* coordinates are transformed into mutually orthogonal *αβ0* coordinates as follows,

$$\begin{bmatrix} v_o \\ v_\alpha \\ v_\beta \end{bmatrix} = \sqrt{\frac{2}{3}} \begin{bmatrix} \frac{1}{\sqrt{2}} & \frac{1}{\sqrt{2}} & \frac{1}{\sqrt{2}} \\ 1 & -\frac{1}{2} & -\frac{1}{2} \\ 0 & \frac{\sqrt{3}}{2} & -\frac{\sqrt{3}}{2} \end{bmatrix} \begin{bmatrix} v_{sa} \\ v_{sb} \\ v_{sc} \end{bmatrix}. \tag{3.23}$$

Similarly, current components i_α, i_β and i_0 can be found out. Let the instantaneous real, reactive and zero sequence powers are denoted by p, q and p_o respectively. These are expressed as,

$$\begin{bmatrix} p \\ q \end{bmatrix} = \begin{bmatrix} v_\alpha & v_\beta \\ -v_\beta & v_\alpha \end{bmatrix} \begin{bmatrix} i_\alpha \\ i_\beta \end{bmatrix}. \tag{3.24}$$

where, three-phase instantaneous power ($p_{3\phi}$) has following relationship with the terms *p* and p_o.

$$\begin{aligned} p_{3\phi} &= v_{sa} i_a + v_{sb} i_b + v_{sc} i_c \\ &= \underbrace{v_\alpha i_\alpha + v_\beta i_\beta}_{p} + \underbrace{v_0 i_0}_{p_0} \end{aligned} \tag{3.25}$$

The instantaneous active and reactive power has two parts: a DC or average value indicated by an overbar (–) and an alternating component indicated by an over tilde (~). Thus, the following can be written as

$$p = \bar{p} + \tilde{p}, \; p_o = \bar{p}_0 + \tilde{p}_o \text{ and } q = \bar{q} + \tilde{q} \tag{3.26}$$

The load powers that can be compensated in terms of *αβ0* coordinates are $\tilde{p}_l, \bar{q}_l, \tilde{q}_l$. Let us assume that the compensator supplies a reactive power q_f, which may be equal to load reactive power. Thus,

$$q_f = q_l. \tag{3.27}$$

Similarly, instantaneous active power supplied by the compensator to the load

$$p_f = \tilde{p}_l + \overline{p}_o . \tag{3.28}$$

The reference currents of the compensator using (3.24) are given as

$$\begin{bmatrix} i_{f\alpha\,ref} \\ i_{f\beta\,ref} \end{bmatrix} = \frac{1}{v_\alpha^2 + v_\beta^2} \begin{bmatrix} v_\alpha & -v_\beta \\ v_\beta & v_\alpha \end{bmatrix} \begin{bmatrix} p_f \\ q_f \end{bmatrix}. \tag{3.29}$$

Substituting filter powers q_f and p_f from (3.27) and (3.28), we get reference filter currents in *αβ0* frame as

$$\begin{bmatrix} i_{f\alpha\,ref} \\ i_{f\beta\,ref} \end{bmatrix} = \frac{1}{v_\alpha^2 + v_\beta^2} \begin{bmatrix} v_\alpha & -v_\beta \\ v_\beta & v_\alpha \end{bmatrix} \begin{bmatrix} \tilde{p}_l + \overline{p}_o \\ q_l \end{bmatrix}. \tag{3.30}$$

The filter reference currents in *abc* phase system can be obtained using inverse *αβ0* transformation as given in the following.

$$\begin{bmatrix} i_{fa\,ref} \\ i_{fb\,ref} \\ i_{fc\,ref} \end{bmatrix} = \sqrt{\frac{2}{3}} \begin{bmatrix} 1/\sqrt{2} & 1 & 0 \\ 1/\sqrt{2} & -1/2 & \sqrt{3}/2 \\ 1/\sqrt{2} & -1/2 & -\sqrt{3}/2 \end{bmatrix} \begin{bmatrix} i_{fo} \\ i_{f\alpha\,ref} \\ i_{f\beta\,ref} \end{bmatrix} \tag{3.31}$$

where $i_{fo}(=i_{lo})$ is the zero sequence load current and is given by

$$i_{lo} = \frac{1}{\sqrt{3}}(i_{la} + i_{lb} + i_{lc}) \tag{3.32}$$

3.9.2 Application of Instantaneous Symmetrical Components (ISC) Theory

The ISC theory can fulfill three fold objectives of load balancing, harmonic suppression, and power factor correction. The control algorithm based on ISC theory can practically compensate any kind of unbalance and harmonics in the load. For any set of three-phase instantaneous currents or voltages, the instantaneous symmetrical components are defined by following transform

$$\begin{bmatrix} i_a^0 \\ i_a^+ \\ i_a^- \end{bmatrix} = \frac{1}{3} \begin{bmatrix} 1 & 1 & 1 \\ 1 & a & a^2 \\ 1 & a^2 & a \end{bmatrix} \begin{bmatrix} i_a \\ i_b \\ i_c \end{bmatrix} \tag{3.33}$$

$$\begin{bmatrix} v_{sa}^{0} \\ v_{sa}^{+} \\ v_{sa}^{-} \end{bmatrix} = \frac{1}{3}\begin{bmatrix} 1 & 1 & 1 \\ 1 & a & a^2 \\ 1 & a^2 & a \end{bmatrix}\begin{bmatrix} v_{sa} \\ v_{sb} \\ v_{sc} \end{bmatrix} \tag{3.34}$$

where $a = e^{j120^{\circ}}$.

The following objectives should be fulfilled in load compensation.

Objective 1: The sum of the source currents after compensation should be zero, i.e.

$$i_{sa} + i_{sb} + i_{sc} = 0 \tag{3.35}$$

Objective 2: There should be control over power factor angle (ϕ^{+}), which is the angle between the positive sequence voltage ($\boldsymbol{v}_{sa}^{+}$) and current ($\boldsymbol{i}_{sa}^{+}$). Thus,

$$\angle\{v_{sa} + av_{sb} + a^2 v_{sc}\} = \angle\{i_{sa} + ai_{sb} + a^2 i_{sc}\} + \phi^{+} \tag{3.36}$$

Objective 3: The source should supply the average value of the load power, P_{lav}, i.e.

$$v_{sa}i_{sa} + v_{sb}i_{sb} + v_{sc}i_{sc} = P_{lav} \tag{3.37}$$

From Fig. (3.11), applying KCL at PCC and assuming balanced supply voltages, the reference compensator currents ($i_{fa\,ref}$, $i_{fb\,ref}$ and $i_{fc\,ref}$) are given as

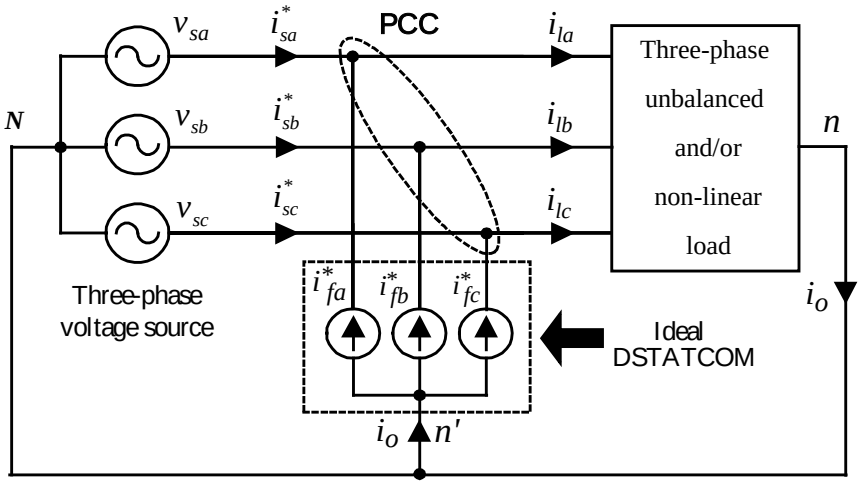

Fig. 3. 11 Schematic diagram of a DSTATCOM based three-phase four-wire compensated system

$$\left.\begin{aligned} i_{fa\,ref} &= i_{la} - i_{sa} = i_{la} - \frac{v_{sa} + \gamma\left(v_{sb} - v_{sc}\right)}{\Delta} P_{lav} \\ i_{fb\,ref} &= i_{lb} - i_{sb} = i_{lb} - \frac{v_{sb} + \gamma\left(v_{sc} - v_{sa}\right)}{\Delta} P_{lav} \\ i_{fc\,ref} &= i_{lc} - i_{sc} = i_{lc} - \frac{v_{sc} + \gamma\left(v_{sa} - v_{sb}\right)}{\Delta} P_{lav} \end{aligned}\right\} \quad (3.38)$$

where $\Delta = \sum_{j=a,b,c} v_{sj}^2 - 3v_{s0}^2$ and $\gamma = \tan\varphi^+ / \sqrt{3}$.

It can be observed that this scheme is computationally much simpler than *pq* theory as it does not require complex transformation of currents and voltages and many definitions of various powers. This scheme provides a direct and comprehensive method of obtaining balanced sinusoids and unity power factor source currents for all kinds of loads. Further, it can generate the source currents at any desired power factor angle. This algorithm was modified with positive sequence extraction in order to provide proper compensation under unbalanced supply voltage conditions [79]

3.9.3 Application of *dq0* Transformation in Synchronous Reference Frame (SRF) Theory

The calculation of reference filter currents using SRF theory is straight forward,

which involves direct *dq0* transformation from *abc* coordinates system and dealing with only DC quantities in *dq0* frame. However, the *dq0* transformation output signal depends on the performance of the phase locked loop (PLL). The PLL circuit provides the rotational speed (rad/sec) of the rotating reference frame, where ' ωt ' is set as fundamental frequency component. Depending on the fundamental, harmonics and negative sequence component in three phase load currents, the corresponding *dq* components can have different frequencies. The analysis of the *dq* components and appropriate filtering can support the generation of the reference filter currents as required by the control. The *dq* component consists of DC and AC components as given below.

$$i_{ld} = \overline{i}_{ld} + \tilde{i}_{ld} \quad (3.39)$$

$$i_{lq} = \overline{i}_{lq} + \tilde{i}_{lq}\,. \quad (3.40)$$

The DC components $\bar{i}_{ld}$ and $\bar{i}_{lq}$ correspond to the fundamental positive sequence load current and the AC components $\tilde{i}_{ld}$ and $\tilde{i}_{lq}$ correspond to the load current harmonics. Component $\bar{i}_{lq}$ corresponds to the reactive power drawn by the load. The reference for the compensator is decided based on the following conditions.

$$\begin{aligned} i^*_{fd} &= \tilde{i}_{ld} \\ i^*_{fq} &= \bar{i}_{lq} + \tilde{i}_{lq} \\ i^*_{f0} &= i_{l0} \end{aligned} \qquad (3.41)$$

Finally, the compensator references in *abc* reference frame are obtained using inverse *dq0* transformation.

3.10 SUMMARY

With *αβ0* transformation the balanced 3-ϕ *abc* voltages get transformed on to a rotating position vector $V_{\alpha\beta}$ consisting of real and imaginary part. The real part corresponds to voltage along α -axis and imaginary part corresponds to voltage along β -axis. The voltages v_α and v_β turns out to be sinusoidal quantities when balanced voltages are transformed. With the help of simulation the transformation is extended to other voltage profiles. Then from *αβ0* frame, *dq0* reference frame is derived and the corresponding *dq0* voltages are obtained. It is observed that the balanced sinusoidal quantities transformed to DC voltages in *dq0* reference frame. There can be different reference frame depending upon the alignment of *d-q* and *α-β* axes. But by defining proper value for 'θ' we can end up getting DC along d and q axes which is the ultimate goal of *dq0* transformation. Towards the end of the chapter loci are obtained for various voltage profiles. If the loci of positive and negative sequence components overlap it indicates a balance in the system and if it doesn't overlap then it symbolizes an unbalance condition. If the system is devoid of harmonics then the loci will either be an ellipse or a circle but if harmonics are present then the loci will be a distorted version of ellipse or circle. In the end application of these transformations to develop control theories required for reference current generation of a Shunt APF is discussed.

CHAPTER 4

GENERALIZATION OF *αβ0* and *dq0* TRANSFORMATIONS

4.1 INTRODUCTION

It has been observed that different reference frames are chosen while transforming *abc* quantities to *αβ0* and *dq0* reference frames. There happens to be different reference frames existing, depending upon the orientation of the axes. There will be a change in the transformation matrix depending upon how you choose your axes orientation that makes it necessary to perform an analysis on the reference frame and find out the transformation matrix corresponding to the selected reference frame. In this chapter generalized transformation for transforming *abc* quantities to *αβ0* and dq0 frames are discussed.

4.2 DIFFERENT REFERENCE FRAMES; *abc* TO *αβ0* TRANSFORMATION

In this section we will consider different *αβ0* reference frames and derive the corresponding transformation matrices. From these matrices we can obtain a generalized matrix which can generate transformation corresponding to all these reference frames. Let us assume that the quantity being transformed is voltage.

4.2.1 *αβ0* Reference Frame -1

αβ0 reference frame-1 is shown in Fig. 4.1(a). Reference frame shown in Fig. 4.1(b) is a mirror image of frame shown in Fig.4.1(a), when the mirror is aligned along the *αβ0* axis. Resolving the *abc* voltages along the *αβ0* axes will result in the transformation matrix as shown in (4.1).

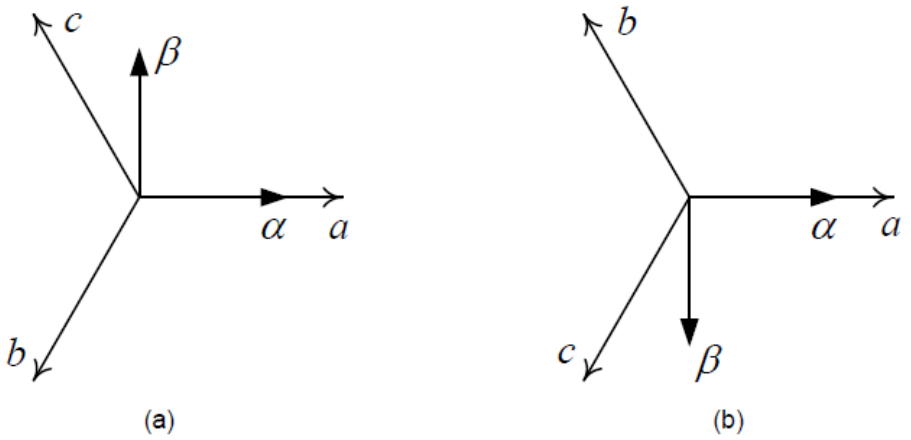

Fig. 4. 1 (a) $\alpha\beta 0$ reference frame-1 (b) Mirror image of $\alpha\beta 0$ reference frame-1

$$v_\alpha = v_a + v_b \cos 120^\circ + v_c \cos 120^\circ$$

$$v_\alpha = v_a - \frac{1}{2}v_b - \frac{1}{2}v_c$$

$$v_\beta = v_b \cos 150^\circ + v_c \cos 30^\circ$$

$$v_\beta = -\frac{\sqrt{3}}{2}v_b + \frac{\sqrt{3}}{2}v_c$$

$$\begin{bmatrix} v_\alpha \\ v_\beta \\ v_0 \end{bmatrix} = \sqrt{\frac{2}{3}} \begin{bmatrix} 1 & -\frac{1}{2} & -\frac{1}{2} \\ 0 & -\frac{\sqrt{3}}{2} & \frac{\sqrt{3}}{2} \\ \frac{1}{\sqrt{2}} & \frac{1}{\sqrt{2}} & \frac{1}{\sqrt{2}} \end{bmatrix} \begin{bmatrix} v_a \\ v_b \\ v_c \end{bmatrix} \tag{4.1}$$

With the help of (4.1), v_α and v_β can be obtained as follows,

$$\begin{aligned} v_\alpha &= \sqrt{\frac{2}{3}}\left[v_a - \frac{1}{2}v_b - \frac{1}{2}v_c \right] \\ &= \sqrt{\frac{2}{3}}\left[\frac{3}{2}v_a \right] \\ &= \sqrt{\frac{2}{3}}\left[\frac{3}{2}\sqrt{2}V \sin \omega t \right] \\ &= \sqrt{3}V \sin \omega t \end{aligned} \tag{4.2}$$

$$v_\beta = \sqrt{\frac{2}{3}}\left[-\frac{\sqrt{3}}{2}v_b + \frac{\sqrt{3}}{2}v_c\right] \tag{4.3}$$

$$= -\frac{1}{\sqrt{2}}v_{bc}$$

$$= -\frac{1}{\sqrt{2}}\left[\sqrt{3}v_a \angle -\pi/2\right]$$

$$= -\frac{1}{\sqrt{2}}\left[\sqrt{3}\sqrt{2}V\sin(\omega t - \pi/2)\right]$$

$$= \sqrt{3}V\sin(\omega t - \pi/2)$$

$$= \sqrt{3}V\cos(\omega t) \tag{4.4}$$

While transforming the *abc* voltages to *αβ0* voltages considering reference frame shown in Fig. 4.1(b), it can be observed that it will result in same transformation shown in (4.1). These reference frames which are mirror images of each other will result in same transformations and they are termed as mirrors of each. Hence we will term the reference frame shown in Fig. 4.1(b) as the mirror of Fig. 4.1(a).

4.2.2 *αβ0* Reference Frame -2

αβ0 Reference Frame-2 is shown in Fig. 4.2(a) and its mirror is shown in Fig. 4.2(b). The transformation matrix for these reference frames can be can be obtained by resolving the *abc* along *α-β* axes as given in (4.5)

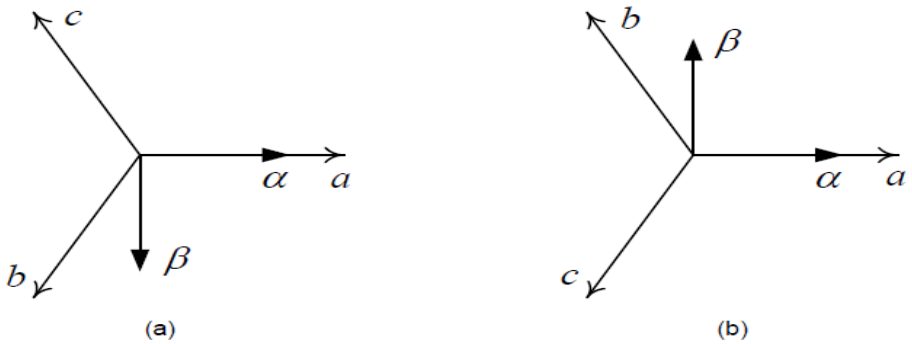

Fig. 4. 2 (a) $\alpha\beta 0$ reference frame-2 (b) Mirror image of *αβ0* reference frame-2

$$\begin{bmatrix} v_\alpha \\ v_\beta \\ v_0 \end{bmatrix} = \sqrt{\frac{2}{3}} \begin{bmatrix} 1 & -\frac{1}{2} & -\frac{1}{2} \\ 0 & \frac{\sqrt{3}}{2} & -\frac{\sqrt{3}}{2} \\ \frac{1}{\sqrt{2}} & \frac{1}{\sqrt{2}} & \frac{1}{\sqrt{2}} \end{bmatrix} \begin{bmatrix} v_a \\ v_b \\ v_c \end{bmatrix} \tag{4.5}$$

4.3 DIFFERENT REFERENCE FRAMES; *abc* TO *dq0* TRANSFORMATION

We have different *dq0* reference frames available depending on the orientation of *dq0* axes with respect to the *abc* and *α-β* axes. We will consider four different reference frames and derive a generalized transformation matrix for the all the frames.

4.3.1 *dq0* Reference Frame - 1

dq0 reference frame -1 is shown in Fig. 4.3(a). The *abc* to *αβ0* transformation is same

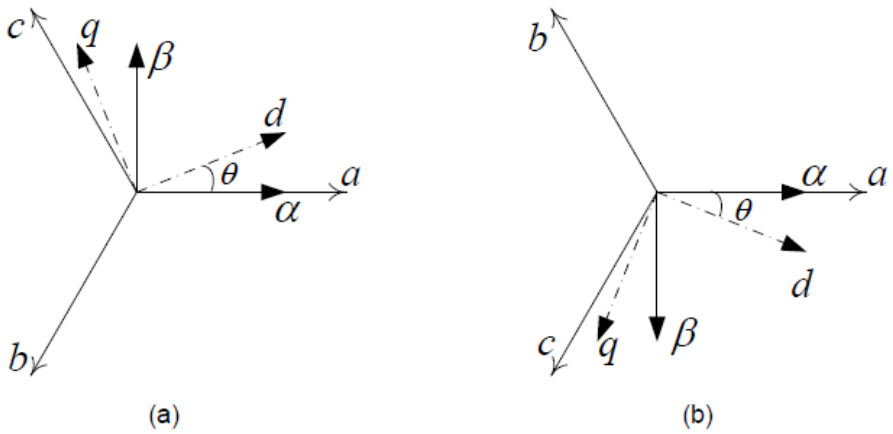

Fig. 4. 3 (a) *dq0* reference frame-1 (b) mirror image of *dq0* reference frame-1

as what is shown in (4.1). The transformation from *αβ0* frame to *dq0* can be found out as follows.

$$v_d = v_\alpha \cos\theta + v_\beta \cos(90^o - \theta) = v_\alpha \cos\theta + v_\beta \sin\theta$$

$$v_q = v_\alpha \cos(90^o + \theta) + v_\beta \cos\theta = -v_\alpha \sin\theta + v_\beta \cos\theta$$

Now we can represent the transformation in matrix form as follows,

$$\begin{bmatrix} v_d \\ v_q \\ v_0 \end{bmatrix} = \begin{bmatrix} \cos\theta & \sin\theta & 0 \\ -\sin\theta & \cos\theta & 0 \\ 0 & 0 & 1 \end{bmatrix} \begin{bmatrix} v_\alpha \\ v_\beta \\ v_0 \end{bmatrix} \tag{4.6}$$

So the whole transformation from natural reference frame to *dq0* reference frame can be obtained as shown in (4.7) by combining (4.1) and (4.6).

$$\begin{bmatrix} v_d \\ v_q \\ v_0 \end{bmatrix} = \sqrt{\frac{2}{3}} \begin{bmatrix} \cos\theta & \sin\theta & 0 \\ -\sin\theta & \cos\theta & 0 \\ 0 & 0 & 1 \end{bmatrix} \begin{bmatrix} 1 & -\frac{1}{2} & -\frac{1}{2} \\ 0 & -\frac{\sqrt{3}}{2} & \frac{\sqrt{3}}{2} \\ \frac{1}{\sqrt{2}} & \frac{1}{\sqrt{2}} & \frac{1}{\sqrt{2}} \end{bmatrix} \begin{bmatrix} v_a \\ v_b \\ v_c \end{bmatrix} \tag{4.7}$$

The transformation can be deducted as shown below using trigonometric simplification.

$$\begin{bmatrix} v_d \\ v_q \\ v_0 \end{bmatrix} = \sqrt{\frac{2}{3}} \begin{bmatrix} \cos\theta & \cos(\theta+\frac{2\pi}{3}) & \cos(\theta-\frac{2\pi}{3}) \\ -\sin\theta & -\sin(\theta+\frac{2\pi}{3}) & -\sin(\theta-\frac{2\pi}{3}) \\ \frac{1}{\sqrt{2}} & \frac{1}{\sqrt{2}} & \frac{1}{\sqrt{2}} \end{bmatrix} \begin{bmatrix} v_a \\ v_b \\ v_c \end{bmatrix} \tag{4.8}$$

We have to obtain a value for θ, which gives constant value for *d* and *q* voltages when balanced voltages in natural reference frame are transformed in these reference frames. The value of θ can be derived as follows,

$$v_d = v_\alpha \cos\theta + v_\beta \sin\theta$$

$$v_q = -v_\alpha \sin\theta + v_\beta \cos\theta$$

Therefore,

$$\begin{aligned} v_d + jv_q &= v_\alpha \cos\theta + v_\beta \sin\theta + j(-v_\alpha \sin\theta + v_\beta \cos\theta) \\ &= (v_\alpha + jv_\beta)\cos\theta - j(v_\alpha + jv_\beta)\sin\theta \\ &= (v_\alpha + jv_\beta)e^{-j\theta} \end{aligned} \tag{4.9}$$

Now substituting for ‘ $v_\alpha + jv_\beta$ ’ from (4.2) in (4.3), we get

$$v_d + jv_q = \sqrt{3}Ve^{j(\pi/2-\omega t)}e^{-j\theta}$$

$$= \sqrt{3}Ve^{j(\pi/2-\omega t-\theta)} \tag{4.10}$$

We will get constant values for v_d and v_q if we get rid of the exponential term in (4.10) Therefore,

$\frac{\pi}{2} - \omega t - \theta = 0$, or

$$\theta = \frac{\pi}{2} - \omega t \tag{4.11}$$

Assuming v_a, v_b, v_c to be balanced voltages i.e.,

$$v_a = \sqrt{2}V \sin \omega t$$

$$v_b = \sqrt{2}V \sin(\omega t - 120^o)$$

$$v_c = \sqrt{2}V \sin(\omega t + 120^o)$$

and substituting the value 'θ' in (4.10) gives

$$v_d = \sqrt{3}V \tag{4.12}$$

$$v_q = 0 \tag{4.13}$$

The frame shown in Fig. 4.3(b) is the mirror of frame shown in Fig. 4.3(a) in terms of *dq0* transformation. By performing similar analysis on the reference frame shown Fig. 4.3(b), it is understood that the transformation is same as that shown in (4.8). The final transformation matrix for both the frames can be obtained by substituting $\theta = \pi/2 - \omega t$ in (4.8) and it is as shown below,

$$\begin{bmatrix} v_d \\ v_q \\ v_0 \end{bmatrix} = \sqrt{\frac{2}{3}} \begin{bmatrix} \sin \omega t & \sin(\omega t - 120^o) & \sin(\omega t + 120^o) \\ -\cos \omega t & -\cos(\omega t - 120^o) & -\cos(\omega t + 120^o) \\ \frac{1}{\sqrt{2}} & \frac{1}{\sqrt{2}} & \frac{1}{\sqrt{2}} \end{bmatrix} \begin{bmatrix} v_a \\ v_b \\ v_c \end{bmatrix} \tag{4.14}$$

4.3.2 *dq0* Reference Frame -2

Now we will consider another reference frame and we will name it as *dq0* reference frame - 2, the reference frame and its mirror are shown in Fig. 4.4(a) and Fig. 4.4(b) respectively. In these frames, the *abc* to *αβ0* transformation is exactly same as (4.5)

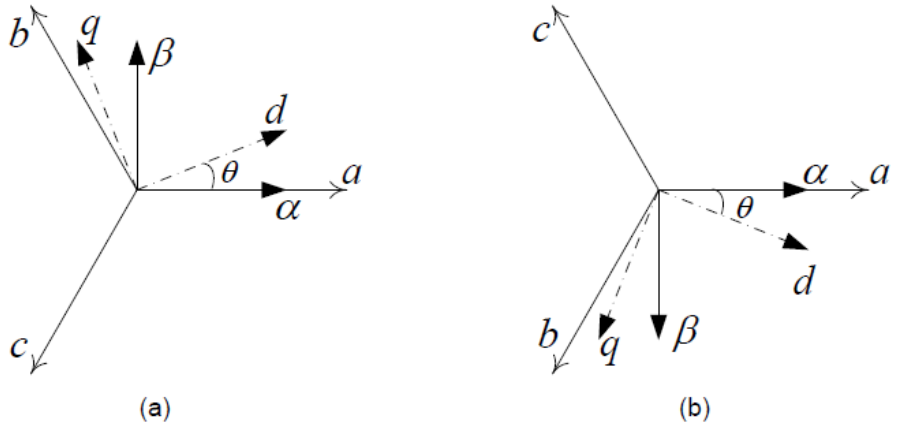

Fig. 4. 4 (a) *dq0* reference frame-2 (b) Mirror image of *dq0* reference frame-2

and the *αβ0* to *dq0* transformation is a replica of (4.6) Combining (4.5) and (4.6) we obtain the *abc* to *αβ0* transformation as shown in (4.16).

$$\begin{bmatrix} v_d \\ v_q \\ v_0 \end{bmatrix} = \sqrt{\frac{2}{3}} \begin{bmatrix} \cos\theta & \sin\theta & 0 \\ -\sin\theta & \cos\theta & 0 \\ 0 & 0 & 1 \end{bmatrix} \begin{bmatrix} 1 & -\frac{1}{2} & -\frac{1}{2} \\ 0 & \frac{\sqrt{3}}{2} & -\frac{\sqrt{3}}{2} \\ \frac{1}{\sqrt{2}} & \frac{1}{\sqrt{2}} & \frac{1}{\sqrt{2}} \end{bmatrix} \begin{bmatrix} v_a \\ v_b \\ v_c \end{bmatrix} \tag{4.15}$$

$$\begin{bmatrix} v_d \\ v_q \\ v_0 \end{bmatrix} = \sqrt{\frac{2}{3}} \begin{bmatrix} \cos\theta & \cos(\theta - \frac{2\pi}{3}) & \cos(\theta + \frac{2\pi}{3}) \\ -\sin\theta & -\sin(\theta - \frac{2\pi}{3}) & -\sin(\theta + \frac{2\pi}{3}) \\ \frac{1}{\sqrt{2}} & \frac{1}{\sqrt{2}} & \frac{1}{\sqrt{2}} \end{bmatrix} \begin{bmatrix} v_a \\ v_b \\ v_c \end{bmatrix} \tag{4.16}$$

Choosing 'θ' as ($\pi/2 - \omega t$) gives DC quantities along *d* and *q* axis in these reference frames. The final transformation matrix can be obtained by substituting $\theta = \pi/2 - \omega t$ in (4.16) and it is shown in (4.17).

$$\begin{bmatrix} v_d \\ v_q \\ v_0 \end{bmatrix} = \sqrt{\frac{2}{3}} \begin{bmatrix} \sin\omega t & \sin(\omega t - \frac{2\pi}{3}) & \sin(\omega t + \frac{2\pi}{3}) \\ \cos\omega t & \cos(\omega t - \frac{2\pi}{3}) & \cos(\omega t + \frac{2\pi}{3}) \\ \frac{1}{\sqrt{2}} & \frac{1}{\sqrt{2}} & \frac{1}{\sqrt{2}} \end{bmatrix} \begin{bmatrix} v_a \\ v_b \\ v_c \end{bmatrix} \tag{4.17}$$

4.3.3 *dq0* Reference Frame - 3

We will analyze another possible reference frame (*dq0* reference frame - 3) shown in Fig. 4.5(a) and its mirror is shown in Fig. 4.5(b). abc to *αβ0* transformation is same as (3.1).

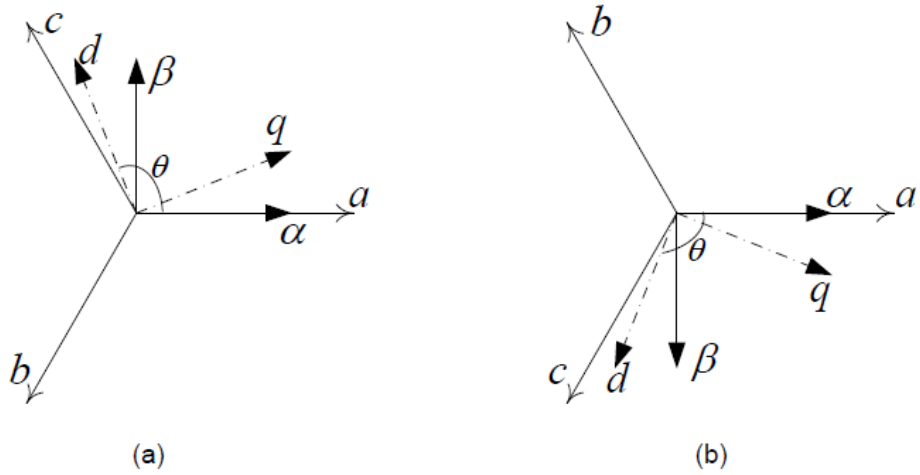

Fig. 4. 5 (a) *dq0* reference frame-3 (b) Mirror image of *dq0* reference frame-3

The *αβ0* to *dq0* transformation can be found out by resolving *α*-*β* components along *dq0* axes as follows.

$$v_d = v_\alpha \cos\theta + v_\beta \cos(\theta - 90^o) = v_\alpha \cos\theta + v_\beta \sin\theta$$

$$v_q = v_\alpha \cos(\theta - 90^o) + v_\beta \cos(\theta - 2(\theta - 90^o)) = v_\alpha \sin\theta - v_\beta \cos\theta$$

We define the *αβ0* to *dq0* transformation as shown in (4.18)

$$\begin{bmatrix} v_d \\ v_q \\ v_0 \end{bmatrix} = \begin{bmatrix} \cos\theta & \sin\theta & 0 \\ \sin\theta & -\cos\theta & 0 \\ 0 & 0 & 1 \end{bmatrix} \begin{bmatrix} v_\alpha \\ v_\beta \\ v_0 \end{bmatrix} \tag{4.18}$$

$$\begin{bmatrix} v_d \\ v_q \\ v_0 \end{bmatrix} = \sqrt{\frac{2}{3}} \begin{bmatrix} \cos\theta & \sin\theta & 0 \\ \sin\theta & -\cos\theta & 0 \\ 0 & 0 & 1 \end{bmatrix} \begin{bmatrix} 1 & -\frac{1}{2} & -\frac{1}{2} \\ 0 & -\frac{\sqrt{3}}{2} & \frac{\sqrt{3}}{2} \\ \frac{1}{\sqrt{2}} & \frac{1}{\sqrt{2}} & \frac{1}{\sqrt{2}} \end{bmatrix} \begin{bmatrix} v_a \\ v_b \\ v_c \end{bmatrix} \tag{4.19}$$

On simplification,

$$\begin{bmatrix} v_d \\ v_q \\ v_0 \end{bmatrix} = \sqrt{\frac{2}{3}} \begin{bmatrix} \cos\theta & \cos(\theta + \frac{2\pi}{3}) & \cos(\theta - \frac{2\pi}{3}) \\ \sin\theta & \sin(\theta + \frac{2\pi}{3}) & \sin(\theta - \frac{2\pi}{3}) \\ \frac{1}{\sqrt{2}} & \frac{1}{\sqrt{2}} & \frac{1}{\sqrt{2}} \end{bmatrix} \begin{bmatrix} v_a \\ v_b \\ v_c \end{bmatrix} \tag{4.20}$$

A choice of $\theta = \pi/2 - \omega t$ gives DC quantities along *d* and *q* axis in these reference frames. The final transformation matrix can be obtained by substituting $\theta = \pi/2 - \omega t$ in (4.20) and it is shown in (4.21).

$$\begin{bmatrix} v_d \\ v_q \\ v_0 \end{bmatrix} = \sqrt{\frac{2}{3}} \begin{bmatrix} \sin\omega t & \sin(\omega t - \frac{2\pi}{3}) & \sin(\omega t + \frac{2\pi}{3}) \\ \cos\omega t & \cos(\omega t - \frac{2\pi}{3}) & \cos(\omega t + \frac{2\pi}{3}) \\ \frac{1}{\sqrt{2}} & \frac{1}{\sqrt{2}} & \frac{1}{\sqrt{2}} \end{bmatrix} \begin{bmatrix} v_a \\ v_b \\ v_c \end{bmatrix} \tag{4.21}$$

4.3.4 *dq0* Reference Frame -4

The last reference frame considered is shown in Fig. 4.6(a) (dq0 reference frame -4) and its mirror is shown in Fig. 4.6(b). The *abc* to *αβ0* transformation is same as (4.5), the *αβ0* to dq0 transformation follows (4.18). The complete *abc* to *dq0* transformation can be obtained as follows by clubbing these equations,

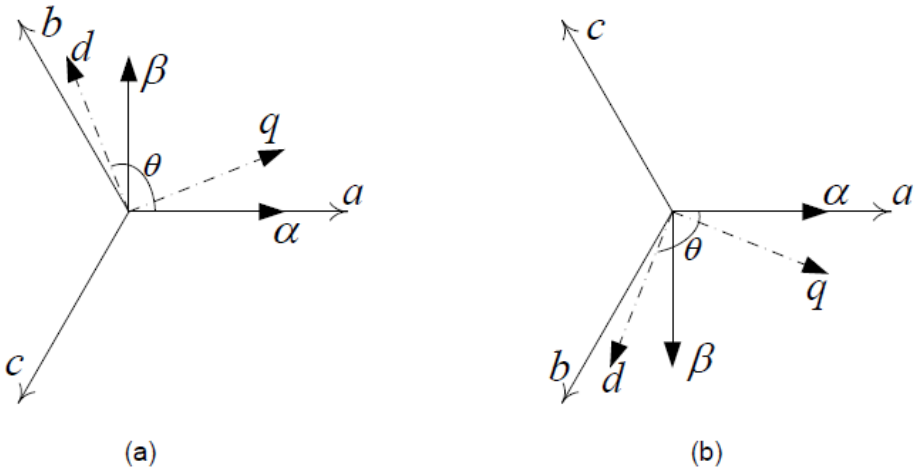

Fig. 4. 6 (a) *dq0* reference frame-4 (b) Mirror image of *dq0* reference frame-4

$$\begin{bmatrix} v_d \\ v_q \\ v_0 \end{bmatrix} = \sqrt{\frac{2}{3}} \begin{bmatrix} \cos\theta & \sin\theta & 0 \\ \sin\theta & -\cos\theta & 0 \\ 0 & 0 & 1 \end{bmatrix} \begin{bmatrix} 1 & -\frac{1}{2} & -\frac{1}{2} \\ 0 & \frac{\sqrt{3}}{2} & -\frac{\sqrt{3}}{2} \\ \frac{1}{\sqrt{2}} & \frac{1}{\sqrt{2}} & \frac{1}{\sqrt{2}} \end{bmatrix} \begin{bmatrix} v_a \\ v_b \\ v_c \end{bmatrix} \tag{4.22}$$

on simplification,

$$\begin{bmatrix} v_d \\ v_q \\ v_0 \end{bmatrix} = \sqrt{\frac{2}{3}} \begin{bmatrix} \cos\theta & \cos(\theta - \frac{2\pi}{3}) & \cos(\theta + \frac{2\pi}{3}) \\ \sin\theta & \sin(\theta - \frac{2\pi}{3}) & \sin(\theta + \frac{2\pi}{3}) \\ \frac{1}{\sqrt{2}} & \frac{1}{\sqrt{2}} & \frac{1}{\sqrt{2}} \end{bmatrix} \begin{bmatrix} v_a \\ v_b \\ v_c \end{bmatrix} \tag{4.23}$$

selecting $\theta = \pi/2 - \omega t$ gives DC quantities along *d* and *q* axis in these reference frames. The final transformation matrix can be obtained by substituting $\theta = \pi/2 - \omega t$ in (4.23) and it is shown in (4.24).

$$\begin{bmatrix} v_d \\ v_q \\ v_0 \end{bmatrix} = \sqrt{\frac{2}{3}} \begin{bmatrix} \sin\omega t & \sin(\omega t - \frac{2\pi}{3}) & \sin(\omega t + \frac{2\pi}{3}) \\ -\cos\omega t & -\cos(\omega t - \frac{2\pi}{3}) & -\cos(\omega t + \frac{2\pi}{3}) \\ \frac{1}{\sqrt{2}} & \frac{1}{\sqrt{2}} & \frac{1}{\sqrt{2}} \end{bmatrix} \begin{bmatrix} v_a \\ v_b \\ v_c \end{bmatrix} \tag{4.24}$$

4.4 GENERALIZING *αβ0* AND *dq0* TRANSFORMATIONS

4.4.1 Generalization of *abc* to *αβ0* Transformation

There are four different reference frames defined and the corresponding two transformations also have been derived. *α*-axis is always aligned along the *a*-axis of *abc* reference frame. Now we require a single transformation matrix to swap between the two transformations (4.1) and 4.5), depending upon the reference frame we choose. To achieve this objective, we will introduce two indices *m* and *n*; *m* represents the alignment of *abc* axes and *n* points at the orientation of *αβ0* axes.

m= 1, when the sequence is *a*-*b*-*c* anticlockwise.
m= -1, when the sequence is *a*-*c*-*b* anticlockwise.
n= *1*, when *β*-axis makes a quadrature with *α*-axis, in anticlockwise direction.
n= -1, when *β*-axis makes a quadrature with *α*-axis, in clockwise direction.

$$l = mn \tag{4.25}$$

Let us define the generalized transformation matrix as,

$$\begin{bmatrix} v_\alpha \\ v_\beta \\ v_0 \end{bmatrix} = \sqrt{\frac{2}{3}} \begin{bmatrix} 1 & -\frac{1}{2} & -\frac{1}{2} \\ 0 & -l\frac{\sqrt{3}}{2} & l\frac{\sqrt{3}}{2} \\ \frac{1}{\sqrt{2}} & \frac{1}{\sqrt{2}} & \frac{1}{\sqrt{2}} \end{bmatrix} \begin{bmatrix} v_a \\ v_b \\ v_c \end{bmatrix} \tag{4.26}$$

It can be observed that now depending upon the values of *m* and *n* we choose, the corresponding transform for all the four reference frames can be directly obtained from the generalized transformation given in (4.26). The inverse transformation can be generalized as shown in (4.27).

$$\begin{bmatrix} v_a \\ v_b \\ v_c \end{bmatrix} = \sqrt{\frac{2}{3}} \begin{bmatrix} 1 & 0 & \frac{1}{\sqrt{2}} \\ -\frac{1}{2} & -l\frac{\sqrt{3}}{2} & \frac{1}{\sqrt{2}} \\ -\frac{1}{2} & l\frac{\sqrt{3}}{2} & \frac{1}{\sqrt{2}} \end{bmatrix} \begin{bmatrix} v_\alpha \\ v_\beta \\ v_0 \end{bmatrix} \tag{4.27}$$

4.4.2 Verification of Generalized *abc* to *αβ0* Transformation

We will verify the generalized transformation with various values of *m* and *n*.

Case 1: *m*=1, *n*=1

Here, *m*=1 corresponds to a reference frame where *abc* axes orients with *a*-*b*-*c* sequence in anticlockwise and *n*=1 indicates *β*-axis makes a quadrature with *α*-axis in anticlockwise direction. This forms the reference frame shown in Fig. 4.1(a).Here,

$$l = mn = 1$$

With the help of (4.26) the transformation can be directly formed as shown below.

$$\begin{bmatrix} v_\alpha \\ v_\beta \\ v_0 \end{bmatrix} = \sqrt{\frac{2}{3}} \begin{bmatrix} 1 & -\frac{1}{2} & -\frac{1}{2} \\ 0 & -\frac{\sqrt{3}}{2} & \frac{\sqrt{3}}{2} \\ \frac{1}{\sqrt{2}} & \frac{1}{\sqrt{2}} & \frac{1}{\sqrt{2}} \end{bmatrix} \begin{bmatrix} v_a \\ v_b \\ v_c \end{bmatrix} \tag{4.28}$$

We can observe that the transformation obtained from generalized matrix i.e, (4.28), exactly matches with the transformation formed by conventional analysis which is (4.1).

Case 2: *m*= -1, *n*= -1

In this case *m*= -1 corresponds to a reference frame where *abc* axes orients with *a*-*c*-*b* sequence in anticlockwise and *n*= -1 indicates *β* -axis makes a quadrature with *α* -axis in clockwise direction. This gives rise to a reference frame shown in Fig. 4.1(b) which is the mirror of frame explained in case1. In this case again

$$l = mn = 1$$

Since, *l* =1, the transformation is same as (4.28) according to the generalized transformation and it is identical to the transformation obtained by conventional analysis i.e, (4.1).

Case 3: *m*=1, *n*= -1 the index *m*=1 produces a reference frame where *abc* axes orients with *a*-*b*-*c* anticlockwise and *n*= -1 indicates *β* -axis makes a quadrature with *α* -axis in clockwise direction. This is identical to the reference frame shown in Fig. 4.2(a).

$$l = mn = -1$$

With the help of (4.26) the transformation can be directly formed as shown below.

$$\begin{bmatrix} v_\alpha \\ v_\beta \\ v_0 \end{bmatrix} = \sqrt{\frac{2}{3}} \begin{bmatrix} 1 & -\frac{1}{2} & -\frac{1}{2} \\ 0 & \frac{\sqrt{3}}{2} & -\frac{\sqrt{3}}{2} \\ \frac{1}{\sqrt{2}} & \frac{1}{\sqrt{2}} & \frac{1}{\sqrt{2}} \end{bmatrix} \begin{bmatrix} v_a \\ v_b \\ v_c \end{bmatrix} \tag{4.29}$$

We can observe that the transformation obtained from generalized matrix i.e, (4.29), exactly matches with transformation formed by conventional analysis which is (4.5).

Case 4: m= -1, n= 1

In this case m= -1 corresponds to a reference frame where *abc* axes orients with *a-c-b* sequence in anticlockwise and n=1 indicates β -axis makes a quadrature with α-axis in anticlockwise direction, the indices chosen in this case gives rise to frame shown in Fig.4.2(b) which is the mirror of frame explained in case3. Since,

$$l = mn = -1$$

The transformation is same as (4.29) according to generalized transformation and it is identical to the transformation obtained by conventional analysis i.e, (4.5).

The indices for various α-β frames are shown in Table 4.1. We have tried all the four

Table 4. 1 Indices corresponding to various *dq0* frames

αβ0	*m*	*n*	*l*
Frame -1	1	1	1
Mirror of Frame -1	-1	-1	1
Frame -2	-1	1	-1
Mirror of Frame -2	1	-1	-1

possible cases and found that the transformation matrices obtained using the generalized transformation and using conventional analysis is one and the same.

4.5 GENERALIZATION OF *abc* TO *dq0* TRANSFORMATION

We have considered total 8 different reference frames and corresponding to this there are 4 different transformation matrices. We require an additional index q to represent

the orientation of *dq0* axes, in addition to indices *m* and *n* to derive a generalized transformation for all these 8 reference frames. Always measure 'θ' as the angle between α-axis and *d*-axis. *l* is the same variable used in generalizing $\alpha\beta 0$ transformation.

q= 1, when q-axis leads d-axis.

q= -1, when q-axis lags d-axis.

$$\begin{bmatrix} v_d \\ v_q \\ v_0 \end{bmatrix} = \sqrt{\frac{2}{3}} \begin{bmatrix} \cos\theta & \cos(\theta + \frac{2\pi}{3} l) & \cos(\theta - \frac{2\pi}{3} l) \\ -q\sin\theta & -q\sin(\theta + \frac{2\pi}{3} l) & -q\sin(\theta - \frac{2\pi}{3} l) \\ \frac{1}{\sqrt{2}} & \frac{1}{\sqrt{2}} & \frac{1}{\sqrt{2}} \end{bmatrix} \begin{bmatrix} v_a \\ v_b \\ v_c \end{bmatrix} \tag{4.30}$$

For obtaining DC quantities along *dq0* axes we need to define the value of 'θ'. The value of 'θ' can be generalized as follows,

$$\theta = l\left(\frac{\pi}{2} - \omega t\right) \tag{4.31}$$

4.5.1 Verification of Generalized *abc* to *dq0* Transformation

The generalized transformation needs to be verified by choosing various values for the indices and whether it matches with the results obtained by conventional analysis. The validity of generalized transform can be verified by comparing the transformations obtained out of the generalized transform and the transformation deduced using the conventional analysis for all the 8 reference frames.

Case 1: *m*=1, *n*=1, *q*=1

m=1 corresponds to a frame where *abc* frame orients with *a*-*b*-*c* anticlockwise, *n*=1 indicates that β-axis makes a quadrature with α-axis in anticlockwise direction and *q*=1 specifies that *q*-axis leads *d*-axis. This is analogous to reference frame shown in Fig. 4.3(a).

$$l = mn = 1$$

The transformation matrix for this reference frame is obtained by substituting *l* and *q* in (4.30) and it is as shown below,

$$\begin{bmatrix} v_d \\ v_q \\ v_0 \end{bmatrix} = \sqrt{\frac{2}{3}} \begin{bmatrix} \cos\theta & \cos(\theta + \frac{2\pi}{3}) & \cos(\theta - \frac{2\pi}{3}) \\ -\sin\theta & -\sin(\theta + \frac{2\pi}{3}) & -\sin(\theta - \frac{2\pi}{3}) \\ \frac{1}{\sqrt{2}} & \frac{1}{\sqrt{2}} & \frac{1}{\sqrt{2}} \end{bmatrix} \begin{bmatrix} v_a \\ v_b \\ v_c \end{bmatrix} \quad (4.32)$$

It is observed that the transformation obtained using generalized transform which is (4.32), is identical to the transformation deducted using conventional analysis i.e, (4.8). The value of 'θ' as per generalization is obtained as $\theta = (\frac{\pi}{2} - \omega t)$ by substituting the value of *l* in (4.31).

Case 2: *m*= -1, *n*= -1, *q*=1

m= -1 reflects a reference frame where *abc* frame orients with *a-c-b* anticlockwise, *n*= -1 specifies that β -axis makes a quadrature with α -axis in clockwise direction and *q*=1 specifies that *q*-axis leads d-axis. These orientations of various axes give rise to reference frame shown in Fig. 4.3(b), which is the mirror of Fig. 4.3(a).

$$l = mn = 1$$

Since *l*=*q*=1, the transformation is same as in (4.32). This is identical to transformation obtained for this frame using conventional analysis i.e,(4.8).

Case 3: *m*= -1, *n*= 1, *q*=1

m= -1 reflects a reference frame where *abc* frame orients with *a-c-b* anticlockwise, *n*=1 points out that β -axis makes a quadrature with α -axis in anticlockwise direction and *q*=1 specifies that *q*-axis leads d-axis. This reference frame is identical to frame shown in Fig. 4.4(a).

$$l = mn = -1$$

The *abc* to *dq0* can be obtained by substituting the values of *l* and *q* in (4.30) and it is as shown below,

$$\begin{bmatrix} v_d \\ v_q \\ v_0 \end{bmatrix} = \sqrt{\frac{2}{3}} \begin{bmatrix} \cos\theta & \cos(\theta - \frac{2\pi}{3}) & \cos(\theta + \frac{2\pi}{3}) \\ -\sin\theta & -\sin(\theta - \frac{2\pi}{3}) & -\sin(\theta + \frac{2\pi}{3}) \\ \frac{1}{\sqrt{2}} & \frac{1}{\sqrt{2}} & \frac{1}{\sqrt{2}} \end{bmatrix} \begin{bmatrix} v_a \\ v_b \\ v_c \end{bmatrix} \quad (4.33)$$

The transformation obtained using generalized transform which is (4.33), is identical to the transformation found out using conventional analysis i.e, (4.16). The value of 'θ' as per generalization is obtained as $(\omega t - \frac{\pi}{2})$ by substituting the value of *l* in (4.31).

Case 4: *m*= 1, *n*= -1, *q*=1

m= 1 reflects a reference frame where *abc* frame orients with *a*-*b*-*c* anticlockwise, *n*= -1 shows that β -axis makes a quadrature with α -axis in clockwise direction and *q*=1 specifies that *q*-axis leads *d*-axis. These orientations of various axes give rise to reference frame shown in Fig. 4.4(b), which turns out to be the mirror of Fig. 4.4(a).

$$l = mn = -1$$

Since l= -1 and q=1, the transformation is same as in (4.33) and it is same as the transformation obtained for this frame using conventional analysis i.e, (4.16).

Case 5: *m*= 1, *n*= 1, *q*= -1

m= -1 reflects a reference frame where *abc* frame orients with *a*-*b*-*c* anticlockwise, *n*=1 points out that β -axis makes a quadrature with α -axis in anticlockwise direction and *q*= -1 specifies that *q*-axis lags *d*-axis. This reference frame is identical to frame shown in Fig. 4.5(a).

$$l = mn = 1$$

The *abc* to *dq0* transformation can be obtained by substituting the values of *l* and *q* in (4.30) and it is as shown below,

$$\begin{bmatrix} v_d \\ v_q \\ v_0 \end{bmatrix} = \sqrt{\frac{2}{3}} \begin{bmatrix} \cos\theta & \cos(\theta + \frac{2\pi}{3}) & \cos(\theta - \frac{2\pi}{3}) \\ -\sin\theta & \sin(\theta + \frac{2\pi}{3}) & \sin(\theta - \frac{2\pi}{3}) \\ \frac{1}{\sqrt{2}} & \frac{1}{\sqrt{2}} & \frac{1}{\sqrt{2}} \end{bmatrix} \begin{bmatrix} v_a \\ v_b \\ v_c \end{bmatrix} \quad (4.34)$$

The transformation obtained using generalized transform which is (4.34), is identical to the transformation found out using conventional analysis i.e, (4.20). The value of 'θ' as per generalization is obtained as $(\frac{\pi}{2} - \omega t)$ by substituting the value of *l* in (3.31).

Case 6: *m*= -1, *n*= -1, *q*=1

m= -1 reflects a reference frame where *abc* frame orients with *a*-*c*-*b* anticlockwise, *n*= -1, β -axis makes a quadrature with α -axis in clockwise direction and *q*= -1

specifies that *q*-axis lags *d*-axis. These orientations of various axes give rise to reference frame shown in Fig. 4.5(b), which turns out to be the mirror of Fig. 4.5(a).

$$l = mn = 1$$

Since *l*=1 and *q*=1, the transformation is same as in (4.34) and it is same as the transformation obtained for this frame using conventional analysis i.e,(4.20).

Case 7: *m*= -1, *n*= 1, *q*= -1

m= -1 reflects a reference frame where *abc* frame orients with *a*-*c*-*b* anticlockwise, *n*=1 points out that β -axis makes a quadrature with α -axis in anticlockwise direction and *q*= -1 specifies that *q*-axis lags *d*-axis. This reference frame is identical to frame shown in Fig. 4.6(a).

$$l = mn = -1$$

The *abc* to *dq0* can be obtained by substituting the values of *l* and *q* in (4.30) and it is as shown below,

$$\begin{bmatrix} v_d \\ v_q \\ v_0 \end{bmatrix} = \sqrt{\frac{2}{3}} \begin{bmatrix} \cos\theta & \cos(\theta - \frac{2\pi}{3}) & \cos(\theta + \frac{2\pi}{3}) \\ \sin\theta & \sin(\theta - \frac{2\pi}{3}) & \sin(\theta + \frac{2\pi}{3}) \\ \frac{1}{\sqrt{2}} & \frac{1}{\sqrt{2}} & \frac{1}{\sqrt{2}} \end{bmatrix} \begin{bmatrix} v_a \\ v_b \\ v_c \end{bmatrix} \tag{4.35}$$

The transformation obtained using generalized transform which is (4.35), is identical to the transformation found out using conventional analysis i.e, (4.23). The value of 'θ' as per generalization is obtained as $(\omega t - \frac{\pi}{2})$ by substituting the value of *l* in (4.31).

Case 8: *m*= 1, *n*= -1, *q*= -1

m=1 reflects a reference frame where *abc* frame orients with *a*-*b*-*c* anticlockwise, *n*= -1, β -axis makes a quadrature with α -axis in clockwise direction and *q*= -1 specifies that *q*-axis lags *d*-axis. These orientations of various axes give rise to reference frame shown in Fig. 4.6(b), which turns out to be the mirror of Fig. 4.6(a).

$$l = mn = -1$$

Since, *l*= -1 and *q*=1, the transformation is same as in (4.35) and it is same as the transformation obtained for this frame using conventional analysis i.e,(4.23).

Table. 3.2, shows the indices for various *dq0* frames. We have used 3 different indices (*m,n,q*) in this *abc* to *dq0* generalization, there are 8 different possible reference frame with different combination of these three indices.

Table 4. 2 Indices Corresponding to Various dq0 Frames

dq0	*m*	*n*	*l*	*q*
Frame -1	1	1	1	1
Mirror of Frame -1	-1	-1	1	1
Frame -2	-1	1	-1	1
Mirror of Frame -2	1	-1	-1	1
Frame -3	1	1	1	-1
Mirror of Frame -3	-1	-1	1	-1
Frame -4	-1	1	-1	-1
Mirror of Frame -4	1	-1	-1	-1

The transformation for all the 8 possibilities has been found from generalized transformation and also through conventional analysis. Transformations deduced through both the methods are found to be identical.

4.6 DEDUCTION OF A MODIFIED GENERALISED TRANSFORMATION FOR *abc* TO *dq0* CONVERSION

Even after the generalization of *abc* to *dq0* transformation we have to substitute the value of 'θ' accordingly, so that we obtain DC quantities along *d* and *q* axes. We will make further analysis and try to integrate the generalized transformation matrix and the generalized value of 'θ', so that we have to look at only one single transformation matrix which takes care of 'θ' and the axes orientation in different reference frames. Name the generalized transformation matrix shown in (4.30) as T'

$$T' = \sqrt{\frac{2}{3}} \begin{bmatrix} \cos\theta & \cos(\theta + \frac{2\pi}{3} l) & \cos(\theta - \frac{2\pi}{3} l) \\ -q\sin\theta & -q\sin(\theta + \frac{2\pi}{3} l) & -q\sin(\theta - \frac{2\pi}{3} l) \\ \frac{1}{\sqrt{2}} & \frac{1}{\sqrt{2}} & \frac{1}{\sqrt{2}} \end{bmatrix} \begin{bmatrix} v_a \\ v_b \\ v_c \end{bmatrix} \qquad (4.36)$$

Substitute the generalized value of 'θ' i.e, (4.31) in (4.36) and call the resultant matrix as *T*.

$$T=\sqrt{\frac{2}{3}}\begin{bmatrix} Cos(l(\frac{\pi}{2}-wt)) & \cos(l(\frac{\pi}{2}-\omega t)+\frac{2\pi}{3}l) & \cos(l(\frac{\pi}{2}-\omega t)-\frac{2\pi}{3}l) \\ -qSin(l(\frac{\pi}{2}-wt)) & -q\sin(l(\frac{\pi}{2}-\omega t)+\frac{2\pi}{3}l) & -q\sin(l(\frac{\pi}{2}-\omega t)-\frac{2\pi}{3}l) \\ \frac{1}{\sqrt{2}} & \frac{1}{\sqrt{2}} & \frac{1}{\sqrt{2}} \end{bmatrix}\begin{bmatrix} v_a \\ v_b \\ v_c \end{bmatrix} \tag{4.37}$$

On simplifying each element of the matrix *T*,

$$T_{11}=\sin\omega t$$

$$T_{12}=\sin(\omega t-\frac{2\pi}{3})$$

$$T_{13}=\sin(\omega t+\frac{2\pi}{3})$$

$$T_{21}=-ql\cos(\omega t)$$

$$T_{22}=-ql\cos(\omega t-\frac{2\pi}{3})$$

$$T_{23}=-ql\cos(\omega t+\frac{2\pi}{3})$$

Let,

$$k = -ql$$

Now *T* can be reformed after simplification as shown in (4.38)

$$T=\begin{bmatrix} \sin\omega t & \sin(\omega t-\frac{2\pi}{3}) & \sin(\omega t+\frac{2\pi}{3}) \\ k\cos\omega t & k\cos(\omega t-\frac{2\pi}{3}) & k\cos(\omega t+\frac{2\pi}{3}) \\ \frac{1}{\sqrt{2}} & \frac{1}{\sqrt{2}} & \frac{1}{\sqrt{2}} \end{bmatrix} \tag{4.38}$$

Now we can modify the generalized transformation as follows,

$$\begin{bmatrix} v_d \\ v_q \\ v_0 \end{bmatrix}=\sqrt{\frac{2}{3}}\begin{bmatrix} \sin\omega t & \sin(\omega t-\frac{2\pi}{3}) & \sin(\omega t+\frac{2\pi}{3}) \\ k\cos\omega t & k\cos(\omega t-\frac{2\pi}{3}) & k\cos(\omega t+\frac{2\pi}{3}) \\ \frac{1}{\sqrt{2}} & \frac{1}{\sqrt{2}} & \frac{1}{\sqrt{2}} \end{bmatrix}\begin{bmatrix} v_a \\ v_b \\ v_c \end{bmatrix} \tag{4.39}$$

We can directly obtain the transformation matrix for any of the 8 reference frames from (4.38), by finding out the value of *k* using the various indices depending upon the orientation of the axes. The different possible indices and the corresponding *k* values are shown in Table 3.3. Since *k* can take only 2 values +1 or -1, there are only two transformation matrices possible and they are as shown below,

$$\begin{bmatrix} v_d \\ v_q \\ v_0 \end{bmatrix} = \sqrt{\frac{2}{3}} \begin{bmatrix} \sin\omega t & \sin(\omega t - \frac{2\pi}{3}) & \sin(\omega t + \frac{2\pi}{3}) \\ \cos\omega t & \cos(\omega t - \frac{2\pi}{3}) & \cos(\omega t + \frac{2\pi}{3}) \\ \frac{1}{\sqrt{2}} & \frac{1}{\sqrt{2}} & \frac{1}{\sqrt{2}} \end{bmatrix} \begin{bmatrix} v_a \\ v_b \\ v_c \end{bmatrix} \tag{4.40}$$

Table 4. 3 Indices corresponding to various *dq0* frames and corresponding *k* values

dqo Frame	*m*	*n*	*l*	*q*	*k*
Frame -1	1	1	1	1	-1
Mirror of Frame -1	-1	-1	1	1	-1
Frame -2	-1	1	-1	1	1
Mirror of Frame -2	1	-1	-1	1	1
Frame -3	1	1	1	-1	1
Mirror of Frame -3	-1	-1	1	-1	1
Frame -4	-1	1	-1	-1	-1
Mirror of Frame -4	1	-1	-1	-1	-1

and

$$\begin{bmatrix} v_d \\ v_q \\ v_0 \end{bmatrix} = \sqrt{\frac{2}{3}} \begin{bmatrix} \sin\omega t & \sin(\omega t - \frac{2\pi}{3}) & \sin(\omega t + \frac{2\pi}{3}) \\ -\cos\omega t & -\cos(\omega t - \frac{2\pi}{3}) & -\cos(\omega t + \frac{2\pi}{3}) \\ \frac{1}{\sqrt{2}} & \frac{1}{\sqrt{2}} & \frac{1}{\sqrt{2}} \end{bmatrix} \begin{bmatrix} v_a \\ v_b \\ v_c \end{bmatrix} \tag{4.41}$$

On finding out the inverse of the above two matrices, the inverse transform of the modified generalized transform can be generalized as shown below,

$$\begin{bmatrix} v_d \\ v_q \\ v_0 \end{bmatrix} = \sqrt{\frac{2}{3}} \begin{bmatrix} \sin\omega t & k\cos\omega t & \frac{1}{\sqrt{2}} \\ \sin(\omega t - \frac{2\pi}{3}) & k\cos(\omega t - \frac{2\pi}{3}) & \frac{1}{\sqrt{2}} \\ \sin(\omega t + \frac{2\pi}{3}) & k\cos(\omega t + \frac{2\pi}{3}) & \frac{1}{\sqrt{2}} \end{bmatrix} \begin{bmatrix} v_a \\ v_b \\ v_c \end{bmatrix} \quad (4.42)$$

4.7 ILLUSTRATION

Find the *abc* to *αβ0* transformation using generalized transform and *abc* to *dq0* transformations using the Modified Generalized Transform for an arbitrarily chosen frame.

Discussion: Consider an arbitrary reference frame given in Fig. 4.7. In this reference frame *abc* orientation is in counter clockwise direction (*m*=1), *β*-axis makes a quadrature with *α*-axis in anticlockwise direction (*n*=1), *q*- axis leads *d*- axis (q=1). To find out *abc* to *αβ0* transformation and its inverse transformation we require the index *l*, which can be found out as shown in (4.43).

$$l = mn = 1$$

By substituting *l*=1 in generalized transform in (4.26) gives us the *abc* to *αβ0* transformation in this chosen reference frame as shown in (4.44).

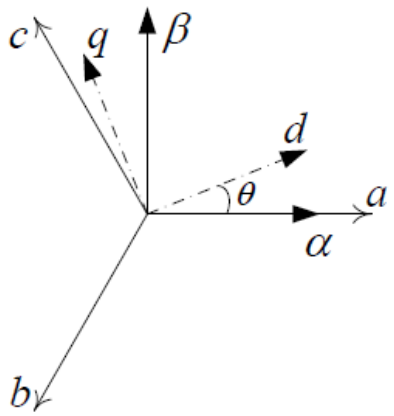

Fig. 4. 7 Arbitrary reference frame-1

$$\begin{bmatrix} v_\alpha \\ v_\beta \\ v_0 \end{bmatrix} = \sqrt{\frac{2}{3}} \begin{bmatrix} 1 & -\frac{1}{2} & -\frac{1}{2} \\ 0 & -\frac{\sqrt{3}}{2} & \frac{\sqrt{3}}{2} \\ \frac{1}{\sqrt{2}} & \frac{1}{\sqrt{2}} & \frac{1}{\sqrt{2}} \end{bmatrix} \begin{bmatrix} v_a \\ v_b \\ v_c \end{bmatrix} \tag{4.44}$$

αβ0 to *abc* transformation can be obtained by substituting *l* in the generalized *αβ0* to *abc* transformation (3.27) and the inverse transformation for this chosen reference frame is obtained as shown in (4.45).

$$\begin{bmatrix} v_a \\ v_b \\ v_c \end{bmatrix} = \sqrt{\frac{2}{3}} \begin{bmatrix} 1 & 0 & \frac{1}{\sqrt{2}} \\ -\frac{1}{2} & -\frac{\sqrt{3}}{2} & \frac{1}{\sqrt{2}} \\ -\frac{1}{2} & \frac{\sqrt{3}}{2} & \frac{1}{\sqrt{2}} \end{bmatrix} \begin{bmatrix} v_\alpha \\ v_\beta \\ v_0 \end{bmatrix} \tag{4.45}$$

To find out the *abc* to *dq0* we have to find the index *k* as shown below,

$$k = -ql = -1$$

$$\begin{bmatrix} v_d \\ v_q \\ v_0 \end{bmatrix} = \sqrt{\frac{2}{3}} \begin{bmatrix} \sin\omega t & \sin(\omega t - \frac{2\pi}{3}) & \sin(\omega t + \frac{2\pi}{3}) \\ -\cos\omega t & -\cos(\omega t - \frac{2\pi}{3}) & -\cos(\omega t + \frac{2\pi}{3}) \\ \frac{1}{\sqrt{2}} & \frac{1}{\sqrt{2}} & \frac{1}{\sqrt{2}} \end{bmatrix} \begin{bmatrix} v_a \\ v_b \\ v_c \end{bmatrix} \tag{4.46}$$

By substituting *k*= -1 in the modified generalized transformation in (4.39) we obtain the *abc* to *dq0* transformation matrix for this reference frame as shown in (4.46).

dq0 to *abc* transformation for this chosen frame can be found out as shown in (3.47) by substituting k in the inverse transformation in (4.42).

$$\begin{bmatrix} v_d \\ v_q \\ v_0 \end{bmatrix} = \sqrt{\frac{2}{3}} \begin{bmatrix} \sin\omega t & -\cos\omega t & \frac{1}{\sqrt{2}} \\ \sin(\omega t - \frac{2\pi}{3}) & -\cos(\omega t - \frac{2\pi}{3}) & \frac{1}{\sqrt{2}} \\ \sin(\omega t + \frac{2\pi}{3}) & -\cos(\omega t + \frac{2\pi}{3}) & \frac{1}{\sqrt{2}} \end{bmatrix} \begin{bmatrix} v_a \\ v_b \\ v_c \end{bmatrix} \tag{4.47}$$

4.8 SUMMARY

In this given chapter various possible reference frames in *αβ0* and *dq0* transformations are analyzed. It was also observed that the variation in the transformation matrix is dependent upon the frame chosen. Finally, generalized *αβ0* and *dq0* transformation matrices are derived, which helps in directly reaching to the final transformation matrix without performing conventional analysis on the selected reference frame. The concept of generalization is useful in saving tremendous intermediate calculations involved in each specific reference frame.

CHAPTER 5

A COMPARATIVE STUDY OF DIFFERENT CONTROL THEORIES FOR REFERENCE CURRENTS GENERATION FOR APFs

This chapter discusses about the differences in control theories, when used for reference currents generation. The chapter aims to bring out a generic comparison in terms of time and space (memory) involved by deriving a polynomial relation, amongst the theories. The scope of the comparison involves, analyzing the formulation of Instantaneous Symmetrical Component (ISC) theory, Instantaneous Reactive power theory (PQ) and Synchronous frame theory (d-q-0) in terms of their execution time and space occupied, under different source voltage conditions.

5.1 INSTANTANEOUS SYMMETRICAL COMPONENT THEORY UNDER BALANCED SOURCE VOLTAGE

The Fig 5.1 depicts the block diagram for formulating the ISC theory. The formulation of ISC theory to derive the reference currents, involves following equations.

$$v_{s0} = \frac{1}{\sqrt{3}}(v_{sa} + v_{sb} + v_{sc}) \tag{5.1}$$

where, v_{s0} is zero sequence component of source voltage, v_{sa}, v_{sb} and v_{sb} are three phase instantaneous source voltages

$$p_l(t) = \begin{bmatrix} v_{sa} & v_{sb} & v_{sc} \end{bmatrix} \begin{bmatrix} i_{la} \\ i_{lb} \\ i_{lc} \end{bmatrix} \tag{5.2}$$

where, $p_l(t)$ is instantaneous active power consumed by load, i_{la}, i_{lb} and i_{lc} are three phase instantaneous load currents

$$P_{lav} = \frac{1}{T}\int_{t_1-T}^{t_1} (v_{sa}i_{la}+v_{sb}i_{lb}+v_{sc}i_{lc})\, dt \tag{5.3}$$

where, P_{lav} is average active power consumed by load over a period T

$$\left.\begin{aligned} i^*_{fa\,ref} &= i_{la} - i_{sa} = i_{la} - \frac{v_{sa}+\gamma\left(v_{sb}-v_{sc}\right)}{\Delta} P_{lav} \\ i^*_{fb\,ref} &= i_{lb} - i_{sb} = i_{lb} - \frac{v_{sb}+\gamma\left(v_{sc}-v_{sa}\right)}{\Delta} P_{lav} \\ i^*_{fc\,ref} &= i_{lc} - i_{sc} = i_{lc} - \frac{v_{sc}+\gamma\left(v_{sa}-v_{sb}\right)}{\Delta} P_{lav} \end{aligned}\right\} \tag{5.4}$$

where $\Delta = \sum_{j=a,b,c} v_{sj}^2 - 3v_{s0}^2$ and $\gamma = \tan\varphi^+ / \sqrt{3}$ and ϕ^+ is the power factor between the positive sequence voltage (v_{sa}^+) and current (i_{sa}^+). (5.4) describes the generation of ideal reference currents, satisfying following objectives:

- Objective 1: The sum of the source currents after compensation should be zero, i.e.

$$i_{sa} + i_{sb} + i_{sc} = 0\,. \tag{5.5}$$

- Objective 2: There should be control over power factor angle (ϕ^+). Thus,

$$\angle\{v_{sa} + av_{sb} + a^2 v_{sc}\} = \angle\{i_{sa} + ai_{sb} + a^2 i_{sc}\} + \phi^+\,. \tag{5.6}$$

- Objective 3: The source should supply the average value of the power required by the load, P_{lav}, i.e.

$$v_{sa}i_{sa} + v_{sb}i_{sb} + v_{sc}i_{sc} = P_{lav}\,. \tag{5.7}$$

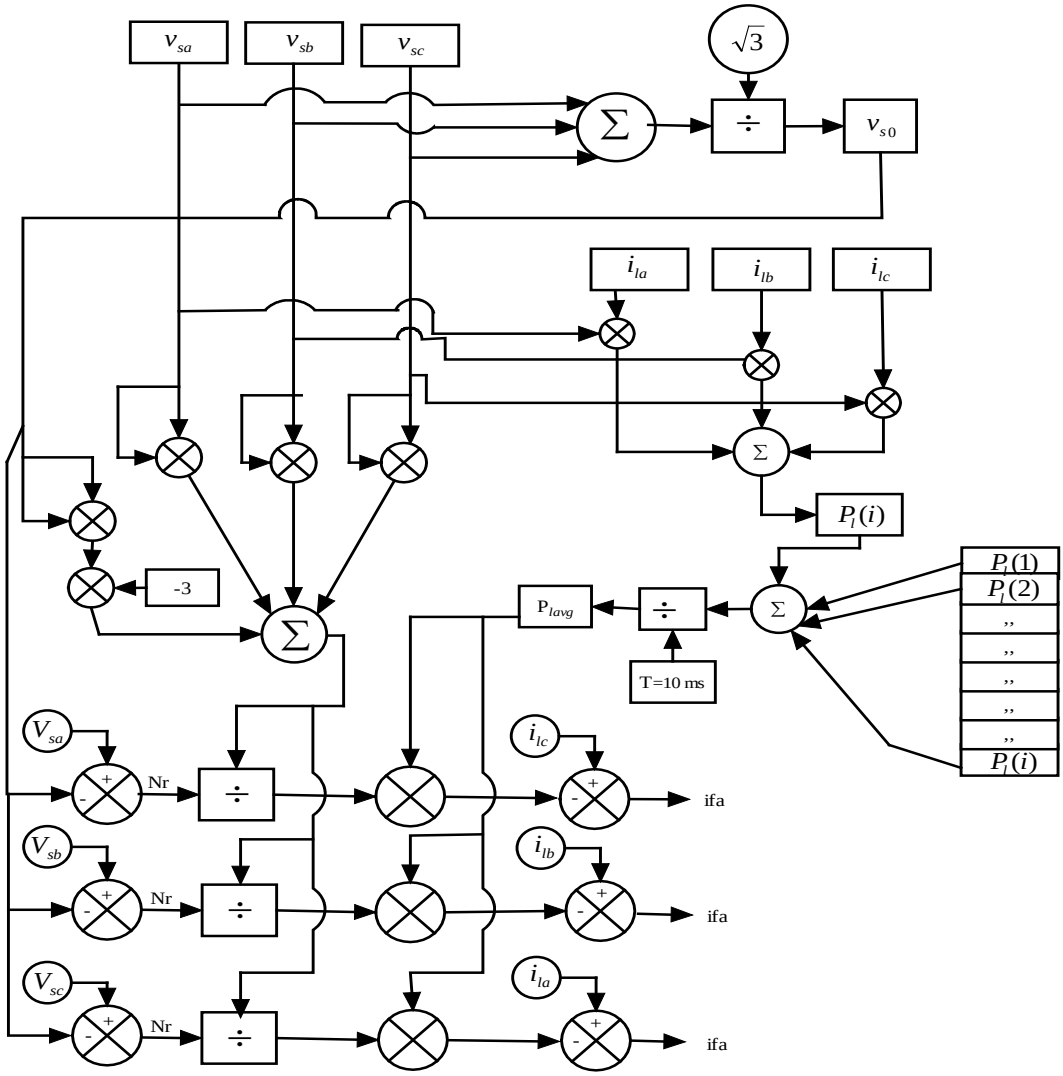

Fig. 5. 1 Block diagram representation for reference current generation using ISC theory

The implementation of (5.1 to 5.4) involve following stages:

- Sensing of Inputs through transducers – v_{sa}, v_{sb}, v_{sc} , and i_{la}, i_{lb}, i_{lc} (total 6)
- Computation of v_{s0} and $p_l(t)$
- Computation of P_{lav}
- Computation of reference currents - $i^*_{fa\,ref}$, $i^*_{fb\,ref}$, $i^*_{fc\,ref}$.

5.1.1 Sensing Input Variables

This stage requires memory allocation for six input variables as shown in Table 5.1. Each of these variables are assumed in Single-precision floating-point format that occupies 4 bytes (32 bits) in computer memory and represents a wide dynamic range of values ($\pm 10^{-38}$ to 10^{38}) as per IEEE 754. For e.g., the value of "Π" in Single-precision floating-point format is equal to 3.141593. This set of 4 bytes is termed as one *float*.

Table 5. 1 Memory for input variables

Input Variables	Memory
v_{sa}	1**float*
v_{sb}	1**float*
v_{sb}	1**float*
i_{la}	1**float*
i_{lb}	1**float*
i_{lc}	1**float*

5.1.2 Computation of Zero Sequence Component of Source Voltage and Instantaneous Active Power

This stage requires memory allocation for two variables (v_{s0} and $p_l(t)$), requiring a total of 2**float* memory allocation. The arithmetic calculations involved in this stage are tabulated in Table 5.2.

Table 5. 2 Arithmetic operations

Variables	Arithmetic operations			
	ADD	SUB	MUL	DIV
v_{s0}	2	-	-	1
$p_l(t)$	2	-	3	-

Similarly, the memory allocation involved in this stage is tabulated in Table 5.3

Table 5. 3 Memory for input variables

Input Variables	Memory
v_{s0}	1x*float*
$p_l(t)$	1x*float*
Constant ($\sqrt{3}$)	1x*float*

5.1.3 Computation of Average Active Power

Average active power is calculated using (5.3). For implementing the same using moving average filter (MAF) takes the discrete form as.

$$P_{lav} = \frac{1}{k}\sum_{i=j-k}^{j} \underbrace{v_{sa}(i).i_{la}(i) + v_{sb}(i).i_{lb}(i) + v_{sc}(i).i_{lc}(i)}_{A(i)} \tag{5.8}$$

where, T = kt_d , t_d is the discretisation time (sec), k is the number of intervals in integers. Therefore, P_{lav} can also be written as:

$$P_{lav} = \frac{1}{k}\sum_{i=j-k}^{j} [A(i)] \tag{5.9}$$

Eqn. (5.9) implies that with $k = \frac{T}{t_d}$, as the total number of intervals (k) picked in one cycle (T) increases, the memory required as well as computational steps increases, linearly. Therefore, k holds an inverse relation with discretisation time (t_d).Therefore, on solving the summation, over a half cycle (*T/2* time period i.e 10ms), the instantaneous real power is calculated at each instant, using 5.2. This instantaneous power is then saved in an array of data type - *float.*

Based on the value of t_d and the number of intervals picked in one half cycle the size of the array will keep updating. The size of this array is (k x 1) i.e (T/t_d x 1). Thus, the total number of variables required in this summation step are k**floats* or T/t_d * *floats*. And the process of summation will require (k-1) or (T/t_d -1) ADD and 1 DIV as shown below.

$$P_{lav} = \frac{1}{k}[A1 + A2 + A3.....AK]$$

Also, 1 x *float* memory is allocated to constant *T*, which is 10ms in our case. The total computational steps and memory requirement in this stage are tabulated in Table 5.4. In practical case, one boundary condition shall also be applied on discretisation time (t_d), while designing the APF.

Boundary Condition:

$$t_{FilterCurrCalc} < t_d < T$$

where, $t_{FilterCurrCalc}$ is the time involved in computation of required filter current and its switching (delay time). However, for an ideal case, where reference current switching is instantaneous; $t_{FilterCurrCalc}$ can be equal to t_d.

Table 5. 4 Memory and computation requirements for P_{lav} calculation

Requirements	Quantity
ADD	(T/t_d -1)
MUL	-
SUB	-
DIV	1
Memory	(T/t_d +1)*_floats_

5.1.4 Computation of Reference Currents

This stage requires implementation of (5.4), which involves assignment of three new variables and their memory allocation; $i^*_{fa\,ref}$, $i^*_{fb\,ref}$, $i^*_{fc\,ref}$, requiring a total of 3**float*. The arithmetic calculations involved in this stage are tabulated in Table 5.5.

Table 5. 5 Arithmetic calculations for reference current generation

Arithmetic operations			
ADD	SUB	MUL	DIV
-	7	8	3

In this step, one constant ("3") appears in equation 5.4, which will be allocated 1**float* of memory. Thus total memory requirement in this step is 4**float*.

5.1.5 Summary

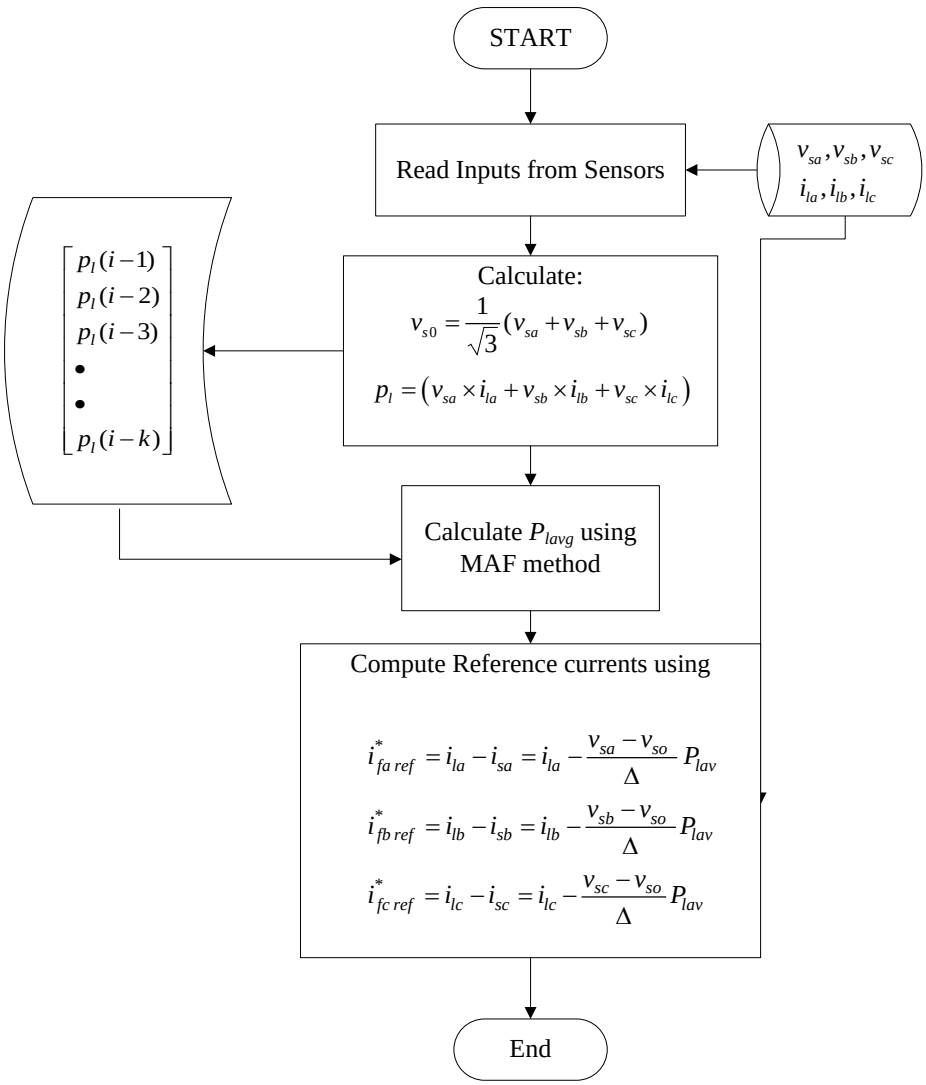

Fig. 5. 2 Flowchart for implementation of ISC control theory under balanced source voltage condition

The generic algorithm for overall implementation of ISC theory for reference current generation under balanced source condition is represented in the form of a flowchart, shown at Fig 5.2. Also, the overall memory required and computational involved is summarized in the Table given below:

Requirements	Quantification
ADD	*T/t*d +3
SUB	7
MUL	11
DIV	5
MEMORY	(*T/t*d + 14) * *float*

The Table shows the computational steps and memory requirement at each instant to generate the instantaneous reference currents of all the three phases using a microprocessor so as to meet the objectives of compensation.

Drawback: Data for MAV till T/2 is not available at the beginning.

5.2 INSTANTANEOUS SYMMETRICAL COMPONENT THEORY UNDER UNBALANCED SOURCE VOLTAGE

The Fig 5.2 depicts the overall block diagram for formulating the ISC theory under unbalanced source voltage condition. The formulation of ISC theory to derive the reference currents, involves following equations:

$$v_{s0} = \frac{1}{\sqrt{3}}(v_{sa} + v_{sb} + v_{sc})$$

$$Cal(i) = \frac{1}{\sqrt{3}}\underbrace{(v_{sa}(i) + a\,v_{sb}(i) + a^2 v_{sc}(i))}_{v^{+}_{sa}(i)}(\sin\omega t(i) + j\cos\omega t(i)) \qquad (5.10)$$

(5.10) transforms the positive sequence component (v^{+}_{sa}) into an orthogonal plane, whose instantaneous complex values are stored in a temporary variable, $Cal(i)$. Average of this temporary variable is calculated using following equation.

$$Cal(i)\_avg = \frac{1}{2T}\int Cal(i)dt \tag{5.11}$$

which in discrete form can be written as,

$$Cal(i)\_avg = \frac{1}{2k}\sum_{i=j-k}^{j} Cal(i) \tag{5.12}$$

The instantaneous active power is calculated using the equation given as under.

$$p_l(t) = \begin{bmatrix} v_{sa} & v_{sb} & v_{sc} \end{bmatrix} \begin{bmatrix} i_{la} \\ i_{lb} \\ i_{lc} \end{bmatrix}$$

Accordingly, the average power consumed by the load is represented using the equation given below.

$$P_{lav} = \frac{1}{T}\int_{t_1-T}^{t_1} (v_{sa}i_{la} + v_{sb}i_{lb} + v_{sc}i_{lc})\, dt$$

However, the reference current generation will now be decided by following equations using the Fundamental positive sequence component of unbalanced/ distorted source voltages - $v_{sa}^{+}, v_{sb}^{+}, v_{sc}^{+}$:

$$\left.\begin{aligned} i_{fa\,ref}^{*} &= i_{la} - i_{sa} = i_{la} - \frac{v_{sa}^{+} + \gamma\left(v_{sb}^{+} - v_{sc}^{+}\right)}{\Delta} P_{lav} \\ i_{fb\,ref}^{*} &= i_{lb} - i_{sb} = i_{lb} - \frac{v_{sb}^{+} + \gamma\left(v_{sc}^{+} - v_{sa}^{+}\right)}{\Delta} P_{lav} \\ i_{fc\,ref}^{*} &= i_{lc} - i_{sc} = i_{lc} - \frac{v_{sc}^{+} + \gamma\left(v_{sa}^{+} - v_{sb}^{+}\right)}{\Delta} P_{lav} \end{aligned}\right\} \tag{5.13}$$

where $\Delta = \sum_{j=a,b,c} v_{sj}^2 - 3v_{s0}^2$ and $\gamma = \tan\varphi^{+}/\sqrt{3}$ and ϕ^{+} is the power factor between the positive sequence voltage (v_{sa}^{+}) and current (i_{sa}^{+}). For ease of analysis γ is assumed to be zero.

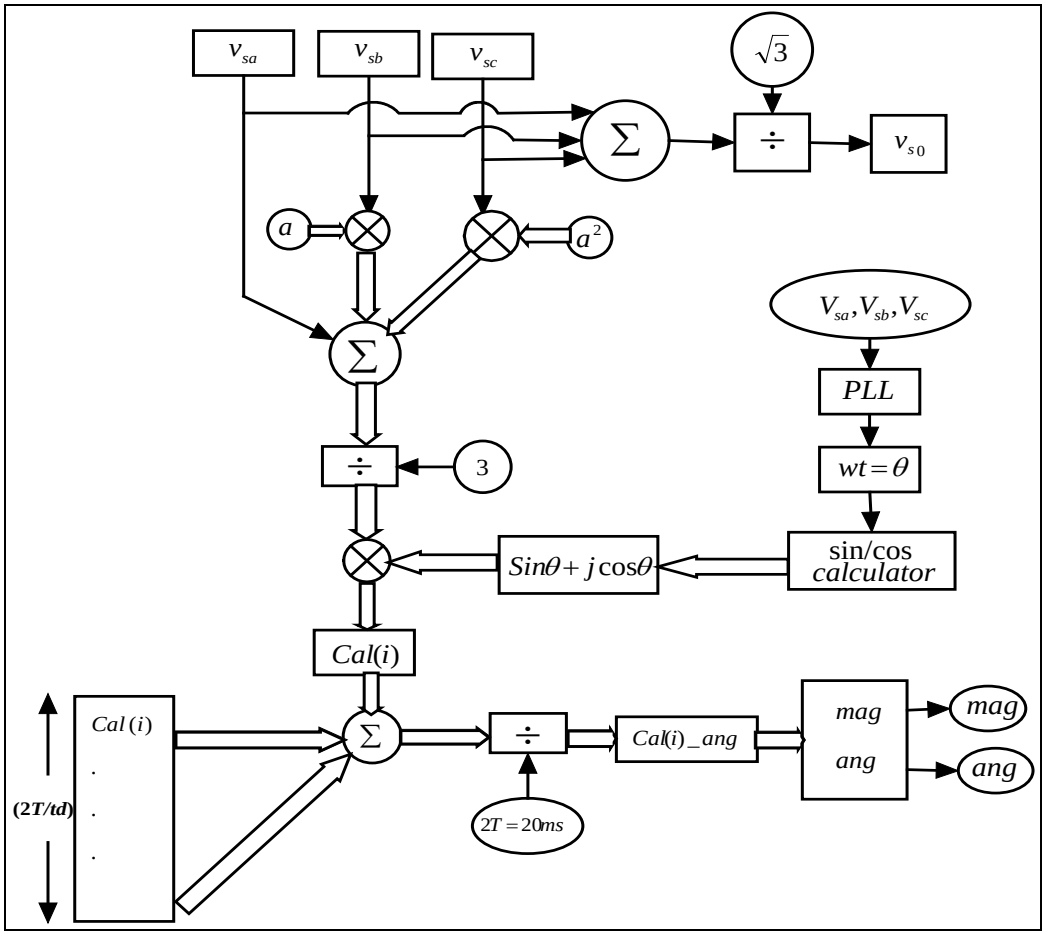
v_{sa}
v_{sb}
v_{sc}
$\sqrt{3}$
Σ
$\div$
v_{s0}
a
a^2
V_{sa}, V_{sb}, V_{sc}
PLL
$wt = \theta$
3
$Sin\theta + j\cos\theta$
sin/cos calculator
$Cal(i)$
$Cal(i)$
(2T/td)
$Cal(i)\_ang$
mag
ang
$2T = 20ms$

(a)

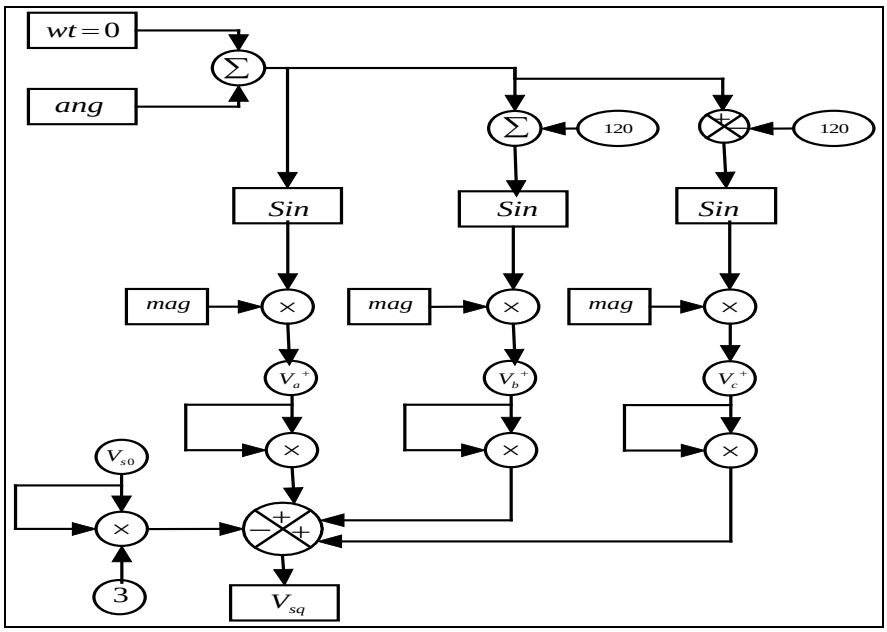
$wt = 0$
ang
120
120
Sin
Sin
Sin
mag
mag
mag
V_a^+
V_b^+
V_c^+
V_{s0}
3
V_{sq}

(b)

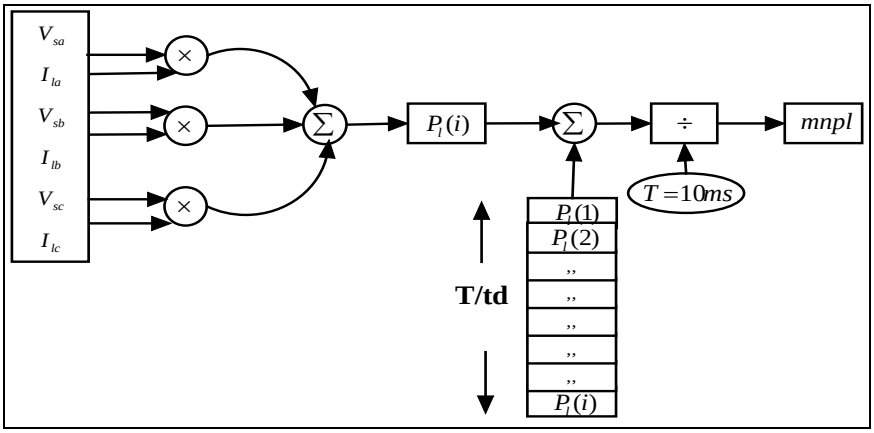

(c)

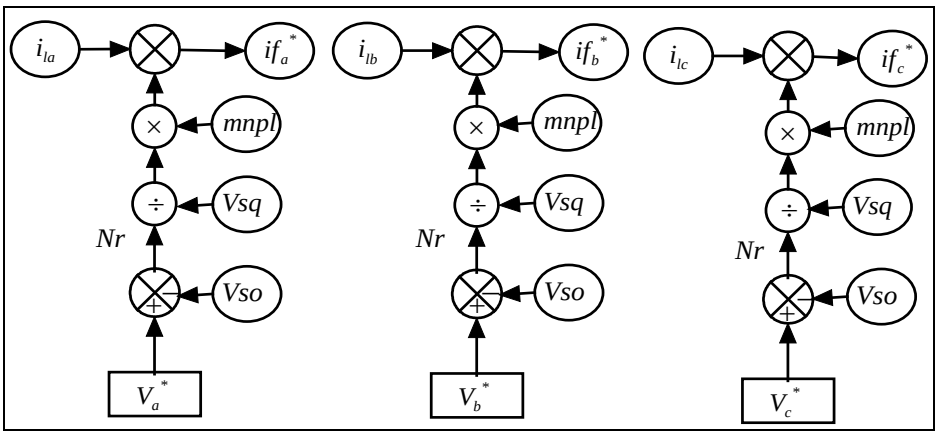

(d)

Fig. 5. 3 Block diagram representation (a)-(b) Positive sequence extraction using *Cal(i)* (c) Computation of average load power using MAF (d) Reference current generation

The implementation of this control theory under unbalanced source voltage condition involves following stages:

- Sensing of Inputs through transducers – v_{sa}, v_{sb}, v_{sc}, and i_{la}, i_{lb}, i_{lc} (total 6)
- Computation of v_{s0} and $p_l(t)$
- Computation of P_{lavg}
- Extraction of Fundamental positive sequence component of unbalanced/ distorted source voltages - $v^+_{sa}, v^+_{sb}, v^+_{sc}$
- Computation of reference currents - $i^*_{fa\,ref}$, $i^*_{fb\,ref}$, $i^*_{fc\,ref}$.

The implementation of stage I to III are same as discussed in Section 5.1.

5.2.1 Extraction of Fundamental Positive Sequence Component of Unbalanced/ Distorted Source Voltages

This stage is implemented in two steps: first, implementing Sine-Cos calculator and then calculation of fundamental positive sequence voltage. The derivations behind the extraction process are given as PROCESS OF FUNDAMENTAL EXTRACTION at Appendix 'A'. One assumption we made here is that the selected processor has an inbuilt PLL block to extract out $\theta = \omega t(i)$, where $\theta < 360^o$. Therefore, θ is readily available (zero delay) for further computations in the theory.

5.2.1.1 Implementation of Sin-Cos Calculator

The Sine and Cosine calculations are carried out by comparisons in a lookup Table (predefined), which is an array of pre fed sine and cosine values at different discretised instants (t_d), represented as under.

θ	$\text{Sin}\,\theta$	$\text{Cos}\,\theta$
0^o	0	1
ωt_d	VALUE	VALUE
$2\omega t_d$	VALUE	VALUE
$3\omega t_d$	VALUE	VALUE
•	VALUE	VALUE
•		
•		
$k\omega t_d$	VALUE	VALUE

where, k is an integer: $k = 360^0 / \omega t_d$. If, k is not an integer, it is rounded off to the nearest integer using a floor function i.e. $floor\left(360^0 / \omega t_d\right)$. This look up Table would require k+1 rows and 3 columns, necessitating (k+1)*3 *floats*. Here, k= 2T/ t_d. As, T= 10 ms, therefore for a full cycle, total memory requirement is (2T/ t_d + 1)*3 *floats*.

On implementing the Sin-Cos calculator, through comparison method there will be a minimum requirement of 1 comparison in the lookup Table, while in the worst

case, a total of k+1 comparisons are required in the first column of the look-up Table, representing angle (θ). All these comparisons include inherent subtractions, which constitutes the major arithmetic operation here. Hence, considering worst case scenario, we can safely conclude that total (k+1) SUB will be needed to implement this step.

5.2.1.2 Implementation of positive sequence extraction step

In the second step, positive sequence extraction would require implementation of (5.10 to 5.12). Accordingly, implementation of (5.10) will require an allocation of 3-constant variables "$\sqrt{3}$", "a", "a^2", necessitating a total of 5**float* of memory (due to the complex nature of a and a^2, 2* *float* per constant). $Cal(i)$ being a complex quantity is saved in an array of size ($2T/t_d$ x1). The computation involved required in this step is tabulated as under.

Arithmetic operations			
ADD	SUB	MUL	DIV
5	1	8	2

The memory requirement of this array is ($2T/t_d$ x 2)* *floats*. This step also requires a memory allocation for a constant, "2T", consuming 1**float*. $Cal(i)\_avg$ is calculated over a period of full cycle (2T) using a MAF as described in equation 5.12. 2**float* memory is also required to accommodate $Cal(i)\_avg$. The arithmetic operations required for calculating the complex quantity $Cal(i)\_avg$ is tabulated below.

Arithmetic operations			
ADD	SUB	MUL	DIV
($2T/t_d$ -1)x2	-	-	2

The next step is finding the magnitude and angle of this complex quantity, $Cal(i)\_avg$ using following equations:

$$M = \sqrt{(v_d^{+})^2 + (v_q^{+})^2} \tag{5.14}$$

$$ang = \tan^{-1}\left(\frac{v_d^{+}}{v_q^{+}}\right) \tag{5.15}$$

The two new variables "*M*" & "*ang*" would require 2* *float* of memory. The computational requirement of this step, involves; 2 MUL, 1 DIV, 1 ADD in addition to 1 SQRT calculation and 1 $\tan^{-1}$ calculation. For comparison purpose, we shall approximate the memory requirement for $\tan^{-1}$ calculation to ($2T/t_d$ +1)* *floats* adding on as 4th column in the look up Table. Also, an excess of ($2T/t_d$ + 1) comparison, approximating to ($2T/t_d$ +1) SUB will also be undertaken in executing $\tan^{-1}$ calculation. Here, it is important to note that the resolution of $\tan^{-1}$ is an independent function to determine the "*ang*" value of $Cal(i)\_avg$ (as number of comparisons for $\tan^{-1}$ would be $\left(\frac{360^0}{res} - 1\right)$, which subsequently will decide the accuracy for computing the reference currents. However, to achieve a high degree of accuracy, we can safely approximate the calculation (comparisons) of $\tan^{-1}$ based on the value of t_d. Therefore, we can safely assume $res = \omega t_d$ for all practical purposes. The 1 SQRT calculation step can be approximated to 1 ADD, 1 SUB, and 1 DIV using Maclaurin series expansion method.

The last step in fundamental positive sequence extraction includes the implementation of following equations:

$$\begin{bmatrix} \boldsymbol{v}_{sa}^{+} \\ \boldsymbol{v}_{sb}^{+} \\ \boldsymbol{v}_{sc}^{+} \end{bmatrix} = M \begin{bmatrix} \sin(\omega t + angle) \\ \sin(\omega t - 120^0 + angle) \\ \sin(\omega t + 120^0 + angle) \end{bmatrix} \tag{5.16}$$

This implementation of equation 5.16 would necessitate assignment of 3**float* variables, 3 MUL, 4 ADD, 1 SUB and 3 sine calculations. The three sine calculation

can be approximate to the worst case scenario of ($2T/t_d$ +1) x3 SUB. The implementation of this stage (section 5.2.4) is summarized in Table as given below.

Requirements	Quantification
ADD	4*T/t*d +9
SUB	10*T/t*d +8
MUL	13
DIV	6
MEMORY	(12*T/t*d + 17) * *float*

5.2.2 Summary

The generic algorithm for overall implementation of ISC theory for reference current generation under unbalanced source condition is represented in the form of a flowchart, shown at Fig 5.4. Also, the overall memory required and computational involved is summarized in the Table given below.

Requirements	Quantification
ADD	*5T/t*d +12
SUB	*10T/t*d +15
MUL	24
DIV	11
MEMORY	(13*T/t*d + 31) * *float*

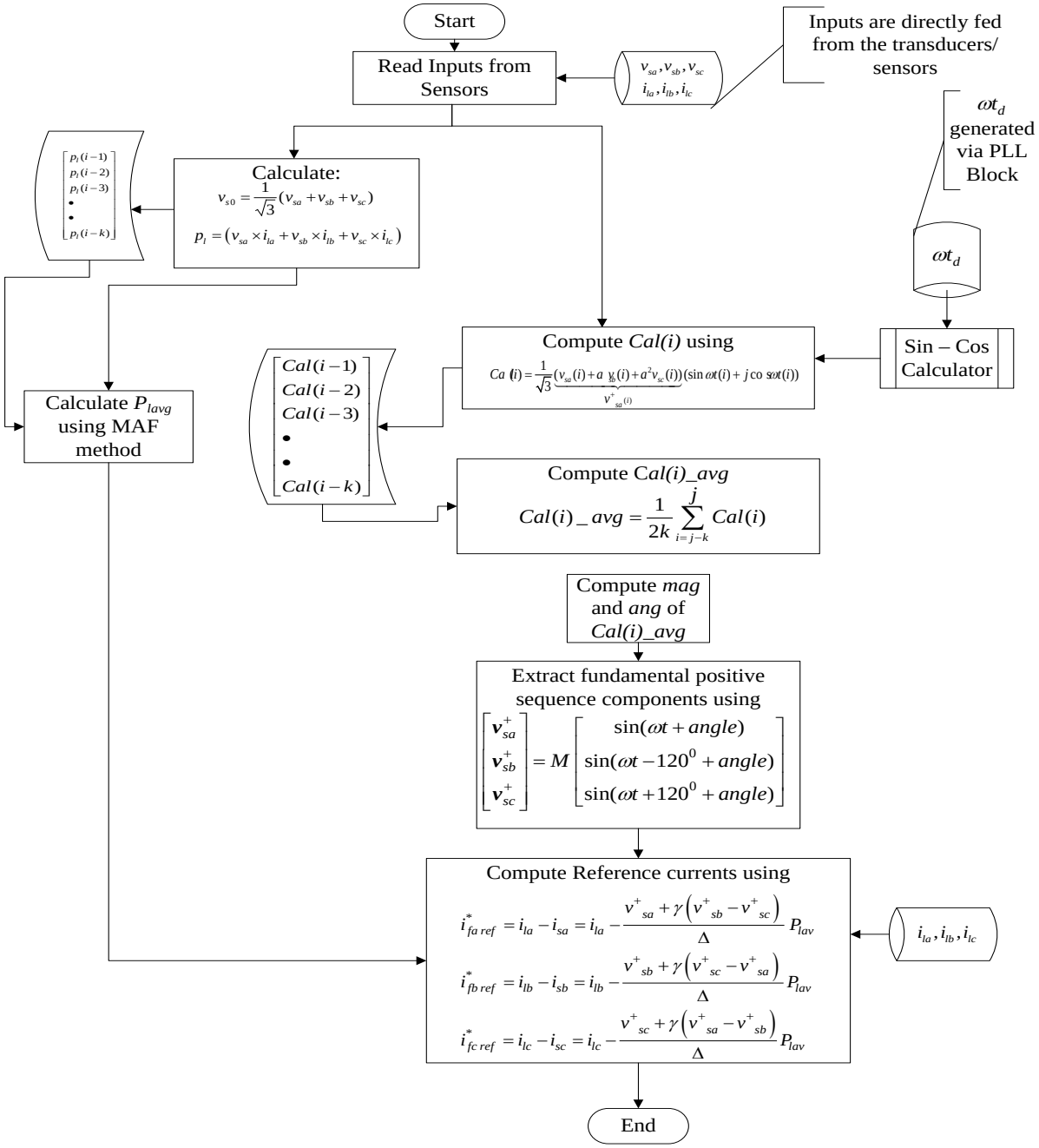

Fig. 5. 4 Flowchart for implementation of ISC control theory under unbalanced source voltage condition

5.3 INSTANTANEOUS REACTIVE POWER THEORY (p-q) UNDER BALANCED SOURCE VOLTAGE

The Fig 5.5 depicts the overall block diagram for formulating the *p-q-0* theory under balanced source voltage condition. The formulation of *p-q* theory to derive the reference currents, involves following equations.

$$\begin{bmatrix} v_o \\ v_\alpha \\ v_\beta \end{bmatrix} = \sqrt{\frac{2}{3}} \begin{bmatrix} \frac{1}{\sqrt{2}} & \frac{1}{\sqrt{2}} & \frac{1}{\sqrt{2}} \\ 1 & -\frac{1}{2} & -\frac{1}{2} \\ 0 & \frac{\sqrt{3}}{2} & -\frac{\sqrt{3}}{2} \end{bmatrix} \begin{bmatrix} v_{sa} \\ v_{sb} \\ v_{sc} \end{bmatrix} \tag{5.17}$$

$$\begin{bmatrix} i_o \\ i_\alpha \\ i_\beta \end{bmatrix} = \sqrt{\frac{2}{3}} \begin{bmatrix} \frac{1}{\sqrt{2}} & \frac{1}{\sqrt{2}} & \frac{1}{\sqrt{2}} \\ 1 & -\frac{1}{2} & -\frac{1}{2} \\ 0 & \frac{\sqrt{3}}{2} & -\frac{\sqrt{3}}{2} \end{bmatrix} \begin{bmatrix} i_{la} \\ i_{lb} \\ i_{lc} \end{bmatrix} \tag{5.18}$$

The instantaneous real, reactive and zero sequence powers, denoted by p, q and p_o are expressed in α-β plane as:

$$\begin{bmatrix} p_{\alpha\beta} \\ q_{\alpha\beta} \end{bmatrix} = \begin{bmatrix} v_\alpha & v_\beta \\ -v_\beta & v_\alpha \end{bmatrix} \begin{bmatrix} i_\alpha \\ i_\beta \end{bmatrix} \tag{5.19}$$

$$p_0 = v_0 \times i_0 . \tag{5.20}$$

In order to calculate the mean active power in α-β plane ($p_{\alpha\beta}$), one temp variable is created, named $\overline{p}_{\alpha\beta}$. The equation of the same is as under.

$$\overline{p}_{\alpha\beta} = \frac{1}{T} \int_{t_1 - T}^{t_1} (v_\alpha i_\alpha + v_\beta i_\beta)\, dt \tag{5.21}$$

Generation of reference currents in α-β plane and in *a-b-c* plane are given in following equations.

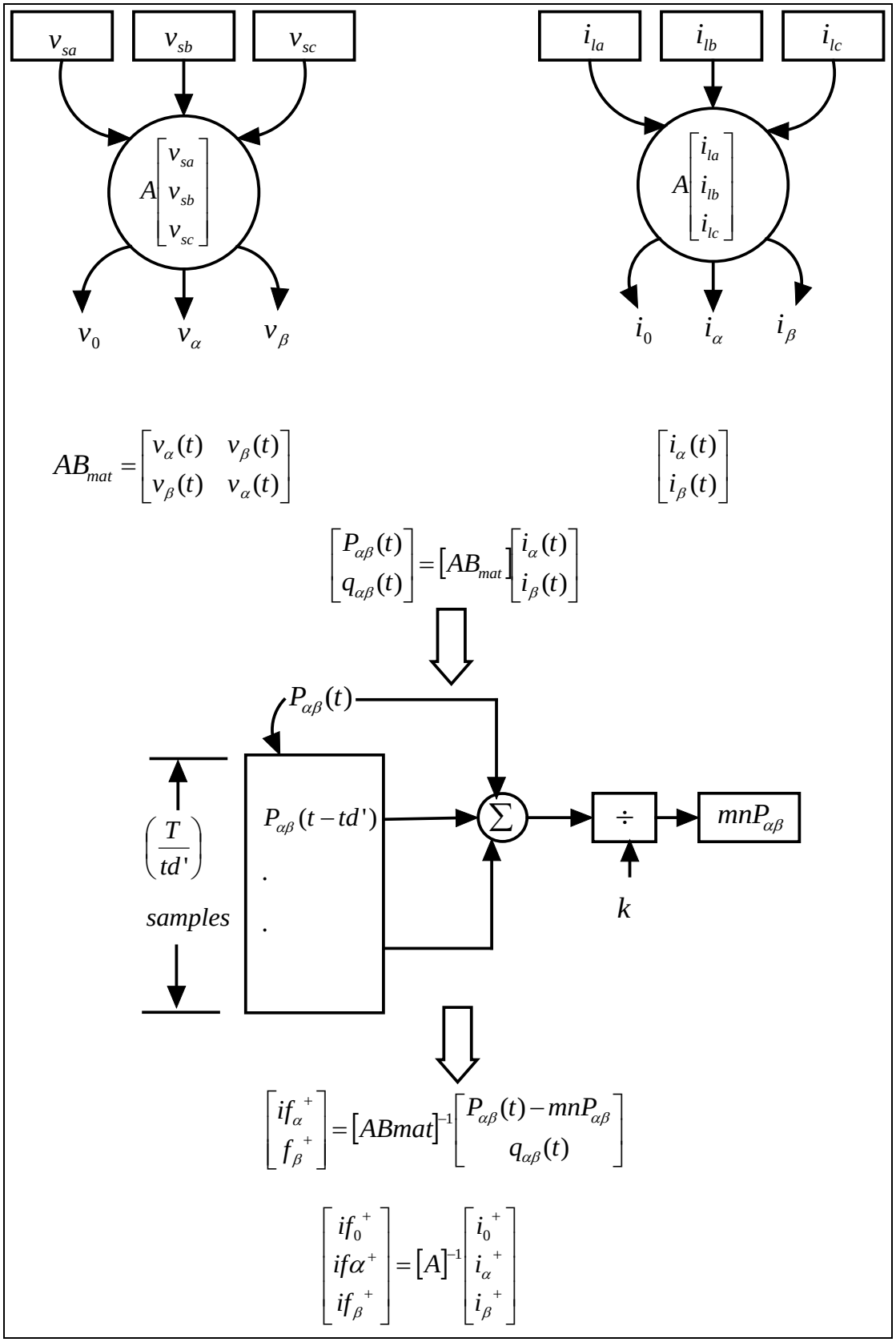

Fig. 5. 5 Block diagram for implementation of IRP control theory under balanced source voltage condition

$$\begin{bmatrix} i^{*}_{f\alpha\,ref} \\ i^{*}_{f\beta\,ref} \end{bmatrix} = \frac{1}{v_\alpha^2 + v_\beta^2} \begin{bmatrix} v_\alpha & -v_\beta \\ v_\beta & v_\alpha \end{bmatrix} \begin{bmatrix} p_{\alpha\beta} - \overline{p}_{\alpha\beta} \\ q_{\alpha\beta} \end{bmatrix} \tag{5.22}$$

$$\begin{bmatrix} i^{*}_{fa\,ref} \\ i^{*}_{fb\,ref} \\ i^{\&}_{fc\,ref} \end{bmatrix} = \sqrt{\frac{2}{3}} \begin{bmatrix} 1/\sqrt{2} & 1 & 0 \\ 1/\sqrt{2} & -1/2 & \sqrt{3}/2 \\ 1/\sqrt{2} & -1/2 & -\sqrt{3}/2 \end{bmatrix} \begin{bmatrix} i_{fo} \\ i^{*}_{f\alpha\,ref} \\ i^{*}_{f\beta\,ref} \end{bmatrix} \tag{5.23}$$

The implementation of this control theory under balanced source voltage condition involves following stages.

- Sensing of Inputs through transducers – v_{sa}, v_{sb}, v_{sc} , and i_{la}, i_{lb}, i_{lc} (total 6)
- Transformation of source voltage and load current to α-β-0 domain
- Computation of instantaneous real ($p_{\alpha\beta}$) and reactive components ($q_{\alpha\beta}$) of power in α-β domain
- Computation of mean real power ($\overline{p}_{\alpha\beta}$) with MAF
- Generation of instantaneous filter currents in α-β domain ($i^{*}_{f\alpha\,ref}$ and $i^{*}_{f\beta\,ref}$)
- Computation of reference currents - $i^{*}_{fa\,ref}$, $i^{*}_{fb\,ref}$, $i^{*}_{fc\,ref}$.

Eqn. (5.22) and (5.23) describes the generation of ideal reference currents, satisfying following objectives.

- Objective 1: All the instantaneous oscillating real power is supplied by the APF, i.e. $p_{\alpha\beta} - \overline{p}_{\alpha\beta}$
- Objective 2: The entire instantaneous reactive power required by the load is supplied by the APF.

5.3.1 Transformation of Source Voltage and Load Current To *α-β*-0 Domain

This stage involves the implementation of (5.17 and 5.18). It would require storing a (3x3) constant Transformation matrix and allocation for 6 new variables: $v_0, v_\alpha, v_\beta, i_o,$ i_α and i_β, thus, requiring 15**floats* of memory. The computational requirement of this stage is tabulated as under.

Arithmetic operations			
ADD	SUB	MUL	DIV
12	-	18	-

5.3.2 Computation of Instantaneous Real ($p_{\alpha\beta}$) and Reactive Components ($q_{\alpha\beta}$) of Power in α-β Domain

This stage requires the implementation of equation 5.19, which shall necessitate one negation operation (element in 2nd row 1st column of matrix), accounting for 1 SUB. This stage would require allocation of 3 new variables, $p_{\alpha\beta}$, $q_{\alpha\beta}$ and $-v_\beta$, thus allocation of 3**float*. The total computational steps including the negation operation are tabulated as under.

Arithmetic operations			
ADD	SUB	MUL	DIV
2	1	4	-

5.3.3 Computation of Mean Real Power $\overline{p}_{\alpha\beta}$ Using MAF

This stage requires implementation of equation number 5.21, which in discrete form is represented as under.

$$\overline{p}_{\alpha\beta} = \frac{1}{k}\sum_{i=j-k}^{j} \underbrace{v_\alpha(i)i_\alpha(i) + v_\beta(i)i_\beta(i)}_{A'} \tag{5.24}$$

$$\overline{p}_{\alpha\beta} = \frac{1}{k}\sum_{i=j-k}^{j} [A'] \tag{5.25}$$

The implementation of the above equations necessitates declaration of an array of size (T/t_d x1), requiring T/t_d **floats*, and an additional 1**float* to save a constant *T*. The computational steps required in this stage are tabulated as under.

Arithmetic operations			
ADD	SUB	MUL	DIV
T/t_d -1	-	-	1

5.3.4 Generation of Instantaneous Filter Currents on α-β DOMAIN ($i^*_{f\alpha\,ref}$) and ($i^*_{f\beta\,ref}$)

This stage requires the implementation of equation number 5.22, which will require an allocation of eight new variables (which includes memory space for $i^*_{f\alpha\,ref}$ and $i^*_{f\beta\,ref}$, and a temporary variable for determinant ($v_\alpha^2 + v_\beta^2$)), thus requiring 8**float*. The computational steps required in this stage are tabulated as under.

Arithmetic operations			
ADD	SUB	MUL	DIV
3	1	6	4

5.3.5 Computation of Reference Currents ($i^*_{fa\,ref}$, $i^*_{fb\,ref}$, and $i^*_{fc\,ref}$)

This stage requires the implementation of equation number 5.23, which requires declaration of a (3x3) matrix, which is nothing but an inverse of a constant transformation matrix used in (5.17 and 5.18), which again turns out to be a new constant matrix, and three variables for $i^*_{fa\,ref}$, $i^*_{fb\,ref}$, $i^*_{fc\,ref}$. Therefore, a total of 12**floats* of memory is required for implementing this stage. The computational steps required in this stage are tabulated as under.

Arithmetic operations			
ADD	SUB	MUL	DIV
6	-	9	-

5.3.6 Summary

The overall memory required and computational involved is summarized in the Table given below.

Requirements	Quantification
ADD	*T/t*d +22
SUB	2
MUL	37
DIV	5
MEMORY	(*T/t*d +45) * *float*

5.4 INSTANTANEOUS REACTIVE POWER THEORY (*p-q*) UNDER UNBALANCED SOURCE VOLTAGE

The Fig 5.6 depicts the overall block diagram for formulating the *p-q* theory under unbalanced source voltage condition. The formulation of *p-q* theory to derive the reference currents, involves following equations.

$$Cal(i) = \frac{1}{\sqrt{3}} \underbrace{(v_{sa}(i) + a\, v_{sb}(i) + a^2 v_{sc}(i))}_{v^{+}_{sa}(i)} (\sin \omega t(i) + j \cos \omega t(i))$$

$$Cal(i)\_avg = \frac{1}{2T} \int Cal(i)dt$$

$$Cal(i)\_avg = \frac{1}{2k} \sum_{i=j-k}^{j} Cal(i)$$

$$\begin{bmatrix} v_o \\ v_\alpha \\ v_\beta \end{bmatrix} = \sqrt{\frac{2}{3}} \begin{bmatrix} \frac{1}{\sqrt{2}} & \frac{1}{\sqrt{2}} & \frac{1}{\sqrt{2}} \\ 1 & -\frac{1}{2} & -\frac{1}{2} \\ 0 & \frac{\sqrt{3}}{2} & -\frac{\sqrt{3}}{2} \end{bmatrix} \begin{bmatrix} v^{+}_{sa} \\ v^{+}_{sb} \\ v^{+}_{sc} \end{bmatrix} \quad (5.26)$$

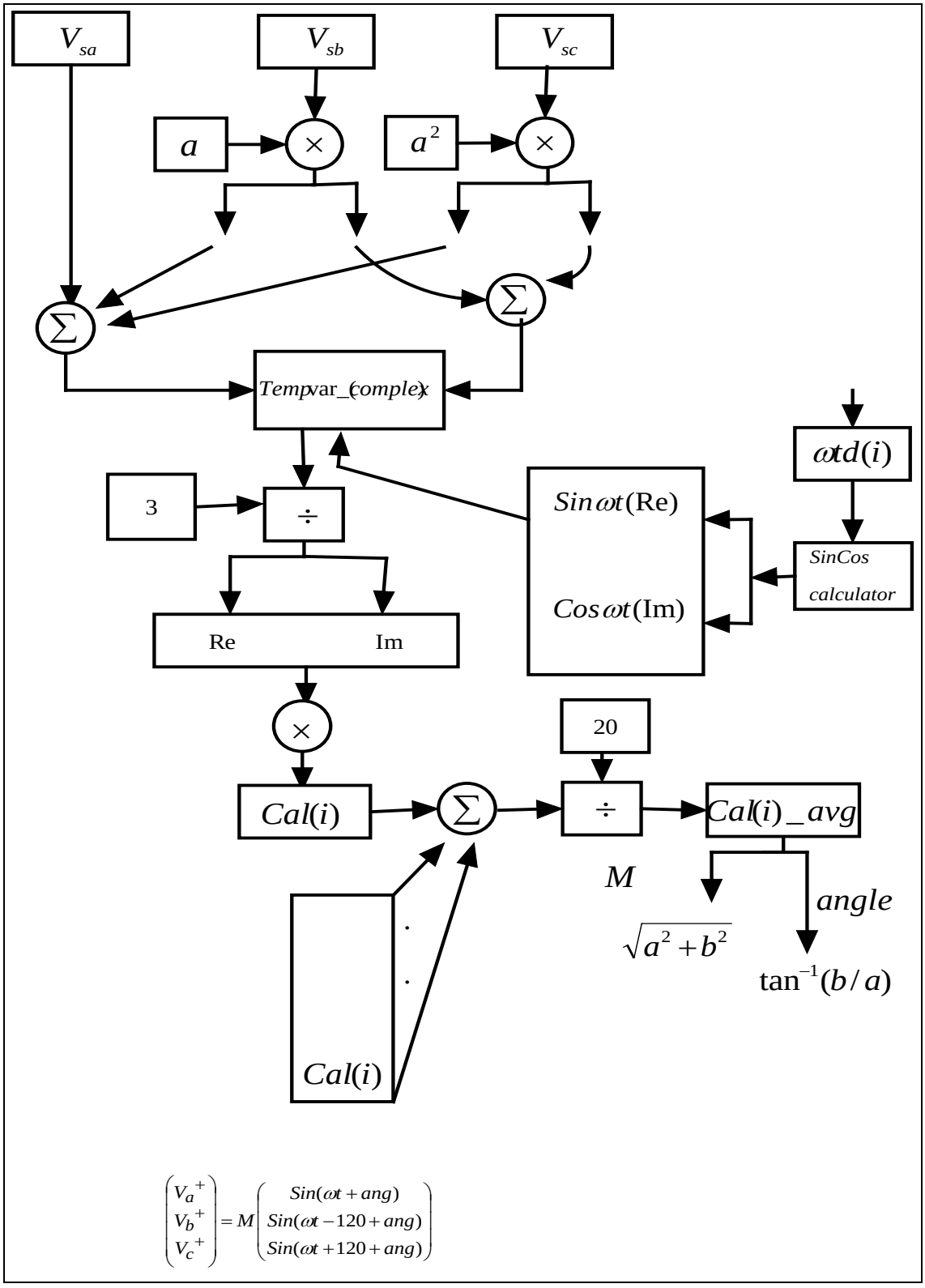
V_{sa}
V_{sb}
V_{sc}
a
a^2
$\times$
$\sum$
Tempvar_(complex)
3
$\div$
Re
Im
$Sin\omega t$(Re)
$Cos\omega t$(Im)
$\omega td(i)$
SinCos calculator
20
$Cal(i)$
$Cal(i)\_avg$
M
$\sqrt{a^2+b^2}$
$angle$
$\tan^{-1}(b/a)$
$\begin{pmatrix} V_a^+ \\ V_b^+ \\ V_c^+ \end{pmatrix} = M \begin{pmatrix} Sin(\omega t + ang) \\ Sin(\omega t - 120 + ang) \\ Sin(\omega t + 120 + ang) \end{pmatrix}$

(a)

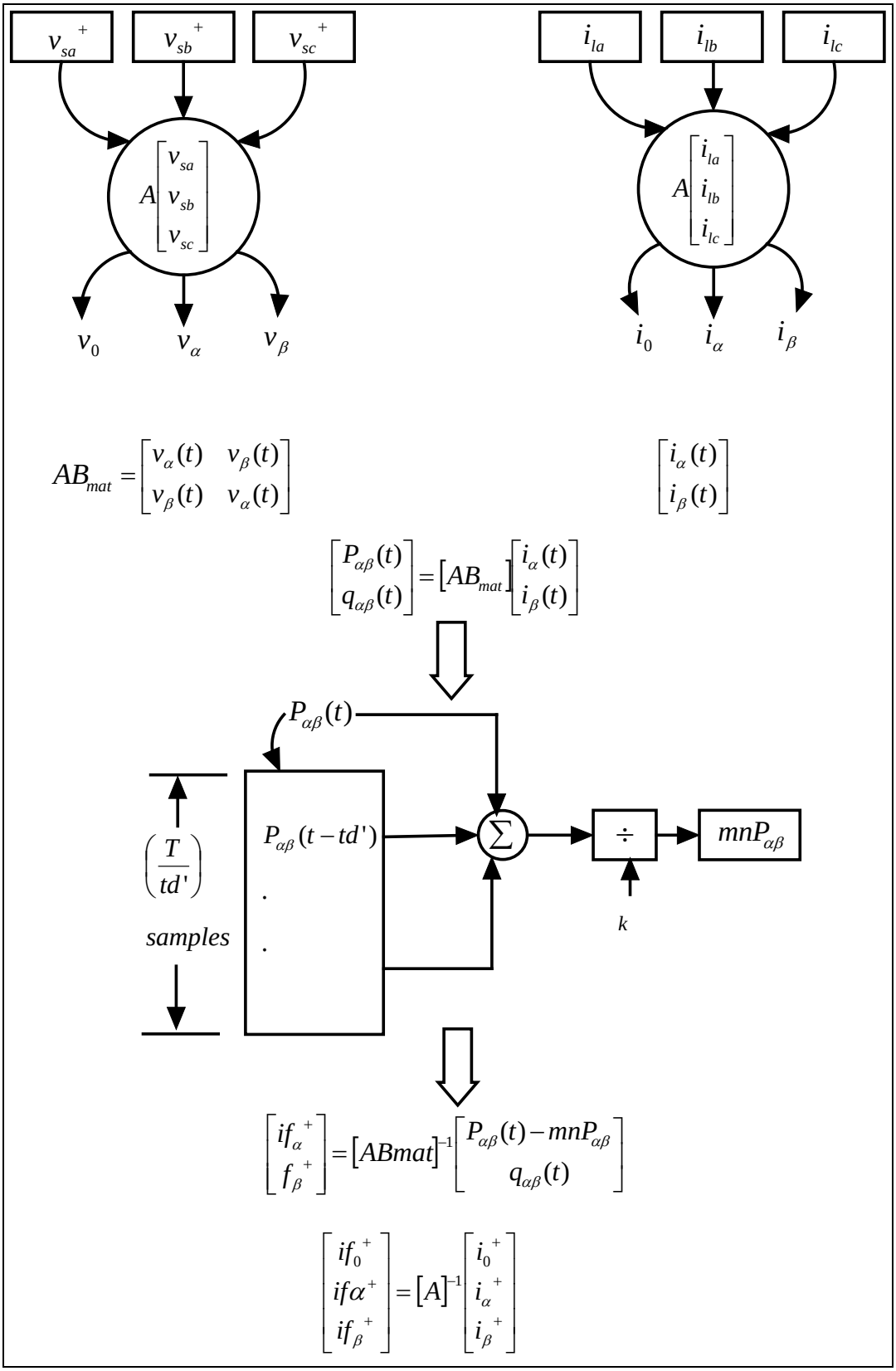

Fig. 5. 6 Block Diagram for (a) process of extraction of fundamental positive sequence voltage component (b) implementation of IRP control theory under unbalanced source voltage condition

Following equations are reproduced again for the sake of completeness, while implementing this theory under unbalanced source voltage condition.

$$\begin{bmatrix} i_o \\ i_\alpha \\ i_\beta \end{bmatrix} = \sqrt{\frac{2}{3}} \begin{bmatrix} \frac{1}{\sqrt{2}} & \frac{1}{\sqrt{2}} & \frac{1}{\sqrt{2}} \\ 1 & -\frac{1}{2} & -\frac{1}{2} \\ 0 & \frac{\sqrt{3}}{2} & -\frac{\sqrt{3}}{2} \end{bmatrix} \begin{bmatrix} i_{la} \\ i_{lb} \\ i_{lc} \end{bmatrix}$$

$$\begin{bmatrix} p_{\alpha\beta} \\ q_{\alpha\beta} \end{bmatrix} = \begin{bmatrix} v_\alpha & v_\beta \\ -v_\beta & v_\alpha \end{bmatrix} \begin{bmatrix} i_\alpha \\ i_\beta \end{bmatrix}$$

$p_0 = v_0 \times i_0$.

$$\overline{p}_{\alpha\beta} = \frac{1}{T} \int_{t_1 - T}^{t_1} (v_\alpha i_\alpha + v_\beta i_\beta)\, dt$$

$$\begin{bmatrix} i^*_{f\alpha\, ref} \\ i^*_{f\beta\, ref} \end{bmatrix} = \frac{1}{v_\alpha^2 + v_\beta^2} \begin{bmatrix} v_\alpha & -v_\beta \\ v_\beta & v_\alpha \end{bmatrix} \begin{bmatrix} p_{\alpha\beta} - \overline{p}_{\alpha\beta} \\ q_{\alpha\beta} \end{bmatrix}$$

$$\begin{bmatrix} i^*_{fa\, ref} \\ i^*_{fb\, ref} \\ i^*_{fc\, ref} \end{bmatrix} = \sqrt{\frac{2}{3}} \begin{bmatrix} 1/\sqrt{2} & 1 & 0 \\ 1/\sqrt{2} & -1/2 & \sqrt{3}/2 \\ 1/\sqrt{2} & -1/2 & -\sqrt{3}/2 \end{bmatrix} \begin{bmatrix} i_{fo} \\ i^*_{f\alpha\, ref} \\ i^*_{f\beta\, ref} \end{bmatrix}$$

Equation 5.22 and 5.23 describes the generation of ideal reference currents, satisfying following objectives:

- Objective 1: All the instantaneous oscillating real power is supplied by the APF, i.e. $p_{\alpha\beta} - \overline{p}_{\alpha\beta}$
- Objective 2: The entire instantaneous reactive power required by the load is supplied by the APF.

The implementation of this control theory under balanced source voltage condition involves following stages:

- Sensing of Inputs through transducers – v_{sa}, v_{sb}, v_{sc}, and i_{la}, i_{lb}, i_{lc} (total 6)

- Extraction of Fundamental positive sequence component of unbalanced/ distorted source voltages - $v^{+}_{sa}, v^{+}_{sb}, v^{+}_{sc}$

- Transformation of fundamental positive sequence source voltage and load current to α-β-0 domain

- Computation of instantaneous real ($p_{\alpha\beta}$) and reactive components ($q_{\alpha\beta}$) of power in α-β domain

- Computation of mean real power ($\overline{p}_{\alpha\beta}$) with MAF

- Generation of instantaneous filter currents in α-β domain ($i^{*}_{f\,\alpha\,ref}$ and $i^{*}_{f\,\beta\,ref}$)

- Computation of reference currents - $i^{*}_{fa\,ref}$, $i^{*}_{fb\,ref}$, $i^{*}_{fc\,ref}$.

5.4.1 Summary of Implementation

The overall memory required and computational involved is summarized in the Table given below.

Requirements	Quantification
ADD	5*T/t*d +31
SUB	10*T/t*d +10
MUL	50
DIV	12
MEMORY	(13*T/t*d +62) * *float*

5.5 SYNCHRONOUS REFERENCE FRAME THEORY (*d-q-0*) UNDER BALANCED AND UNBALANCED SOURCE VOLTAGE

The Fig 5.8 depicts the overall block diagram for formulating the *d-q-0* theory under balanced and unbalanced source voltage condition. Based on Fig. 5.7, the formulation of *d-q-0* theory to derive the reference currents, involves following equations.

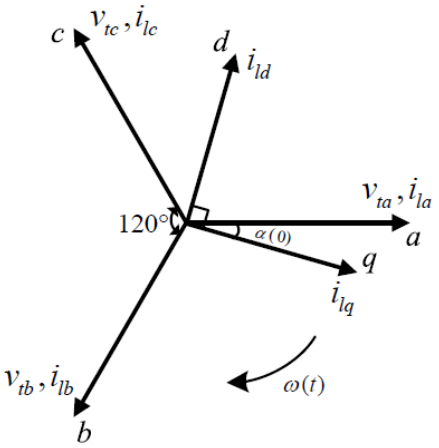

Fig. 5. 7 Axis *a-b-c* and *d-q-0* orientation

$$\begin{bmatrix} i_{lq} \\ i_{ld} \\ i_{l0} \end{bmatrix} = \sqrt{\frac{2}{3}} \begin{bmatrix} \cos\omega t & \cos(\omega t - 2\pi/3) & \cos(\omega t + 2\pi/3) \\ \sin\omega t & \sin(\omega t - 2\pi/3) & \sin(\omega t + 2\pi/3) \\ 1/\sqrt{2} & 1/\sqrt{2} & 1/\sqrt{2} \end{bmatrix} \begin{bmatrix} i_{la} \\ i_{lb} \\ i_{lc} \end{bmatrix} \tag{5.27}$$

$$I_{ld} = \frac{1}{2T} \int_{t_1 - T}^{t_1} i_{ld}(t)\, dt \tag{5.28}$$

$$\boldsymbol{I_{ld}} = \frac{\boldsymbol{1}}{\boldsymbol{k}} \sum_{i=j-k}^{\boldsymbol{j}} [\boldsymbol{i_{ld}(i)}] \tag{5.29}$$

$$\begin{bmatrix} i^*_{fa} \\ i^*_{fb} \\ i^*_{fc} \end{bmatrix} = \sqrt{\frac{2}{3}} \begin{bmatrix} \cos\omega t & \sin\omega t & 1/\sqrt{2} \\ \cos(\omega t - 2\pi/3) & \sin(\omega t - 2\pi/3) & 1/\sqrt{2} \\ \cos(\omega t + 2\pi/3) & \sin(\omega t + 2\pi/3) & 1/\sqrt{2} \end{bmatrix} \begin{bmatrix} i_{ld} - I_{ld} \\ i_{lq} \\ i_{l0} \end{bmatrix} \tag{5.30}$$

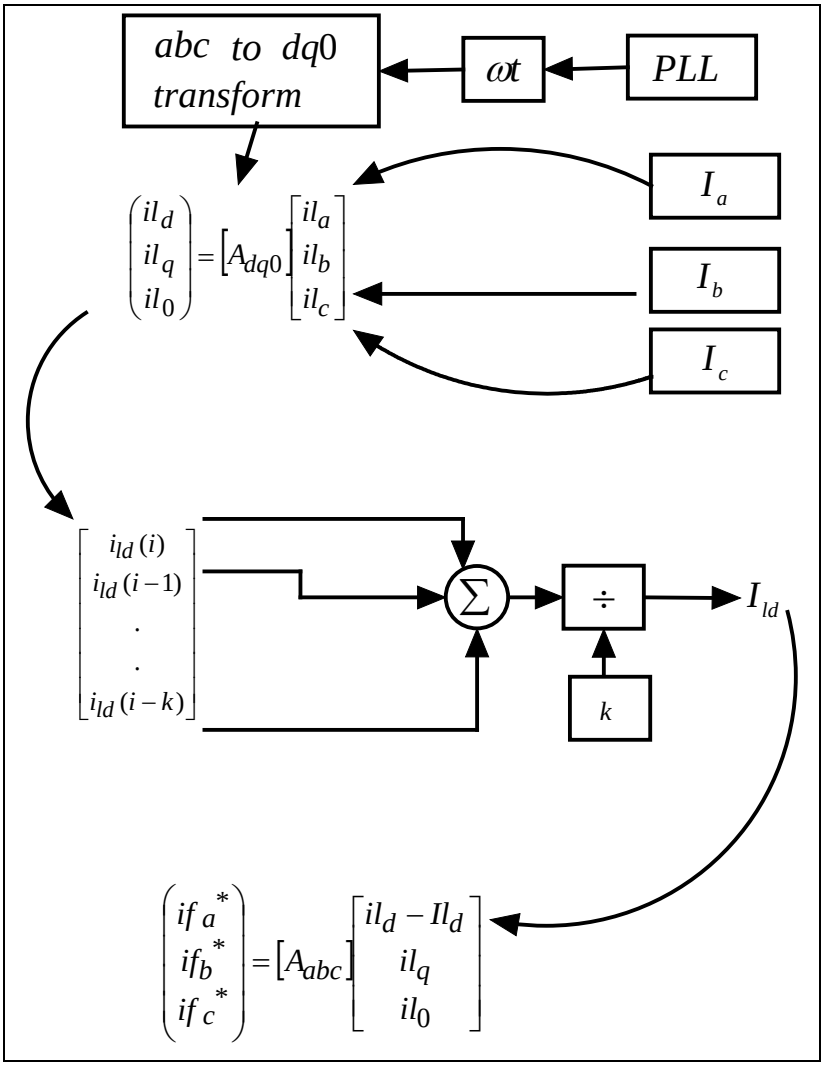

Fig. 5. 8 Block diagram for formulation of SRF theory

The implementation of this control theory under balanced and unbalanced source voltage condition requires following stages.

- Sensing of Inputs through transducers – i_{la}, i_{lb}, i_{lc} (total 3)
- Transformation of load current to *dq0* domain
- Computing average of *d*-component of load current (I_{ld}) using MAF.

- Computation of reference currents - $i^*_{fa\,ref}$, $i^*_{fb\,ref}$, $i^*_{fc\,ref}$.

Eqn. 5.30 describes the generation of ideal reference currents, satisfying following objectives:

- Objective 1: The oscillating *d*-component of instantaneous load current is supplied by the APF
- Objective 2: The entire instantaneous *q*-component current required by the load is supplied by the APF.

5.5.1 Sensing Input Variables

This stage requires memory allocation for three input variables: i_{la} , i_{lb} and $\boldsymbol{i}_{lc}$, necessitating total 3*float memory.

5.5.2 Transformation of Load Current to *d-q-0* Domain

The assumption made for extraction of ($\theta = \omega t(i)$ in section 5.2.4 holds true for this section as well. Therefore, information on θ is provided by the inbuilt PLL block. This stage necessitates three Cosine calculations and three Sine calculations sequentially after 1 SUB and 1 ADD. This sine and cosine calculations would therefore require, (2T/td +1)*3 *floats* and (2T/td +1) SUB for implementing Sin-Cos calculator as discussed in sub-sub section 5.2.4. After Sine and Cosine calculations the step requires allocation of 11 distinct variables that includes 7 distinct matrix variables (incl $1/\sqrt{2}$, preloaded in decimal format), one constant ($\sqrt{2/3}$, preloaded in decimal format), and three variables for i_{ld} , i_{lq} , i_{l0} . , necessitating 11**floats*. These matrix operations require 13 MUL, 6 ADD. After removing all the redundancies in memory allocations and arithmetic operations, the total requirements of this stage is tabulated as under.

Requirements	Quantification
ADD	7
SUB	2*T*/*t*d + 2
MUL	13
DIV	-
MEMORY	6*T*/*t*d + 14

5.5.3 Computing Average *d*-Component Load Current (I_{ld}) using MAF

This stage requires implementation of equation 5.29, which necessitates a memory allocation of an array of size (2T/td x 1) requiring 2T/td**float*. This stage also requires 1*float for a constant (2*T*). The computational steps in this stage are tabulated as under.

Arithmetic operations			
ADD	SUB	MUL	DIV
2 *T*/*t*d - 1	-	-	1

5.5.4 Computation of Reference Currents ($i^*_{fa\,ref}$, $i^*_{fb\,ref}$, and $i^*_{fc\,ref}$)

Analysis of this section requires implementation of equation 5.30, which requires allocation of four new distinct variables, necessitating 4**float* memory ($i^*_{fa\,ref}$, $i^*_{fb\,ref}$, $i^*_{fc\,ref}$ and 1 temporary variable, accounting for 1 SUB). Calculations involved in computation of other elements of this equation have been performed already. The computational steps in this stage including 1 SUB required for the temporary variable are tabulated below:

Arithmetic operations			
ADD	SUB	MUL	DIV
6	1	9	-

The matrix in equation 5.30 is the transpose matrix of equation 5.27. Therefore, while implementing this equation no new memory is allocated for this stage as memory addressing mode is used to optimize the memory space as there were no distinct values involved.

5.5.5 Summary

The overall memory required and computational efforts involved are summarized in the Table given below.

Requirements	Quantification
ADD	2*T/t*d +12
SUB	2*T/t*d +3
MUL	22
DIV	1
MEMORY	(8*T/t*d +22) * *float*

5.6 COMPARATIVE ANALYSIS OF CONTROL THEORIES UNDER DIFFERENT SOURCE CONDITIONS

In this section, the performance of these control theories are quantified in terms of memory occupied and execution time involved. The *Big-O* analysis, which is generally used in solving a computer science problem when there are usually more than one method/ algorithm is available to solve a problem, is used here in MATLAB. The definition of *Big-O* analysis is that it measures the efficiency of an algorithm based on the time it takes for the algorithm to run as a function of the input size (here *td*). Finally, the performance of each control theory is represented in the form of a general polynomial, which can be analysed and compared based on the available microprocessor used for implementing the APF. Following cases are organized to analyze and compare the performance of these control theories in time and space domain:

- Case I: Comparison of control theories under balanced source voltage condition.
- Case II: Comparison of control theories under unbalanced source voltage condition.

5.6.1 Case I: Comparison of control theories under balanced source voltage condition

The overall comparison amongst the control theories is represented in the form of Tables given below.

Mathematical Operations											
ADD			SUB			MUL			DIV		
ISC	*p-q*	*d-q*	ISC	*p-q*	*d-q*	ISC	*p-q*	*d-q*	ISC	*p-q*	*d-q*
*T/t*d +3	*T/t*d +22	2*T/t*d +12	7	2	2*T/t*d +3	11	37	22	5	5	1

Memory		
ISC	p-q	d-q
(*T/t*d +12) * *float*	(*T/t*d +45) * *float*	(8*T/t*d +22) * *float*

Big-O Polynomial: With the help of the Table given above, the total execution time for a particular control theory to generate the ideal reference current using a particular processor is represented as its *Big O polynomial*, given as under:

- *Big-O (ISC):*

$$T_{total} = \left(\frac{T}{t_d}+3\right) \times T_{ADD} + 7 \times T_{SUB} + 11 \times T_{MUL} + 5 \times T_{DIV} \tag{5.31}$$

- *Big-O (p-q):*

$$T_{total} = \left(\frac{T}{t_d}+22\right) \times T_{ADD} + 2 \times T_{SUB} + 37 \times T_{MUL} + 5 \times T_{DIV} \tag{5.32}$$

- *Big-O (d-q):*

$$T_{total} = \left(\frac{2T}{t_d}+12\right) \times T_{ADD} + \left(\frac{2T}{t_d}+3\right) \times T_{SUB} + 22 \times T_{MUL} + 1 \times T_{DIV} \tag{5.33}$$

Overall the same is represented as:

$$\begin{bmatrix} Ttotal(Sym) \\ Ttotal(pq) \\ Ttotal(dq) \end{bmatrix} = \begin{bmatrix} \frac{T}{t_d}+3 & 7 & 11 & 5 \\ \frac{T}{t_d}+22 & 2 & 37 & 5 \\ \frac{2T}{t_d}+12 & \frac{2T}{t_d}+3 & 22 & 1 \end{bmatrix} \begin{bmatrix} T_{ADD} \\ T_{SUB} \\ T_{MUL} \\ T_{DIV} \end{bmatrix}$$

5.6.2 Case II: Comparison of control theories under unbalanced source voltage condition

The overall comparison amongst the control theories is represented in the form of Tables given below:

Mathematical Operations											
ADD			SUB			MUL			DIV		
ISC	*p-q*	*d-q*	ISC	*p-q*	*d-q*	ISC	*p-q*	*d-q*	ISC	*p-q*	*d-q*
5*T*/*t*d	5*T*/*t*d+31	2*T*/*t*d+12	10*T*/*t*d+15	10*T*/*t*d+10	2*T*/*t*d+3	24	50	22	11	12	1

Memory		
ISC	p-q	d-q
(13*T*/*t*d +31) * *float*	(13*T*/*t*d +62) * *float*	(8*T*/*t*d +22) * *float*

Big O Polynomial:With the help of the Table given above, the total execution time for a particular control theory to generate the ideal reference current using a particular processor is represented as its *Big O polynomial*, given as under:

- *Big-O (ISC):*

$$T_{total(sym)} = \left(\frac{5T}{t_d}\right) \times T_{ADD} + \left(\frac{10T}{t_d}+15\right) \times T_{SUB} + 24 \times T_{MUL} + 11 \times T_{DIV} \qquad (5.31)$$

- *Big-O (p-q):*

$$T_{total(p-q)} = \left(\frac{5T}{t_d}+31\right) \times T_{ADD} + \left(\frac{10T}{t_d}+10\right) \times T_{SUB} + 50 \times T_{MUL} + 12 \times T_{DIV} \qquad (5.32)$$

- *Big-O (d-q):*

$$T_{total}(d-q) = \left(\frac{2T}{t_d}+12\right)\times T_{ADD} + \left(\frac{2T}{t_d}+3\right)\times T_{SUB} + 22\times T_{MUL} + 1\times T_{DIV} \qquad (5.33)$$

Overall the same is represented as.

$$\begin{bmatrix} Ttotal(Sym) \\ Ttotal(pq) \\ Ttotal(dq) \end{bmatrix} = \begin{bmatrix} \frac{5T}{t_d} & \frac{10T}{t_d}+15 & 24 & 11 \\ \frac{5T}{t_d}+31 & \frac{10T}{t_d}+10 & 50 & 12 \\ \frac{2T}{t_d}+12 & \frac{2T}{t_d}+3 & 22 & 1 \end{bmatrix} \begin{bmatrix} T_{ADD} \\ T_{SUB} \\ T_{MUL} \\ T_{DIV} \end{bmatrix}$$

5.6.3 Case Study: Implementation of Control Theories on TMS320F28377S processor

The performance of the control theories in terms of their execution time is analyzed on TI processor - TMS320F28377S using Code Composer Studio (CCS) software. The Datasheet pertaining to TMS320C28x Floating Point Unit and Instruction Set are referred for understanding the instruction cycles involved. The results obtained by using the CCS on TMS320F28377S are summarized as under:

Operations	Instruction cycles	Execution time per cycle (1 clock = 5nsec)
ADD	6 clocks	T_{ADD} = 30nsec
SUB	6 clocks	T_{SUB} = 30nsec
MUL	6 clocks	T_{MUL} =30nsec
DIV	236 clocks	T_{DIV} = 1180nsec

5.6.3.1 *Big-O* polynomial for comparison of various theories under balanced source conditions

The performance of the control theories in terms of their execution time and memory requirement is analyzed on TI processor - TMS320F28377S. The results obtained in the MATLAB are plotted as Fig. 5.9 to 5.11.

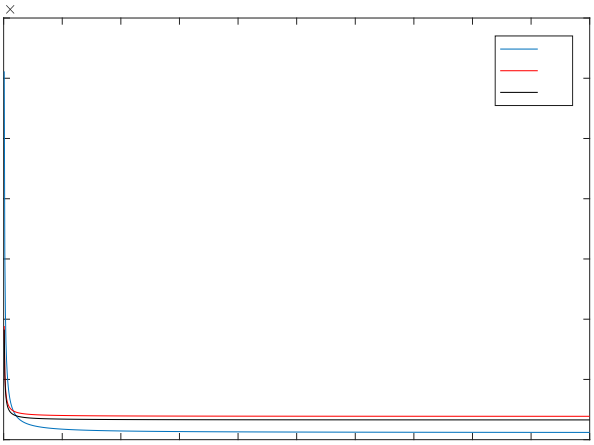

(a)

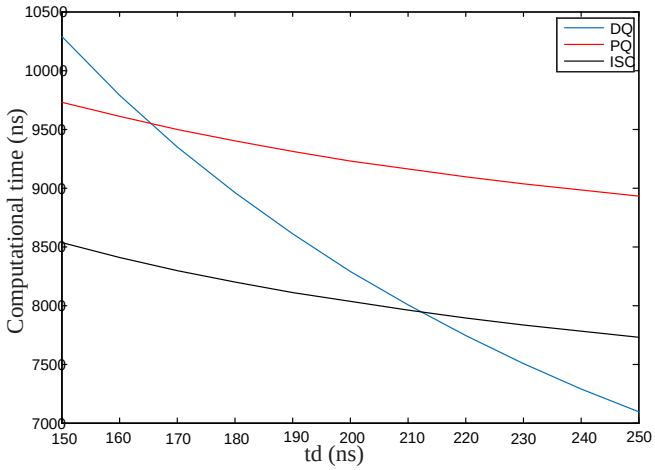

(b)

Fig. 5. 9 Graphs depicting nature of computational efficiency of control theories under balanced source voltage conditions (a) Overall performance (b) Intersection points

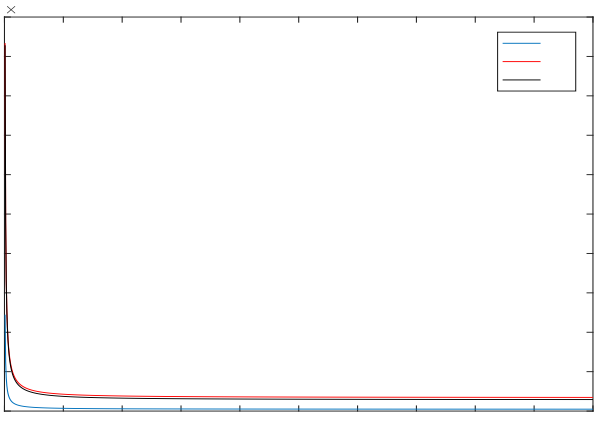

(a)

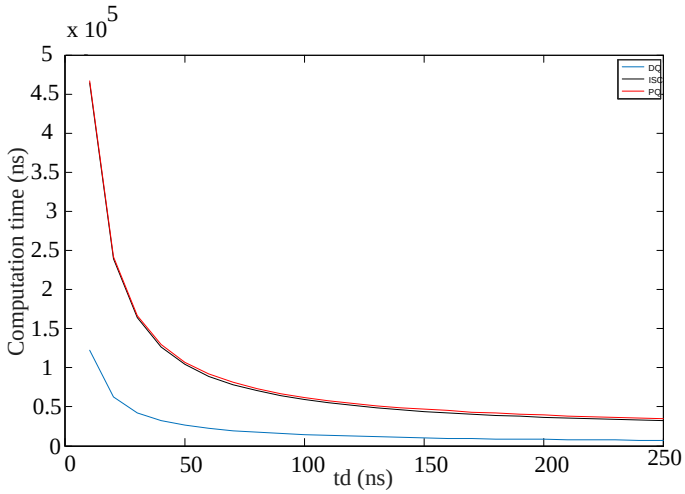

(b)

Fig. 5. 10 Graphs depicting nature of computational efficiency of control theories under unbalanced source voltage conditions; (a) Overall performance (b) Intersection points

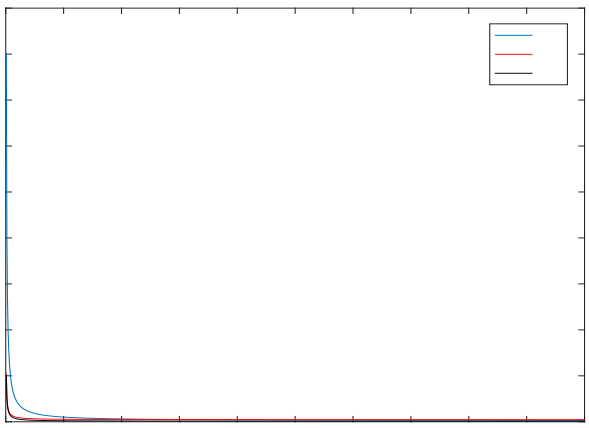

(a)

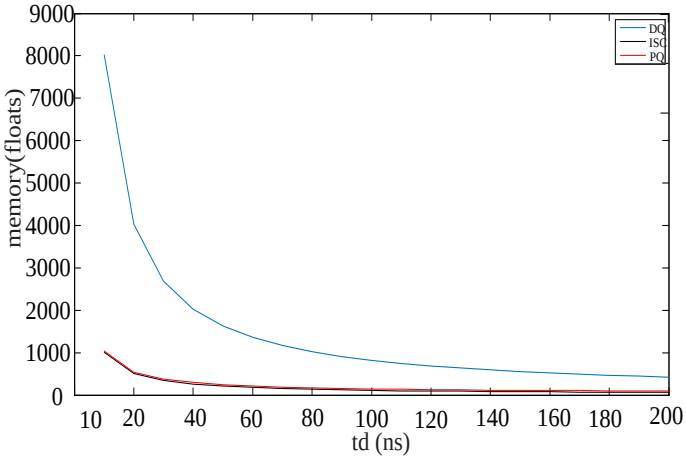

(b)

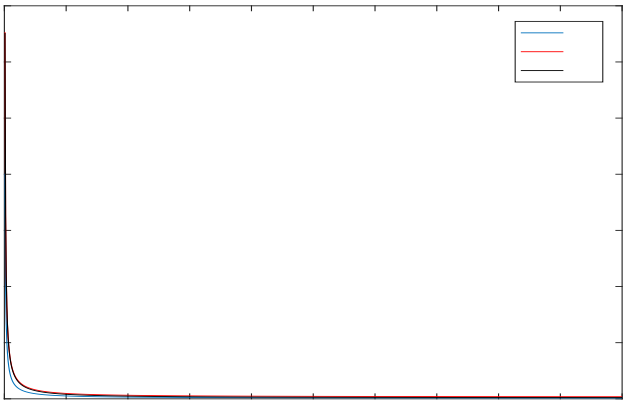

(c)

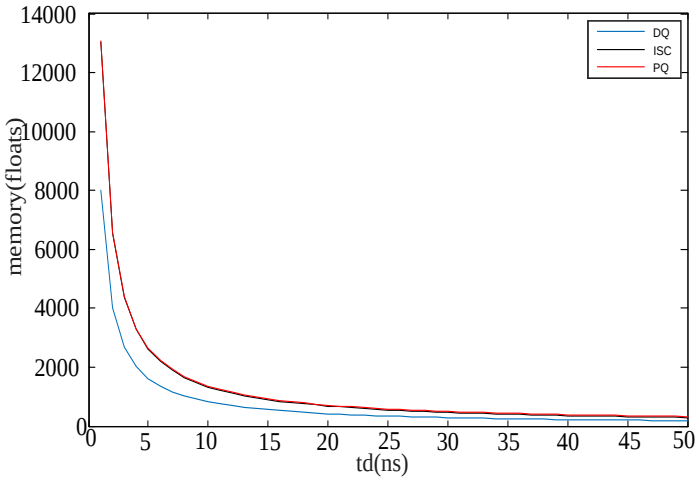

(d)

Fig. 5. 11 Graphs depicting nature of memory allocation for control theories (a) Overall performance under balanced source (b) Intersection of curves under balanced source (c) Overall performance under unbalanced source (d) Intersection of curves under unbalanced source

5.6.3.2 Results and Discussions

The nature of the computational efficiency versus discretisation time for different control theories is plotted in Fig. 5.9 and 5.10. The intersection of these curves as shown in Fig. 5.9(b) infers following:

- Below the discretisation time of 168ns, the computational efficiency of different theories according to their rank is enlisted below:

- ✓ Instantaneous Symmetrical component theory takes the lowest computational time in implementation, thereby having - Highest computational efficiency,
- ✓ *p-q* theory ranks next best in terms of computational efficiency,
- ✓ *d-q* theory takes higher computational time amongst all, thereby having- Lowest computational efficiency.

- Between the discretisation time of 168ns to 212 ns, the order of computational efficiency is:
  - ✓ Instantaneous Symmetrical component theory having - Highest computational efficiency,
  - ✓ *d-q* theory ranks next best in terms of computational efficiency,
  - ✓ *p-q* theory having - Lowest computational efficiency.
- For any case where the discretisation time is greater than 212ns, the order of computational efficiency is:
  - ✓ *d-q* theory ranks best in terms of computational efficiency having- Highest computational efficiency,
  - ✓ Instantaneous Symmetrical component theory ranks next best in terms of computational efficiency,
  - ✓ *p-q* theory having - Lowest computational efficiency.

In case of memory allocation under balanced voltage source, Fig. 5.11(a) and 5.11(b) infers that ISC theory has the lowest memory requirement. Memory requirement for implementing *p-q* theory is close to ISC theory. However, in case of *d-q* theory the memory requirement is highest.

In case of unbalanced voltage source, Fig 5.11(c) and 5.11(d), highlights that the memory requirement for implementing d-q theory is least against ISC and *p-q* theory, while after around 500ns of discretisation time, the difference is marginal in all the three theories.

5.7 CONCLUSIONS

In this chapter the three different control theories were formulated when used for generation of reference currents for shunt APF. The theories were compared wrt the discretisation time to generalize the differences amongst them. The comparative study on TI processor - TMS320F28377S processor brings out that for a filter current generation when discretisation time is low (implying high accuracy), ISC theory has the highest computational efficiency. However, for less demanded accuracy (a high discretisation time) *d-q* theory takes on the rest theories in computational speed. Also, on varying the source condition to unbalanced source, *dq* theory has highest computational speed amongst all, where computational speeds of ISC and p-q theory are nearly the same.

Similarly, the comparison of memory requirement in implementing the reference current generation algorithm under balanced source brings out ISC theory far superior than rest. However, in case of unbalanced source *dq* theory accrue more savings in memory from implementation point of view.

CHAPTER 6

SIMULATION STUDIES ON DSTATCOM USING DIFFERENT CONTROL THEORIES

In preceding chapter we have discussed the formulation of different control theories and their application in generation of ideal reference currents for a shunt APF. The preceding chapters, brings out a theoretical comparison amongst the theories, in specific to their performance in terms of computational time and memory. The present chapter focuses on implementation of these control theories on DSTATCOM with an aim to verify the goals of compensation achieved by the theories when implemented on a shunt APF under the same working conditions (designed parameters). Consequently, transient performance of the theories is also compared when implemented on time varying load, however, without DSTATCOM.

6.1 SIMULATION STUDIES

MATLAB simulink model of three phase DSTATCOM is as shown in Fig. 6.1 is developed to perform the simulation studies. The system parameters used for carrying out the studies are tabulated in Table 6.1. In order to verify the functionality of the control theories on the DSTATCOM, following objectives of compensation needs to be performed:

- The primary aim of compensation is to obtain the balanced source currents
- Source must supply the load active power and the losses of the DSTATCOM in Power factor correction (PFC) mode i.e $P_{lav} = P_{loss} = v_{sa}i^{*}_{la} + v_{sb}i^{*}_{lb} + v_{sc}i^{*}_{lc}$. In PFC mode the supply currents have zero phase shift wrt PCC voltage i.e $\beta = 0$. This also implies that the entire requisite reactive power demand of the load is met by the DSTATCOM
- In case of non-linear loads, harmonics reduction and neutral current elimination.

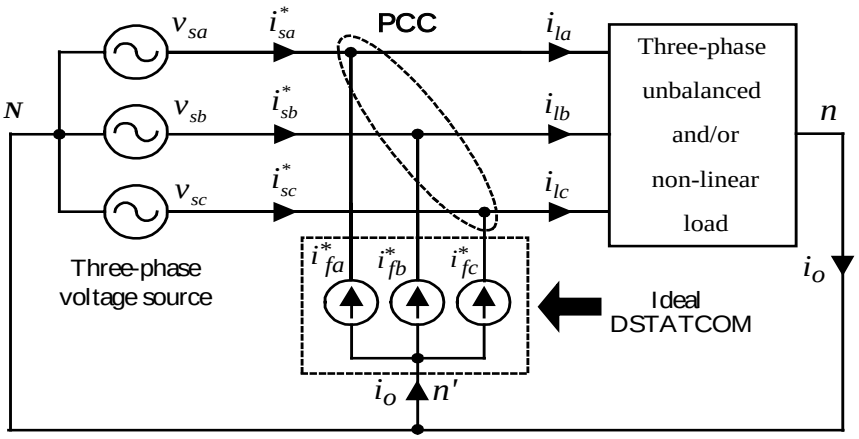

Fig. 6. 1 Schematic diagram of a DSTATCOM based three-phase four-wire compensated system

In order to obtain a comparative evaluation amongst the theories, following system conditions are considered and followed throughout, while simulating all the control theories on DSTATCOM.

- Three phase four wire system.
- Split capacitor, three leg VSI topology.

Table 6. 1 Simulation parameters

Source parameters	▪ V_{rms} (L-L) = 400 V, 50 Hz
Load parameters at 50Hz	▪ Unbalanced Load (phases *a*, *b* and *c*) 20+j15.8 Ω, 30+j20 Ω & 454+j18.85 Ω ▪ Non-Linear Load Three-phase Diode Bridge with load of R_L=30 Ω and L_L=40mH
Interface inductances	▪ L_f = 15 mH, ▪ R_f = 0.3 Ω (all phases)
VSI parameters	▪ $C_{dc1} = C_{dc2}$ = 3,300 µF ▪ V_{dcref} =1100 V
Hysteresis band	▪ 0.05 A
PI controller	▪ PI gains; Kp = 12, Ki = 0.02

- Fixed Hysteresis current control strategy. The schematic of the same is shown at Fig. 6.2. This is chosen because of following advantages:

  ✓ Simpler implementation

  ✓ Enhanced system stability

  ✓ Increased reliability

  ✓ Fast response.

A hysteresis band (± *h*) within which actual current has to be tracked is fixed to 0.05A. The narrower the band (smaller value of *h*) the more accurate is the tracking. But this also results in higher switching frequency, resulting higher switching losses.

- MAF is used to compute the average components of power or current components, whenever required.

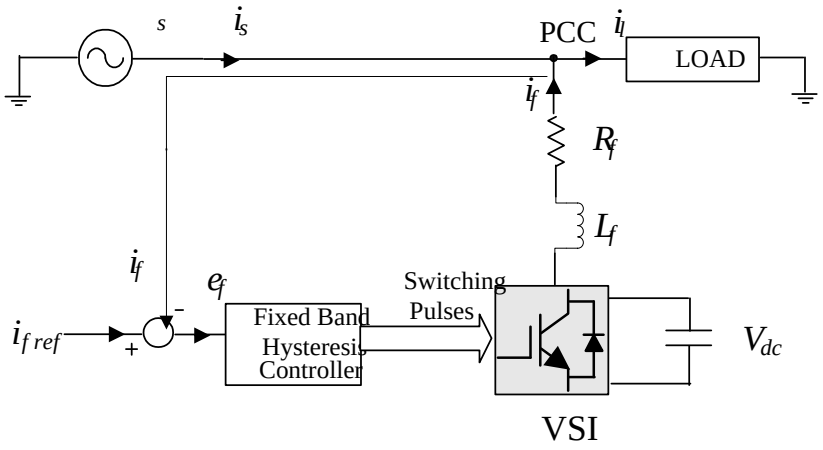

Fig. 6. 2 Block diagram of a fixed hysteresis band current controller

6.2 SIMULATION STUDIES OF ISC THEORY WHEN IMPLEMENTED ON DSTATCOM

Eqn. (5.4) used for reference current generation are modified to (6.1), in order to accommodate the active losses in the inverter (P_{loss}). Here the source power factor can

be set to any desired value. However, for simulation purpose the same has been taken as unity (γ=0). The reference shunt filter currents to be injected at the PCC for phases a, b and c is therefore given by,

$$\left.\begin{aligned} i_{fa\,ref} &= i_{la} - \frac{v_{sa} - v_{s0}}{v_{sa}^{\,2} + v_{sb}^{\,2} + v_{sc}^{\,2}} (P_{lav} + P_{loss}) \\ i_{fb\,ref} &= i_{lb} - \frac{v_{sb} - v_{s0}}{v_{sa}^{\,2} + v_{sb}^{\,2} + v_{sc}^{\,2}} (P_{lav} + P_{loss}) \\ i_{fc\,ref} &= i_{lc} - \frac{v_{sc} - v_{s0}}{v_{sa}^{\,2} + v_{sb}^{\,2} + v_{sc}^{\,2}} (P_{lav} + P_{loss}) \end{aligned}\right\} \quad (6.1)$$

The term P_{lav} in (5.3) is obtained using MAF of one cycle window to ensure good dynamic response as compared to low pass filters. P_{loss} is generated through a suiTable feedback control. Here this is achieved by using a simple proportional-plus-integral (PI) controller of the following form.

$$P_{loss} = K_p e_v + K_i \int e_v \, dt \quad (6.2)$$

where, $e_v = V_{dc\,ref} - V_{dc}$, $V_{dc\,ref}$ and V_{dc} are the values of the capacitor voltage reference and its value at the end of a cycle of phase-*a* system voltage respectively.

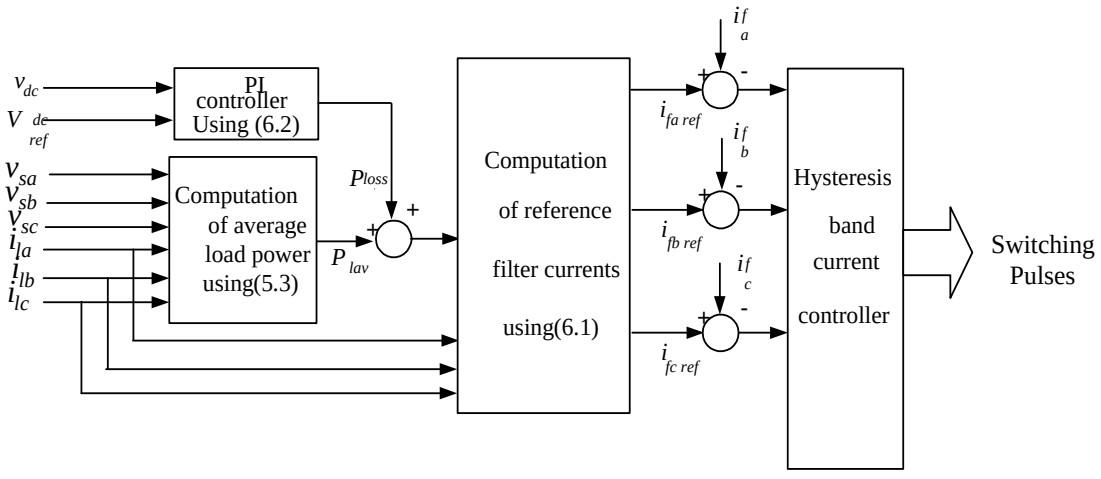

Fig. 6. 3 Overall block diagram for generation of switching pulses

Here the switching commands for the inverter switches are generated using hysteresis band current control method. The algorithm used for generating gating pulses for the VSI shown in Fig. 6.3 is as follows:

If $i_f \geq i_{f\,ref} + h$,

bottom switch is turned ON whereas top switch is turned OFF,

else if $i_f \leq i_{f\,ref} - h$,

top switch is turned ON whereas bottom switch is turned OFF,

else if,

maintain previous state,

end.

In order to achieve the objectives of compensation first an unbalanced linear load is compensated followed by a non-linear load. The simulation results obtained on compensation of both type of loads are given at Fig 6.4 and 6.5. The results elucidates that the primary aim of compensation has been met as shown in Fig 6.4(c) and Fig 6.5(c). In addition, unity power factor is also obtained.

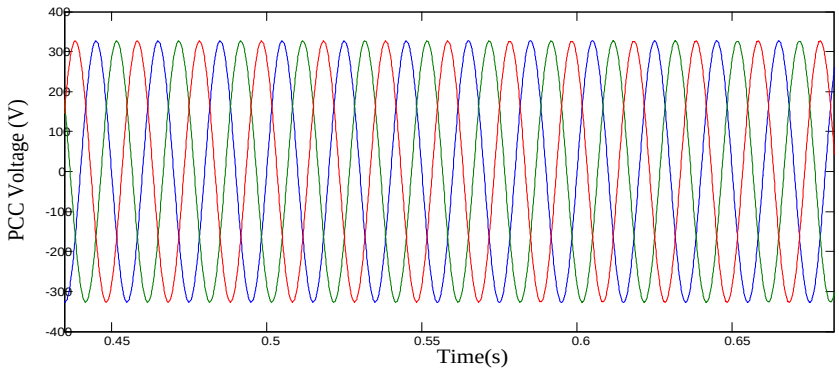

(a)

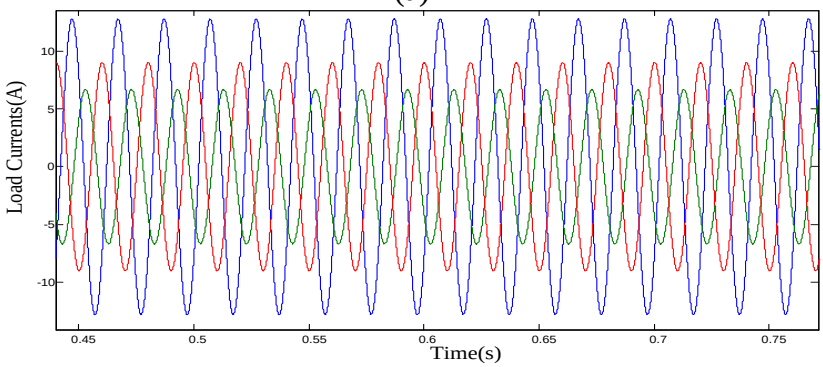

(b)

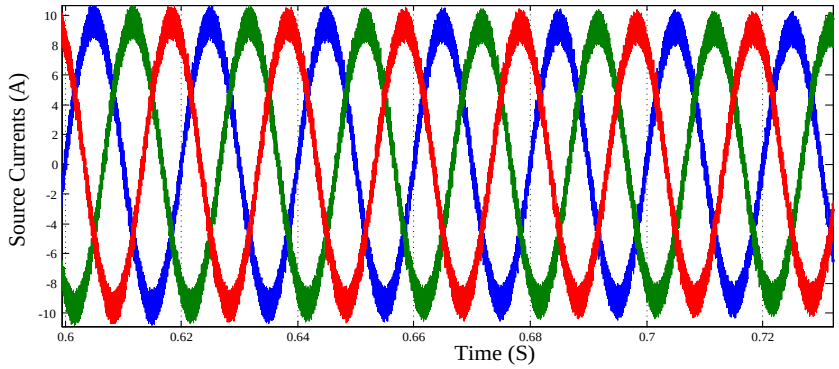

(c)

Fig. 6. 4 Simulation results for unbalanced load (a) Voltages at PCC (ii) Load currents (iii) Compensated Source currents

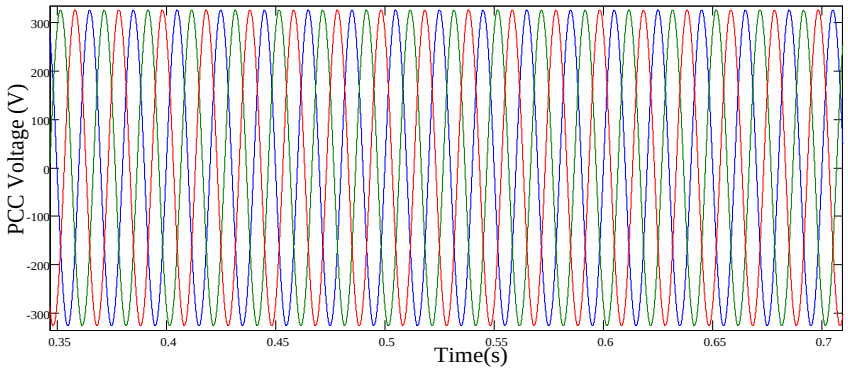

(a)

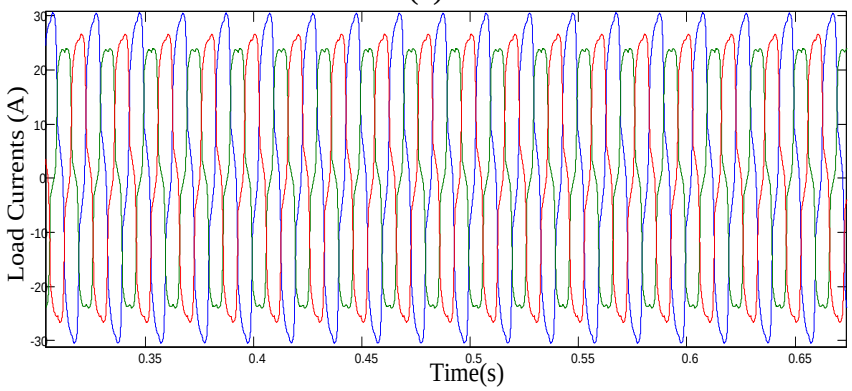

(b)

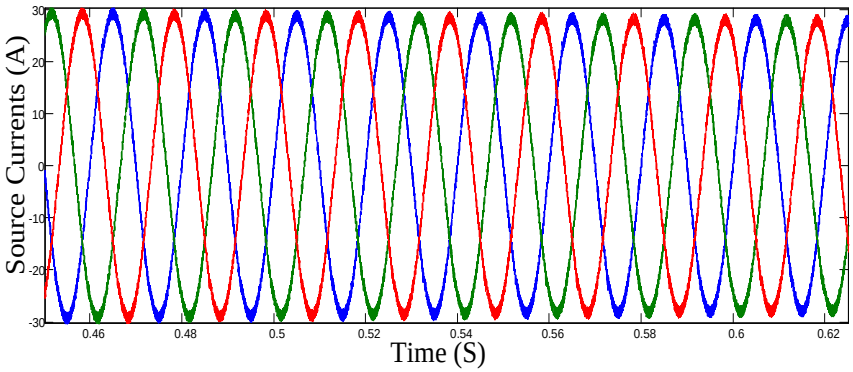

(c)

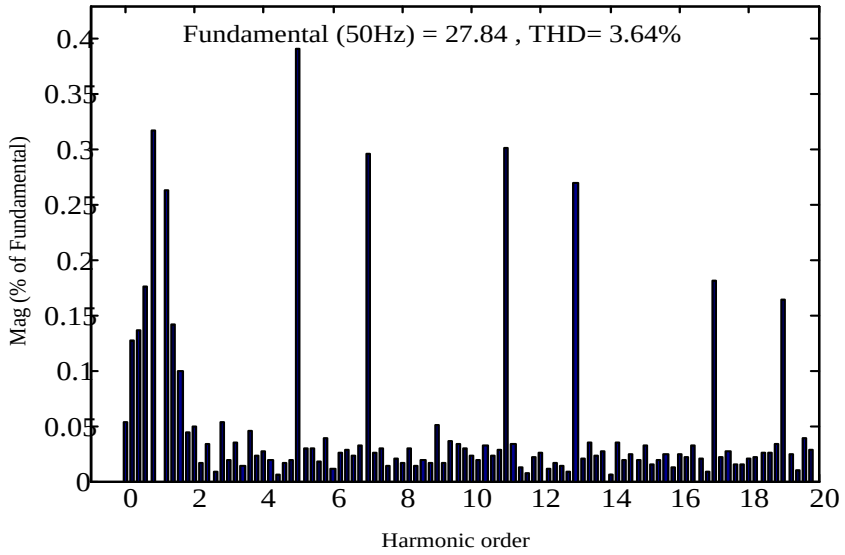

(d)

Fig. 6. 5 Simulation results for Non-Linear load (a) Voltages at PCC (b) Load currents (c) Compensated Source currents (d) THD in source current

6.3 SIMULATION STUDIES OF p-q THEORY WHEN IMPLEMENTED ON DSTATCOM

Keeping the simulation parameters same as what mentioned in Table 6.1 and the system conditions, the results obtained after implementing the *p-q* theory on DSTATCOM are given at Fig 6.6 and 6.7, respectively.

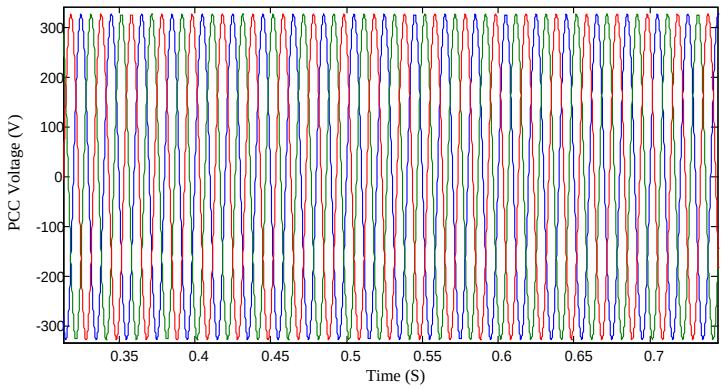

(a)

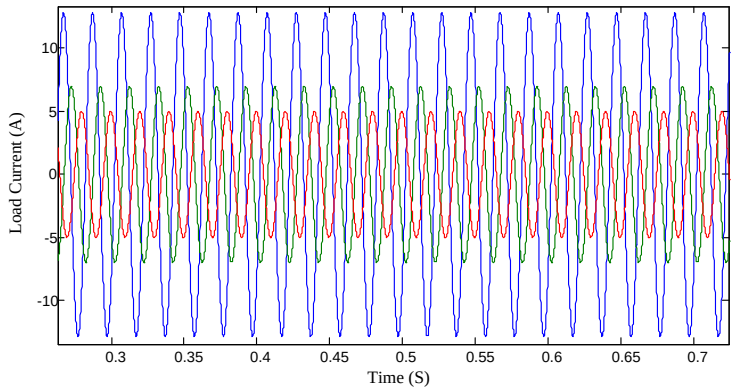

(b)

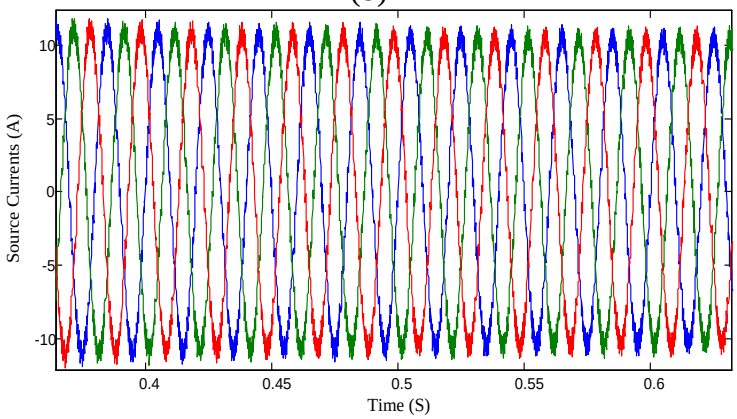

(c)

Fig. 6. 6 Simulation results for unbalanced load (a) Voltages at PCC (b) Load currents (c) Compensated Source currents

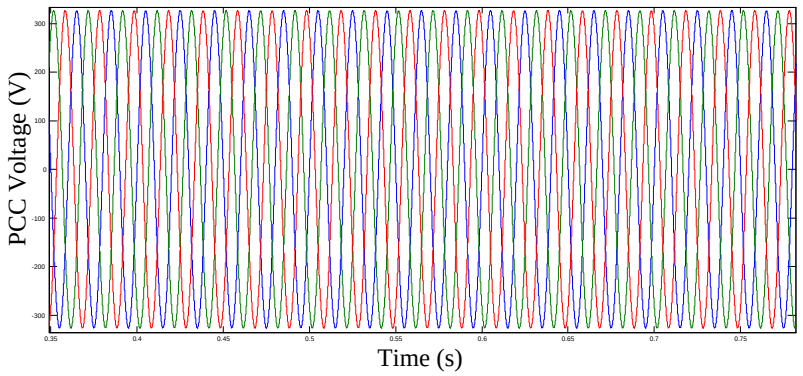

(a)

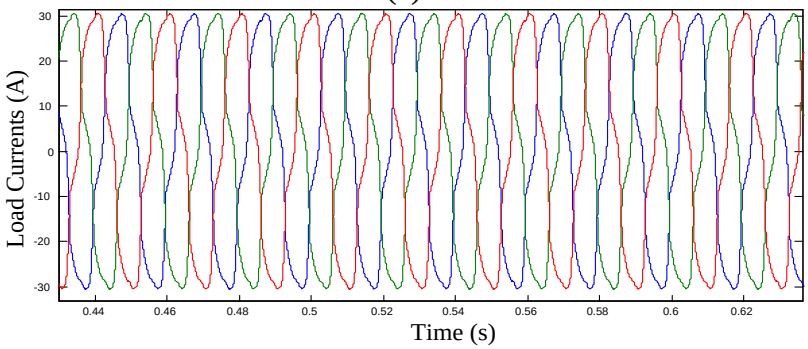

(b)

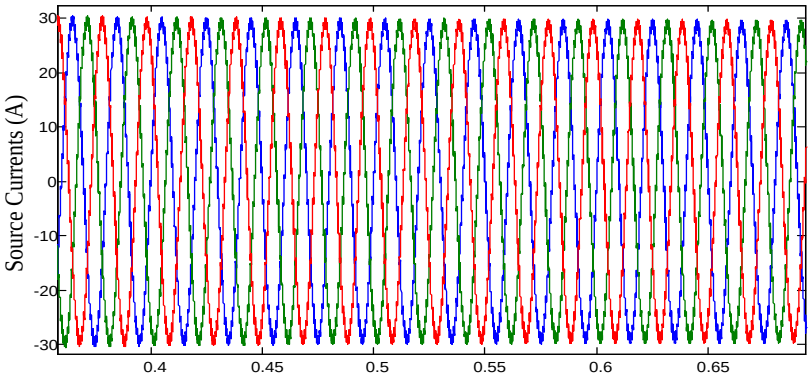

(c)

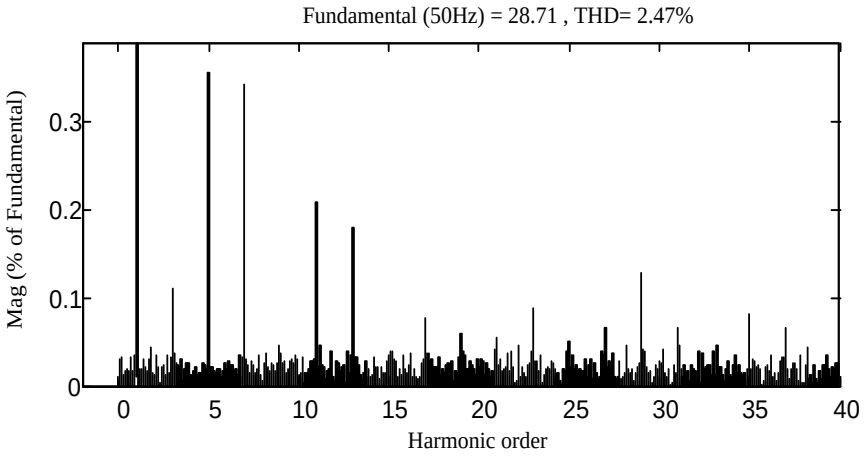

(d)

Fig. 6. 7 Simulation results for non-Linear load (a) Voltages at PCC (b) Load currents (c) Compensated Source currents (d) THD in source current

6.4 SIMULATION STUDIES OF d-q THEORY WHEN IMPLEMENTED ON DSTATCOM

Keeping the simulation parameters same as what mentioned in Table 6.1 and the system conditions, the results obtained after implementing the *d-q* theory on DSTATCOM are given at Fig 6.8 and 6.9, respectively. In addition a 3-phase PLL block is also used to derive the information of ' ωt ', used in Park's transformation matrix.

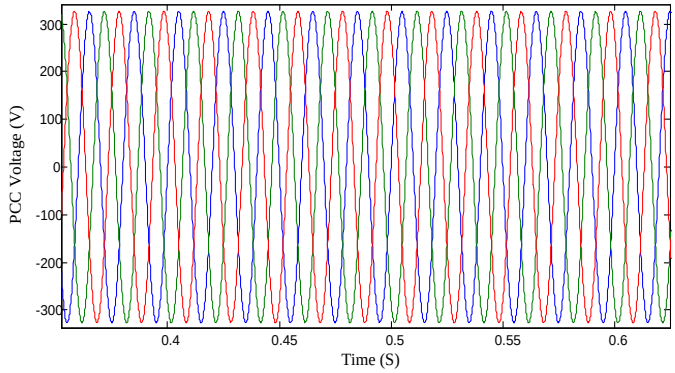

(a)

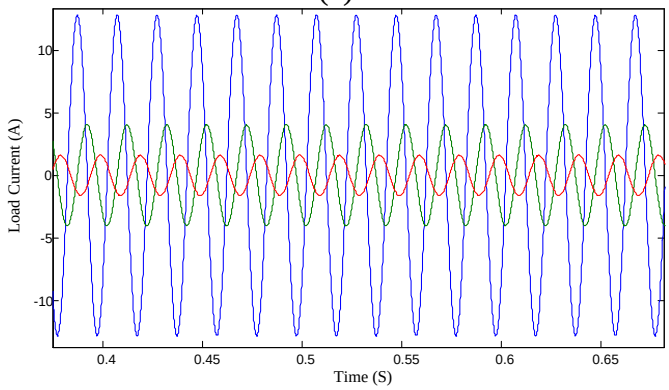

(b)

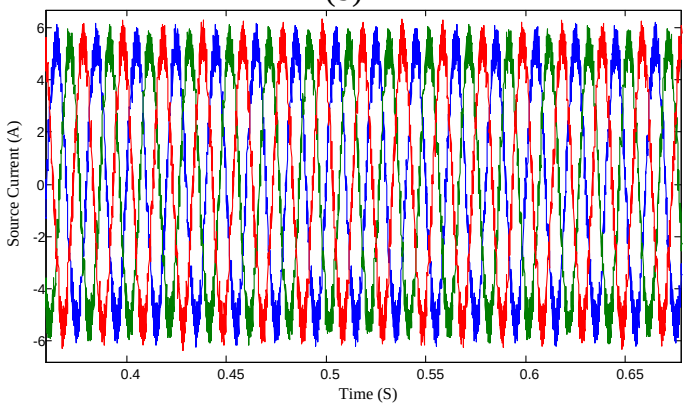

(c)

Fig. 6. 8 Simulation results for unbalanced load (a) Voltages at PCC (b) Load currents (c) Compensated Source currents

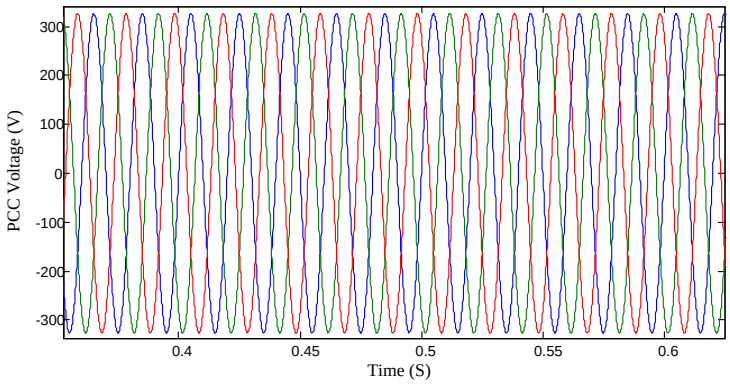

(a)

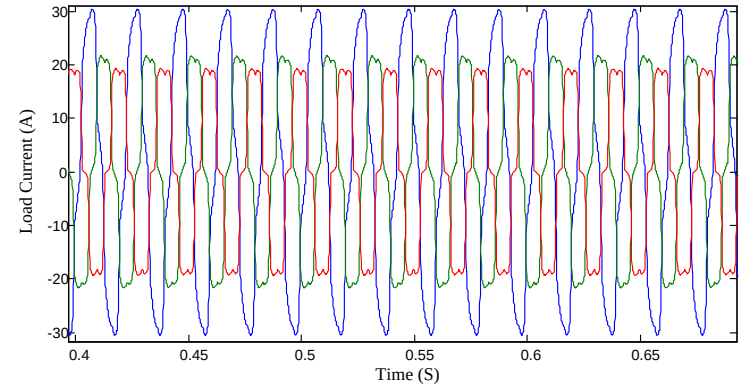

(b)

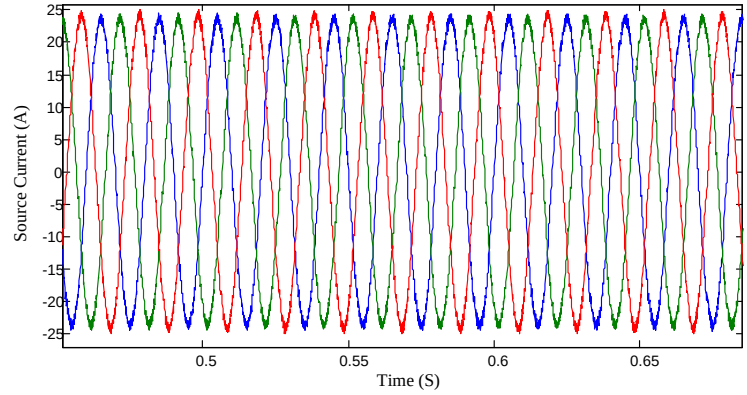

(c)

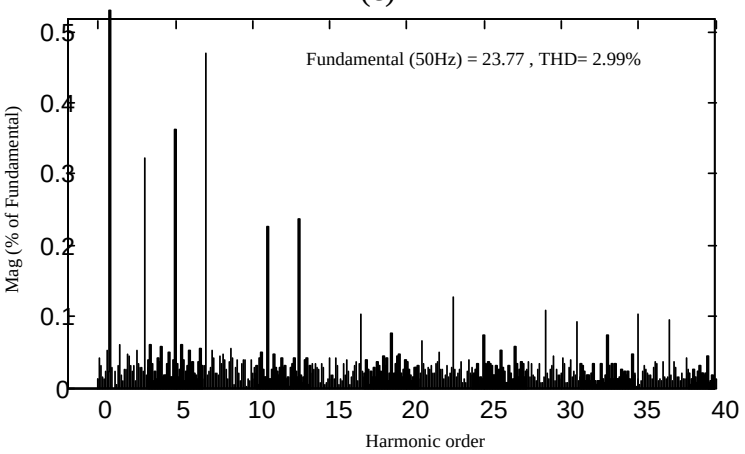

(d)

Fig. 6. 9 Simulation results for non-Linear load (a) Voltages at PCC (b) Load currents (c) Compensated Source currents (d) THD in source current

The % THD in the source current after compensation is tabulated in Table 6.2, which highlights that all the three theories have successfully restricted the harmonics within the stipulated limits if IEEE- 519.

Table 6. 2 %THD with and without compensation

%THD in source currents	ISC	*p-q*	*d-q*
Without compensation	13.93	13.93	13.93
With compensation	3.64	2.47	2.99

6.5 TRANSIENT PERFORMANCE ANALYSIS OF CONTROL THEORIES WHEN IMPLEMENTED AS SHUNT APF

In order to analyze the performance of the control theories with time varying loads a transient model of the load is simulated. As shown in Fig 6.10 step changes in load are introduced symmetrically each after 0.5ms and in a worst case one of the phase is open circuited at 1.5ms to analyze the transient performance.

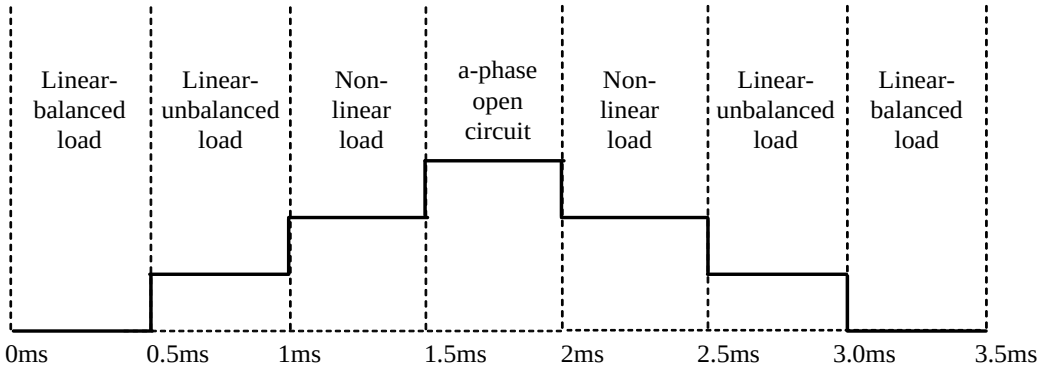

Fig. 6. 10 Step changes in load

6.5.1 Simulation Study of Time Varying Load with ISC Theory

Fig. 6.11 gives the transient performance of the ISC theory by introducing step changes in the load as per step changes in load.

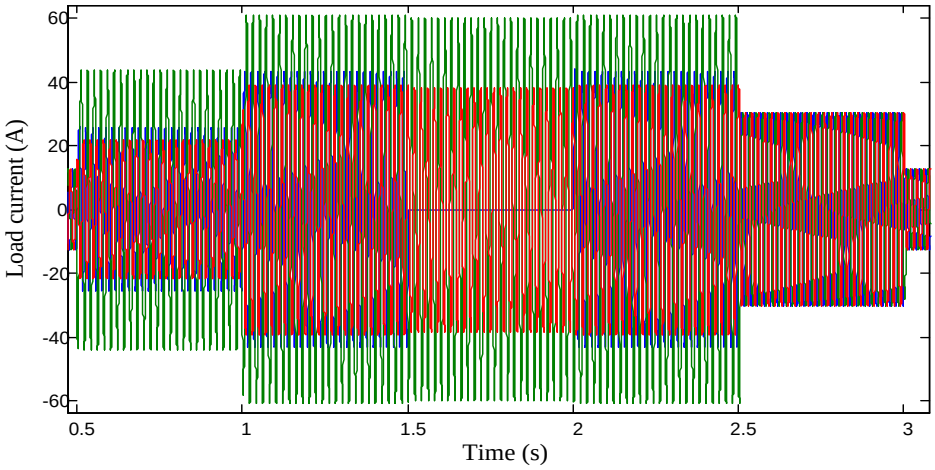
Load current (A)
Time (s)

(a)

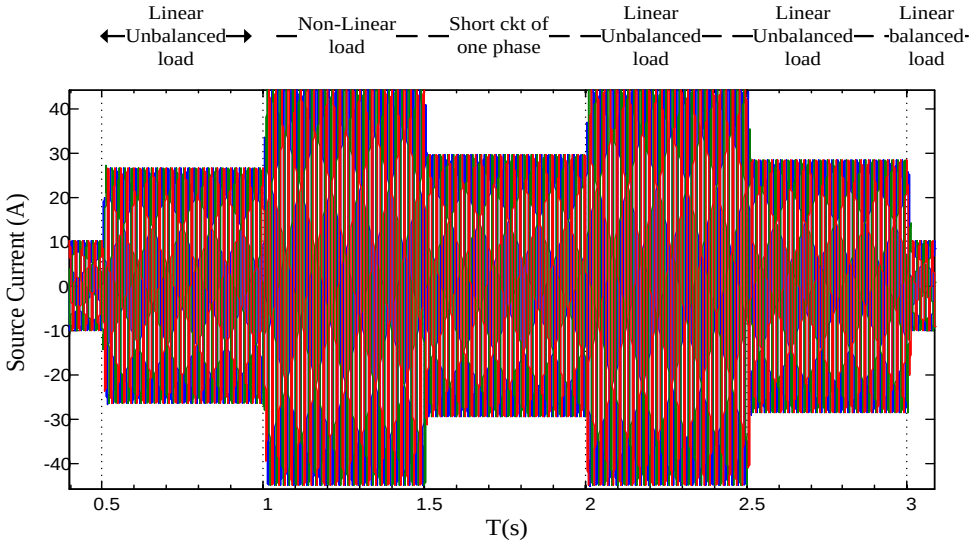
Linear Unbalanced load
Non-Linear load
Short ckt of one phase
Linear Unbalanced load
Linear Unbalanced load
Linear balanced load
Source Current (A)
T(s)

(b)

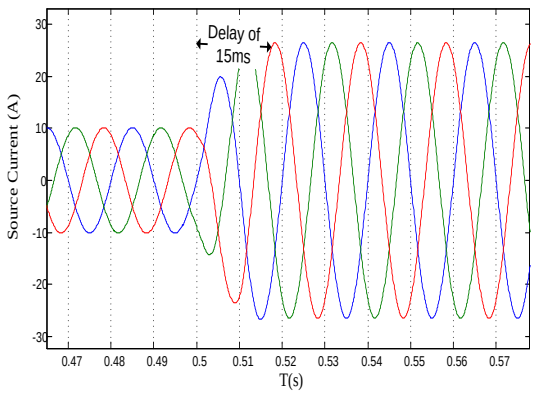
Delay of 15ms
Source Current (A)
T(s)

(c)

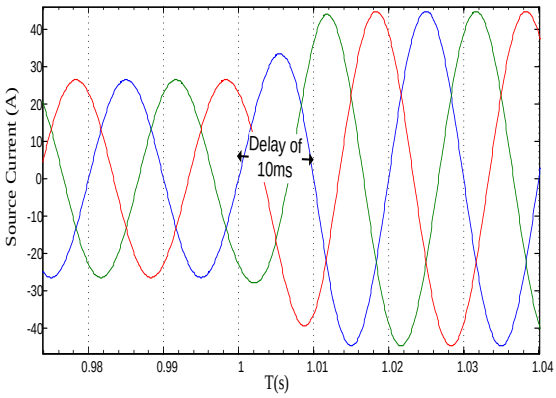
Delay of 10ms
Source Current (A)
T(s)

(d)

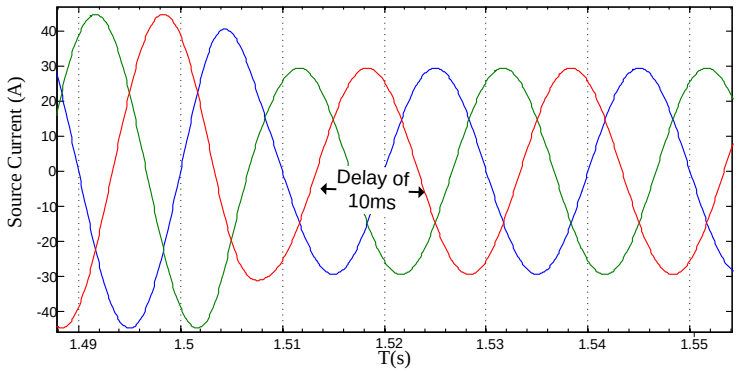

(e)

Fig. 6. 11 Transient response of time varying load (b) Overall response to step change (c) Response to linear, unbalanced load (d) Response to non linear load (e) Response to short circuit fault in one phase

6.5.2 Simulation Study of Time Varying Load with p-q theory

Fig. 6.12 gives the transient performance of the *p-q* theory by introducing step changes in the load as per Figure 6.10.

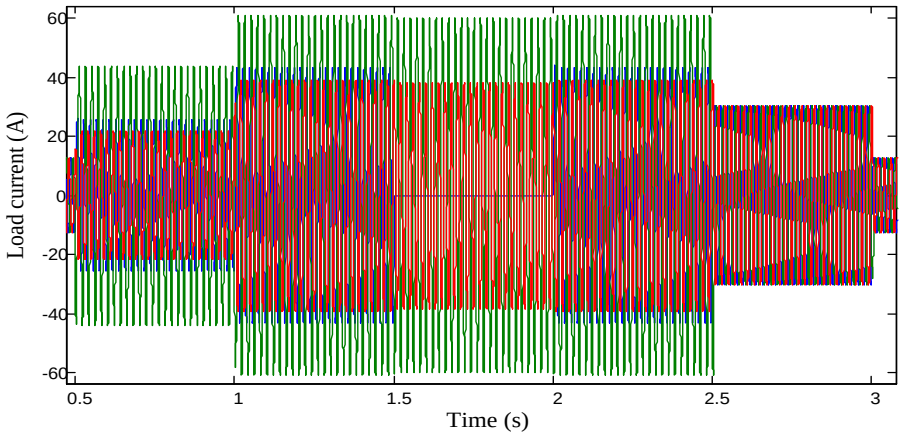

(a)

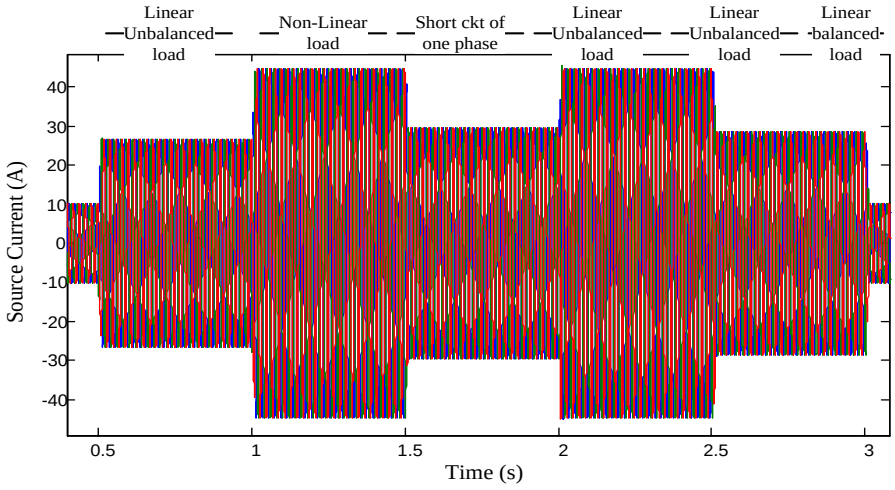

(b)

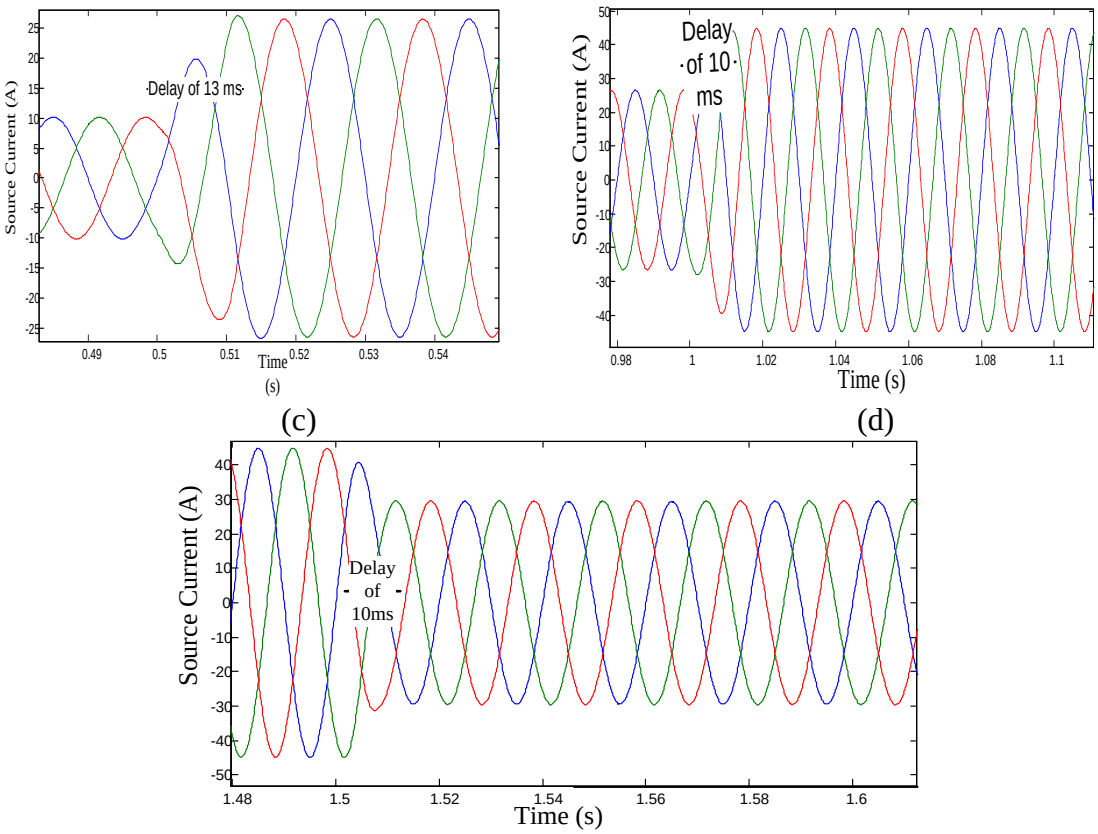

Fig. 6. 12 Transient response of time varying load with *p-q* theory(b) Overall response to step change (c) Response to linear, unbalanced load (d) Response to non linear load (e) Response to short circuit fault in one phase

6.5.3 Simulation Study of Time Varying Load with d-q theory

Figure 6.13 gives the transient performance of the *d-q* theory by introducing step changes in the load as per Figure 6.10.

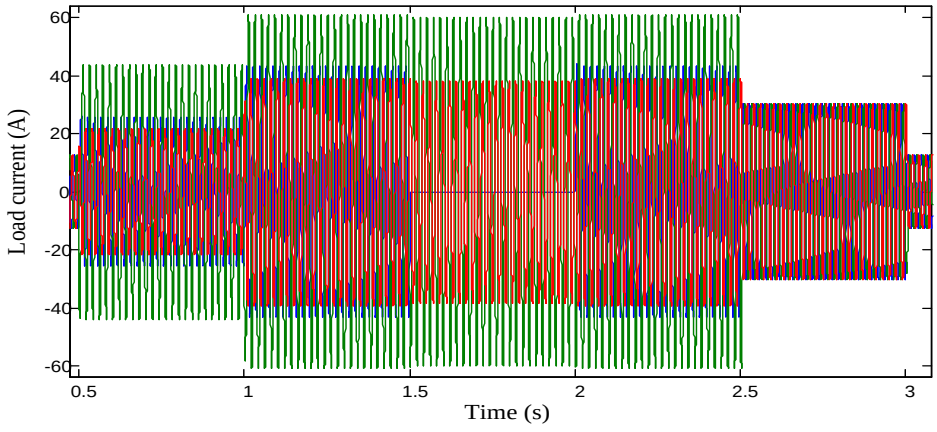

(a)

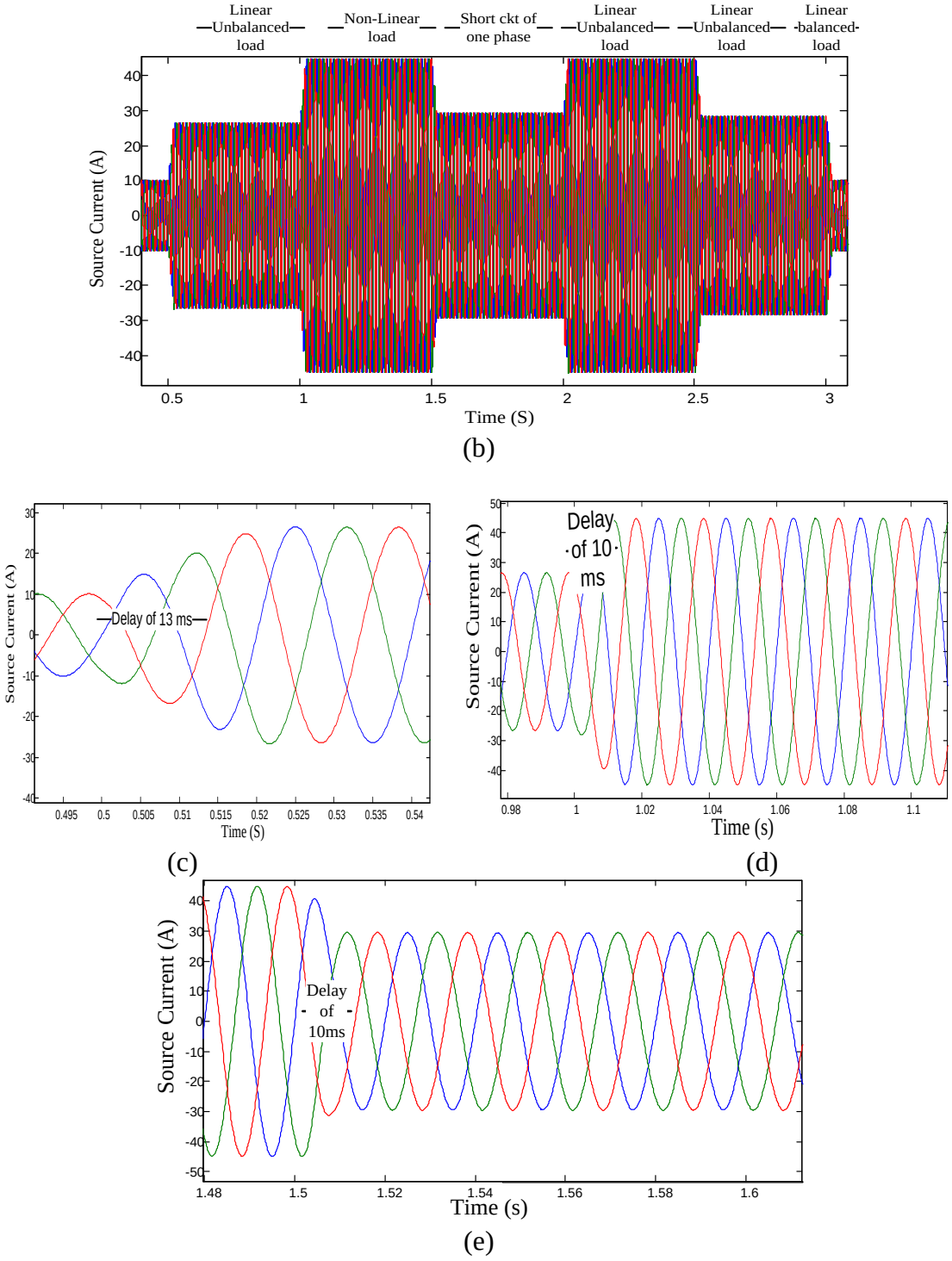

Fig. 6. 13 Transient response of time varying load with *d-q* theory(b) Overall response to step change (c) Response to linear, unbalanced load (d) Response to non linear load (e) Response to short circuit fault in one phase

The performance of the theories with a time varying load has been compared in terms of their response time to track the change and it was found that the transient response of the theories was instantaneous with a response time given in Table 6.3.

Table 6. 3 Comparative analysis with time varying load

Control theory	Response to step change from linear, balanced load to		
	Linear, unbalanced	Non linear	Short circuit in one phase
ISC	$\geq 10ms$	$\geq 10ms$	$\geq 10ms$
p-q	$\geq 10ms$	$\geq 10ms$	$\geq 10ms$
d-q	$\geq 20ms$	$\geq 20ms$	$\geq 20ms$

6.6 CONCLUSIONS

The performance of the control theories in achieving the compensation goals has been verified on DSTATCOM and compared with respect to the %THDs obtained. The three theories have successfully mitigated the harmonics in the load current to the stipulated limits. The transient performance of the theories was more or less same with a response time varying from 10 ms to 20 ms. The delay period due to the time taken in tracking the fundamental component will actually attribute in the equivalent amount of power dissipation in the inverter switches, when realized and therefore will result in certain percentage of power loss per load cycle.

CHAPTER 7

CONCLUSIONS

7.1 SUMMARY

Concerns of power quality problems, especially for sensitive loads are well known challenge for the power quality engineers. The integration of microgrid and renewable energy sources with the help of power converters is propounding this problem day by day. Thus, pushing us to know more about their control techniques so as to optimize their performance, both in terms of time and memory involved.

As part of the M.Tech project this thesis has described the need of understanding the existing control theories in a deeper sense and to present a comparative analysis in terms of their performance. The important results/ inferences drawn out of this work are enumerated as under:

- The performance of the theories is purely dependent on the discretisation time involved, which actually depends on the accuracy desired.

- In a practical case, where the grid is balanced and sinusoidal, the ISC theory performs far better than rest, both in terms of computational efficiency and memory requirement. However, when the scenario changes with unbalance and/ or distorted source supply, *dq* theory takes over the rest due to its inherent property of using PLL but the difference in terms of speed and memory requirement is marginal after certain discretisation time i.e, when accuracy is reduced.

- As far as the transient performance of the three theories is concerned, the performance found is more or less same with a delay varying from 10 ms to 20 ms.

7.2 SCOPE FOR FUTURE WORK

The comparative study of the control theories was performed for reference current generation for a shunt APF. However, the scope of future research which may be planned to:

- Optimization of selected signal processing algorithms related to specific applications for mitigating power quality problems on the lines of embedded system designing.

- The comparative study may be performed on other topologies of APF, like DVR and UPQC to derive overall better understanding in designing and optimizing an active filter for selected processor.

- The transient studies may be performed on various existing or modified practical filters to compute overall delay in response, thereby to deduce the equivalent amount of power dissipation occurred in the inverter switches and therefore the resulting power loss per load cycle.

- The scope of this comparative study on control theories may be increased to cover other modified versions of these theories or other harmonic extraction algorithms like, Non linear Least Squares Approach (NLS method).

APPENDIX "A"

A PROCESS OF POSITIVE SEQUENCE EXTRACTION [83]

The alternate method implemented in this thesis is described below. The positive sequence of source voltages can be extracted from the instantaneous source voltages by the following equation.

$$\begin{bmatrix} v_0 \\ v_1 \\ v_2 \end{bmatrix} = \frac{1}{\sqrt{3}} \begin{bmatrix} 1 & 1 & 1 \\ 1 & a & a^2 \\ 1 & a^2 & a \end{bmatrix} \begin{bmatrix} v_{sa} \\ v_{sb} \\ v_{sc} \end{bmatrix} \tag{A.1}$$

In case the source voltage has harmonics (or distortions) it would be imperative to extract the fundamental component of positive sequence for the implementation of control theories. For this the positive sequence voltages are inherently converted to *dq* reference frame and processed through a MAF to extract the fundamental part. This fundamental source voltage in *dq* frame is converted back to *abc* frame to finally obtain the fundamental positive sequence source voltage, via an indirect inverse matrix computation as described in succeeding equations.

$$v_1 = \frac{1}{\sqrt{3}}(v_a + a v_b + a^2 v_c) \tag{A.2}$$

$$Cal(i) = \frac{1}{\sqrt{3}} \underbrace{(v_{sa}(i) + a v_{sb}(i) + a^2 v_{sc}(i))}_{v^{+}_{sa}(i)} (\sin wt(i) + j \cos wt(i)) \tag{A.3}$$

(A.3) on simplification reduces to $Cal(i) = \frac{1}{\sqrt{2}}\left(v_d + j v_q\right)$, where

$$\begin{bmatrix} v_d \\ \\ v_q \\ \\ \end{bmatrix} = \sqrt{\frac{2}{3}} \begin{bmatrix} \cos\theta & \cos(\theta - 120^o) & \cos(\theta + 120^o) \\ \sin\theta & \sin(\theta - 120^o) & \sin(\theta + 120^o) \end{bmatrix} \begin{bmatrix} v_a \\ \\ v_b \\ \\ v_c \end{bmatrix} \tag{A.4}$$

This instantaneous positive sequence voltage in *dq* reference frame is paced through a MAF, if it has harmonics (distortions). The output of MAF is (A.5)

$$Cal(i)\_avg = \frac{1}{\sqrt{2}}\left(\bar{v}_d + j\bar{v}_q\right) \tag{A.5}$$

The output of (A.5) is devoid of any harmonics (distortions) and has the information of fundamental positive sequence of source voltages in *d-q* frame only. This is converted back to *abc* frame of reference for the implementation of control theories as shown below.

$$\begin{bmatrix} v_{sa} \\ v_{sb} \\ v_{sc} \end{bmatrix} = \sqrt{\frac{2}{3}} \begin{bmatrix} \cos\omega t & \sin\omega t \\ \cos(\omega t - 2\pi/3) & \sin(\omega t - 2\pi/3) \\ \cos(\omega t + 2\pi/3) & \sin(\omega t + 2\pi/3) \end{bmatrix} \begin{bmatrix} \bar{v}_q \\ \bar{v}_d \end{bmatrix} \tag{A.6}$$

Here,

$$v_a = \sqrt{\frac{2}{3}}\left(\bar{v}_q \cos\omega t + \bar{v}_d \sin\omega t\right) \tag{A.7}$$

$$v_a = \sqrt{\frac{2}{3}}(\sqrt{\bar{v}_d{}^2 + \bar{v}_q{}^2}\left(\frac{\bar{v}_q}{\sqrt{\bar{v}_d{}^2 + \bar{v}_q{}^2}}\cos\omega t + \frac{\bar{v}_d}{\sqrt{\bar{v}_d{}^2 + \bar{v}_q{}^2}}\sin\omega t\right) \tag{A.8}$$

$$v_a = \frac{2}{\sqrt{3}} M \sin(\omega t + \phi) \tag{A.9}$$

where,

$$M = \frac{1}{\sqrt{2}}(\sqrt{\bar{v}_d{}^2 + \bar{v}_q{}^2})$$

$$angle = \phi = \left(\sin^{-1}\frac{\bar{v}_q}{\sqrt{\bar{v}_d{}^2 + \bar{v}_q{}^2}}\right)$$

Re-writing the (A.9) for all the three voltage components in polar form gives (A.10).

$$\begin{bmatrix} \boldsymbol{v}_{sa}^{+} \\ \boldsymbol{v}_{sb}^{+} \\ \boldsymbol{v}_{sc}^{+} \end{bmatrix} = \frac{2}{\sqrt{3}} M \begin{bmatrix} \sin(\omega t + \phi) \\ \sin(\omega t - 120^{0} + \phi) \\ \sin(\omega t + 120^{0} + \phi) \end{bmatrix} \tag{5.16}$$

REFERENCES

[1] Santoso, Surya, and W. M. Grady, "Understanding Power System Harmonics. *IEEE Power Engineering Review*," vol. 21, no. 1, pp. 8-11, 2011.

[2] João Afonso, Carlos Couto, and Júlio Martins, "Active Filters with Control Based on the p-q Theory," *IEEE Industrial Electronics Society Newsletter,* Sept. 2000

[3] F.Z. Peng, "Harmonic sources and filtering approaches," *IEEE Industrial Application Magazine*, vol. 7, pp. 18-25, 2001.

[4] J.C. Das, "Passive filters –potentialities and limitations. *IEEE Transactions on Power Industry Application*," vol. 40, no. 1, pp. 232-241, 2004.

[5] H. Akagi**,** "Active harmonic filters," *Proceedings of the IEEE,* vol. 93, no. 12, pp. 2128-2141, 2005.

[6] B. Singh, V. Verma, A. Chandra, and K. Al Hadded, "Hybrid filters for power quality improvements," *IEE Proceedings – Generation, Transmission and Distribution,* vol. 152, no. 3, pp. 365-378, 2005.

[7] El-Habrouk, M. K. Darwish, and P. Mehta, "Active power filters: A review," *IEE Proceedings on Electrical Power Application,* vol. 147, no. 5, pp. 403-413, 2000.

[8] B. Singh, K. Al Hadded, and, A. Chandra, "A review of active filters for power quality improvement," *IEE Transactions on Industrial Electronics,* Vol. 46, no. 5, 1999.

[9] T.C. Green, and J.H Marks. "Control techniques for active power filters," *IEE Proceedings – Electric Power Application,* vol. 152, no. 5, pp. 369-381, 2005.

[10] Chennai Salim and Benchouia Mohamed Toufik, "Intelligent controllers for shunt active filter to compensate current harmonics based on SRF and SCR control strategies," *International Journal on Electrical Engineering and Informatics,* vol. 3, no. 3, 2011

[11] H. Akagi, Y. Kanazawa, and A. Nabae, "Instantaneous reactive power compensators comprising switching devices without energy storage components," *IEEE Trans. Ind. Applicat.,* vol. IA-20, pp. 625–630,1984.

[12] S. Bhattacharya, M. Divan, and B. Benerjee, "Synchronous reference frame harmonic isolator using series active filter," in Proc 4th Eur. Power Electron. Conf., Italy, vol. 3, pp. 30-35, 1991.

[13] S. Bhattacharya and D. Divan, "Synchronous frame based controller implementation for a hybrid series active filter system," *IEEE Conf. on Industry Applications*, Vol.4, pp no. 2531–2540, 1995.

[14] G.Arthy1, and Dr.C.N.Marimuthu, "Review of Digital control schemes for Active Power Filters," *IOSR-JECE*, pp. 53-62, 2001.

[15] M. Suresh, S.S.Patnaik, Y. Suresh and A.K. Panda, "Comparison of two tompensation tontrol strategies for shunt active power filter in three-phase four-wire system," *IEEE,* 2011.

[16] A. Ghosh and G. Ledwich, "Load compensating DSTATCOM in weak ac systems," IEEE Transactions on Power Delivery, vol. 18, no. 4, pp. 1302–1309, Oct. 2003

[17] A. Ghosh and A. Joshi, "A new approach to load balancing and power factor correction in power distribution system," IEEE Transactions on Power Delivery, vol. 15, no. 1, pp. 417–422, 2000.

[18] Y. Pal, A. Swarup and B. Singh, "A review of compensating type custom power devices for power quality improvement," *in proc of Joint International Conference on Power System Technology and IEEE Power India Conference, Power conf*, pp. 1-8, 2008

[19] N. Maruin, A. Alam, and S. Mahmod, and H. Hizam, "Review of control strategies for power quality conditioners," in *proc. of IEEE PECon 2004*, pp.109-115, Nov. 2004.

[20] L. Asiminoaei, F. Blaabjerg, and S. Hansen, "Detection is key-Harmonic detection methods for active power filter applications," *IEEE Ind. Appl. Mag.*, vol. 13, no. 4, pp. 22–33, Aug. 2007.

[21] Blajszczak, G "Non-active power compensation using time-window method," *Eur. Trans. Electr. Power Eng*, vol. 2. no. 5, pp.285-290, Sept/Oct. 1992.

[22] M.El-Habrouk, M. K Darwish and P. Mehta ''A survey of active filters and reactive power compensation techniques," in *proc. 8th lnt Conf on Power Electronics and Variabie Speed Drives, 2000, (IEE Conf Publ.No. 475)*, pp. 7-12, Sept. 2000.

[23] W. M. Grady, M. J. Samotyj, and A. H. Noyola, "Survey of active power line conditioning methodologies" *IEEE Trans on Power Delivery*, vol. *5*, no. 3, pp. 1536 - 1542, July 1990.

[24] M.El-Habrouk and M. K. Darwish "Design and implementation of a modified Fourier analysis harmonic current computation technique for power active filters using DSPs," *IEE Proceedings- Electric Powcr Applications*, vol. 148, no. 1, pp. 21 - 28, Jan. 2001.

[25] M. K.Mishra, A. Ghosh, and A. Joshi, “Operation of a DSTATCOM in voltage control mode,” *IEEE Tran. Pow .Del*., vol. 18, pp.258-264, Jan.2003.

[26] D. A. Marshal and J. D. van Wyk, “An evaluation of the real-time compensation of fictitious power in electric energy networks”, *IEEE Transaction on Power Delivery*, vol. 6. no. 4. pp. 1774-1780, October 1991.

[27] A. Nabae, H. Nakano and S. Togasawa, “An instantaneous distortion current compensator without any coordinate transformation,” in *Proc. IEEJ Int. Power Electro. Conf. (IPEC-Yokohama),* pp. 1651-1655, 1995.

[28] H. Akagi, S. Ogasawara, and H. Kim “The theory of instantaneous power in three-phase four-wire systems: A comprehensive approach,” in *proc. of Industry Application Conf. 34th IAS Annual Meeting*, vol. 1, pp. 431-439, 1999.

[29] M. T. Haque, S. H. Hosseini and T. Ise, “A control strategy for parallel active filters using extended p-q theory and quasi instantaneous positive sequence extraction method,” in *proc. ISIE. Puson, Korea.* pp. 348-353, 2001.

[30] H. Kim and H. Akagi, “The instantaneous power theory on the Rotating p-q-r Reference Frame,” *IEEE 1999 Int. Conf. On Power EIectronics and Drive Systems, PEDS,* Hong Kong, pp. 422- 427, *1999.*

[31] S. Bhattacharya. D. M. Divan and B. Banerjee, “Synchronous frame harmonics Isolator using active series filter,” *European Power Electronics Conf. EPE 1991* ,vol. 3, pp. 30-35, Fircnzi, Italy.

[32] V. Soares. P. Verdelho, C. D. Marques, “Active power filter control circuit based on the instantaneous active and reactive current id-iq method”, *Power Elecfronrcs Specialists Conference. PESC ‘91*. St Louis. Missouri, pp. 1096-1101, 1997.

[33] *G.* W. Chang, “A new method for determining reference compensating currents of the three-phase shunt active power filter,” *IEEE Power Engineering Review,* pp, 63-65, March 2001.

[34] C. L. Chen, C. E. Lin, C. L. Huang, “The reference active source current for active power filter in an unbalanced three-phase power system via the synchronous detection method,” *in Conf Proc. IMTU 94.*, vol.2, pp. 502-505, 1994.

[35] C. E. Lin, C. L. Chen, and C. L. Huang, “Calculating approach, implementation for active filters in unbalanced three-phase system using synchronous detection method,” in *Proc. IEEE IECON'92,* pp. 374-380, 1992.

[36] L. F. C. Monteiro, M. Aredes, J. A. Moor Neto, “A control strategy lor unified power quality conditioner,” *in IEEE int. Symp. on Industrial Elecrronics. 2003,* vol. 1, pp.391-396, 2003.

[37] P. Li, Y. H. Yang; Z. Ma, H. Li, “The study and simulation verifying of the controlling signal detecting method about UPQC,” in Proc. 6th Int. Conf. on Electrical Machines and systems, vol. 2, pp 657-660, 2003.

[38] S Bhattachaya, and A. Vellman. D. M. Divan, R. D. Lorenz, “Flux-bascd active filter controller,” *IEEE Transaction on Industrial Applications,* vol. 32, no. 3, pp. 491-502, 1996.

[39] J. H. R Enslin, J. D. Van Wyk, “A new control philosophy for power electronic converters as fictitious power compensators,” *IEEE Transaction on Power Electronics.* vol. 5, no. 1, pp 88-97, Jan. I990.

[40] S. Luo, Z. Hou “An adaptive detecting method for harmonic and reactive currents” *IEEE Trans. on Industrial Electronics,* vol. 42, no. 1, pp. 85–89, Feb. 1995.

[41] H. Karimi, M. Karimi-Ghartemani. M. R. Iravani, A. R Bakhshai. “An adaptive filter for synchronous extraction of harmonics and distortions,” *IEEE Transactions an Power Delivery,* vol. 18, no. 4, pp. 1350-1356, Oct. 2003.

[42] A. Abellan. G. Garccra, M. Pascual, E. Figucrcs, “A new current controller applied to Four-brach inverter shunt activc filters with UPF control method,” *IEEE 32nd AnnuaI Power Elccrronics Specialist Conference, 2001,* vol. 3. pp. 1402-1407.

[43] C. Y. Hsu, H. Y. Wu, “ A new single-phase active filter with reduced energy storage capacity,” *IEE proc. Electric Power Applications,* vol. 143, no. 1, pp. 25-30, Jan 1996.

[44] R. Kazemzadeh “Sigma-delta modulation applied to a 3-phase shunt active power filter using compensation with instantaneous power theory,” in *proc of IEEE international conference on Computer and Automation Engineering*, 2010, vol. 5, pp. 88-92.

[45] E. Wiebe-Quintana, J. L. Duran-Gomez, P. R. Acosta-Cano, “Delta-Sigma Integral Sliding-Mode Control Strategy of a Three-Phase Active Power Filter using d-q Frame Theory,” in proc. *of IEEE conf on Electronics, Robotics and Automotive Mechanics,* pp. 291-298, 2006.

[46] R. Zahira and A. P. Fathima, “A technical survey on control strategies of active filter for harmonic suppression,” in *proc of ICCTSD 2011, procedia Engineering*, vol. 30, pp. 686-693, 2012.

[47] M. Fatiha, M. Mohamed and A Nadia, “New hysteresis control band of an unified power quality conditioner,” in *Electric Power System Research*, vol. 81, pp. 1743-1753, 2001.

[48] M. Suresh, A. K. Panda, S. S. Patnaik and Y. Suresh, “Comparison of two compensation control strategies for SHAF in 3ph 4wire system By using PI controller,” in *proc. of the IICPE 2010*, pp. 1-7, 2012.

[49] M. Suresh, A. K. Panda , "Instantaneous Active and Reactive Power and Current Strategies for Current Harmonics Cancellation in 3-ph 4-Wire SHAF with Both PI and Fuzzy Controllers," *Journal of energy and power engineering* vol. 3, pp.285-298, 2011.

[50] S. Mikkili, A. K. Panda "PI and Fuzzy Logic Controller based 3-phase 4-wire Shunt active filter for mitigation of Current harmonics with Id-Iq Control Strategy," *Journal of power Electronics (JPE),* vol. 11, no. 6, Nov. 2011.

[51] S. K. Jain, P. Agarwal and H. O. Gupta, "Fuzzy Logic Controlled Shunt Active Power Filter for Power Quality Improvement," *IEEE Proceedings of Electric Power Applications*, vol. 149, no. 5, pp. 317-328, 2002.

[52] Z. Changjiang *et al*. "Dynamic voltage restorer based on voltage-spacevector PWM control," IEEE Trans. on Ind. Application vol.37, pp.1855-1863, Dec. 2001.

[53] R. R. Errabelli, Y. Y. Kolhatkar and S. P. Das, "Experimental investigation of sliding mode control of inverter for custom power applications," in *Proc.IEEE PES General Meeting*, pp. 1-8, June2006.

[54] G. Ledwich and A. Ghosh, "A flexible DSTATCOM operating in voltage or current control mode," Proc. *IEE Generation, Transmission and Distribution*, vol. 149, pp.215-224, March 2002.

[55] S. Bhattacharya and D. M. Divan, "Hybrid series active/parallel passive power line conditioner with controlled harmonic injection," U.S. Patent 5 465 203, Nov. 1995.

[56] C. K. Sao, P. W. Lehn, M. R. Iravani and J. A. Martinez, "A benchmark system for digital time-domain simulation of a pulse-width-modulated D-STATCOM," *IEEE Trans. Pow. Del*., vol. 17, pp. 1113-1120, Oct. 2002.

[57] B. Singh, S. S. Murthy and S. Gupta, "STATCOM-based voltage regulator for self-excited induction generator feeding nonlinear loads," *IEEE Transaction on Industrial Electronics*, vol. 53, issue 5, pp. 1437-1452, 2006.

[58] B. Singh, K. Al Haddad and A. Chandra, "Harmonic elimination, reactive power compensation and load balancing in three-phase, four wire electric distribution systems supplying non-linear loads," Electric Power Systems Research , vol. 44, pp. 93–100, 1998.

[59] A. Banerji, S. K. Biswas and B. Singh, "DSTATCOM control algorithms: A review," *International Journal of Power Electronics and Drive System (IJPEDS)* vol.2, no.3, pp. 285-296, September 2012.

[60] B. Singh, S.S. Murthy and S. Gupta, "STATCOM-based voltage regulator for self-excited induction generator feeding nonlinear loads", *IEEE Transactions on Industrial Electronics*, vol. 53, no. 5, October 2006.

[61] B. Singh, S. S. Murthy and S. Gupta, “Modelling of STATCOM based voltage regulator for self-excited induction generator with dynamic loads,” in *proc. of IEEE int. conf. on PEDES ’06*, pp.1-6, 2006

[62] A. Chandra, B. Singh, B. N. Singh and K. Al-Haddad, “An improved control algorithm of shunt active filter for voltage regulation, harmonic elimination, power-factor correction, and balancing of nonlinear loads”, *IEEE Transactions On Power Electronics*, vol. 15, no. 3, pp. 495-507, May 2000.

[63] B. Singh, K. Al Haddad and A. chandra, “A new control approach to three-phase active filter for harmonics and reactive power compensation”, *IEEE Transactions on Power Systems*, vol. 13, no. 1, pp. 133-138, February 1998.

[64] Y. K. Chauhan, S. K. Jain, and B. Singh, “A prospective on voltage regulation of self-excited induction generators for industry applications,” *IEEE Transactions On Industry Applications*, vol. 46, no. 2, pp. 720-730, march/april 2010.

[65] B. K. Bose “An adaptive hysteresis-band current control technique of voltage-fed PWM inverter for machine drive system,” *IEEE Transaction on Industrial Electronics*, vol.337, no.5, pp.402-406, October 1990.

[66] M. Kale and E. Ozdemir, “A novel adaptive hysteresis band current controller for shunt active power filter” *Electric Power Systems Research*, vol. 73, Issue 2, pp 113-119, February 2005.

[67] B.S. Rajpurohit and S.N. Singh “An efficient adaptive hysteresis band current controller for active power filters”, *IEEE-Bangalore Secton-15th Annual Symposiium on Technological Advances and IT Applications for Indian Power Sector*, Nov. 2006.

[68] B.S. Rajpurohit and S.N. Singh “Performance evaluation of current control algorithms used for active power filters”, in *proc of EUROCON 2007, The International Conference on “Computer as a Tool”*, pp. 2570-2575, 2007.

[69] S. R. Prusty, S. K. Ram, B. D. Subudhi and K. K. Mahapatra, “Performance analysis of adaptive band hysteresis current controller for shunt active power filter” in *proc. of IEEE int conf on Emerging Trends in Electrical Computer Technology (ICETECT)*, pp. 425-429, 2011.

[70] V. Khadkikar, M. Singh, Chandra A and B. Singh, “Implementation of single-phase synchronous d-q reference frame controller for shunt active filter under distorted voltage conditioner, ” In *Proc. of Int. Conf. on Power Electron. Drives and Energy syst.*, pp. 1-6, 2010.

[71] Anzari M, R. Chandran and A. Kumar R, “Single-phase shunt active power filter using indirect control method,” *Advance in Electronic and Electric Engineering*, vol. 3, no. 1, pp. 81-90, 2013.

[72] A. Ghosh, A. K. Jindal and A. Joshi, “Inverter Control Using Output Feedback for Power Compensating Devices,” in *Proc. TENCON 2003*, vol. 1, pp.48-52, Oct.2003.

[73] A. Ghosh and G. Ledwich, “Characterization of electric power,” in *Power quality enhancement using custom power devices*. Kluwer Academic Publishers, 2002.

[74] P. Rodriguez, A. Luna, R. Mun andoz Aguilar, I. Etxeberria-Otadui, R. Teodorescu, and F. Blaabjerg, “A stationary reference frame grid synchronization system for three-phase grid-connected power converters under adverse grid conditions,” Power Electronics, IEEE Transactions on, vol. 27, no. 1, pp. 99 –112, Jan. 2012.

[75] M. Schonardie and D. Martins, “Three-phase grid-connected photovoltaic system with active and reactive power control using dq0 transformation,” in Power Electronics Specialists Conference, 2008. PESC 2008. IEEE, June 2008, pp. 1202–1207.

[76] W. C. Duesterhoeft, M.W. Schulz, and E. Clarke, “Determination of instantaneous currents and voltages by means of alpha, beta, and zero components,” American Institute of Electrical Engineers, Transactions of the, vol. 70, no. 2, pp. 1248 –1255, July 1951.

[77] R. H. Park, “Two-reaction theory of synchronous machines generalized method of analysis-part i,” American Institute of Electrical Engineers, Transactions of the, vol. 48, no. 3, pp. 716 –727, July 1929.

[78] C. L. Fortescue, “Method of symmetrical co-ordinates applied to the solution of polyphase networks,” American Institute of Electrical Engineers, Transactions of the, vol. XXXVII, no. 2, pp. 1027 –1140, July 1918.

[79] K. Karthikeyan and Mahesh K. Mishra, “ A novel load compensation algorithm under unbalanced and distorted supply voltages,” International Journal of emerging electric power systems, vol. 8(5), 2007.